Solvent Induced Microcracking in High Performance Polymeric Composites

by

A. Paige Clifton

Thesis submitted to the faculty of the
Virginia Polytechnic Institute and State University
in partial fulfillment of the requirements for the degree of
Master of Science
in
Engineering Mechanics

APPROVED:

Dr. David A. Dillard, Chairman

Dr. Kenneth L. Reifsnider

Dr. Ron G. Kander

Dr. Terry L. St. Clair

Dr. Jeffrey A. Hinkley

January 1996
Blacksburg, Virginia

Keywords: Environmental stress cracking, microcracking, matrix cracking, solvent effects, dye penetrant effects, fracture mechanics, transverse flexure tests

LD
5655
V855
1996
C554
c.2

SOLVENT INDUCED MICROCRACKING IN HIGH PERFORMANCE POLYMERIC COMPOSITES

by
A. Paige Clifton
Dr. David A. Dillard, Chairman
Engineering Mechanics

ABSTRACT

The first paper, "Dye Penetrant Induced Microcracking in High Performance Thermoplastic Polyimide Composites", studied the possibility of spurious microcracking in three high performance thermoplastic polyimide composite materials due to zinc iodine dye penetrant. The material systems were IM7/LaRC™-IAX, IM7/LaRC™-IAX2, and IM7/LaRC™-8515. Specimens from each material system were subjected to one of three immersion tests. The first immersion test involved soaking composite specimens previously prepared with different polishing techniques in dye penetrant. In the second test, specimens were immersed in the individual components of the dye penetrant. The final test involved exposure of specimens to one of six solvents followed by exposure to dye penetrant. Results showed that the composite materials have sufficiently high thermal residual stresses to drive microcracking in the presence of dye penetrant without external mechanical loading. There was no evidence that the different polishing techniques had an effect on dye penetrant induced stress cracking. The dye penetrant components did not produce microcracks in the composites. Some combination of the components must be present to induce microcracking. Observations also revealed that polishing had an effect on the microcracking process of the composites that were initially exposed to solvents then dye penetrant.

The second paper, "The Effect of Environmental Stress Cracking on High Performance Polymeric Composites", studied solvent stress cracking and solvent induced strength degradation on four polyimide matrix materials developed at NASA-Langley Research Center. These materials are LaRC™-IAX, LaRC™-IAX2, LaRC™-8515, and LaRC™-PETI-5. Cross-ply specimens were used to characterize solvent stress cracking in composites. Matrix cracking due to solvent exposure was observed in all of the materials. The solvent exposure time of the materials ranged from 1 minute to 96 hours. The results

show that residual thermal stresses due to processing in the cross-ply composite specimens are sufficient to drive solvent stress cracking in the matrix. Solvent application lowers the microcracking toughness, G_{mc} ,values such that the available strain energy, G_m, within the transverse ply groups is sufficient to initiate microcracking. In the absence of a solvent, the same G_m value would not induce microcracking.

Transverse flexure tests were performed on unidirectional specimens to determine the effects of the solvents on the material strengths. The presence of certain solvents severely degraded the materials. The manner in which the solvents were applied to the materials determined the degree of material degradation. The results revealed a synergistic effect between stress and solvent.

The tests showed that diglyme, MEK, and acetone produced the most severe damage to the materials. The most solvent resistant material was LaRC™-PETI-5. This is followed by LaRC™-8515, LaRC™-IAX2, and LaRC™-IAX respectively. LaRC™-PETI-5 is a thermoset whereas the remaining materials are thermoplastics.

PREFACE

This thesis is written in the form of two journal articles. The first article is entitled "Dye Penetrant Induced Microcracking in High Performance Thermoplastic Polyimide Composites" which is to be submitted to the *Journal of Thermoplastic Composites* in February 1996. The second article, to be submitted to the *Journal of Composites* in February 1996, is entitled "The Effect of Environmental Stress Cracking on High Performance Polymeric Composites".

ACKNOWLEDGEMENTS

This work was supported primarily by NASA Langley Research Center under grant number NGT-51116 monitored by Dr. Terry L. St. Clair, and also by the National Science Foundation Science & Technology Center: High Performance Adhesives and Composites under contract DMR 9120004. I would also like to thank Keith Furrow, Roberto Cano, Dr. Brian Jensen, Jeane Kurtz, John Snoha, Buddy Stotler, and Scott Warrington for their technical support. Special thanks are given to my parents, Charles and Phyllis Clifton, for their constant love and support.

TABLE OF CONTENTS

1. Dye Penetrant Induced Microcracking in High Performance Thermoplastic Polyimide Composites 1

INTRODUCTION 1

LITERATURE REVIEW 2

EXPERIMENTAL PROCEDURE 5

Materials 5

Specimen Preparation 6

Test Procedures 8

Immersion Tests in Dye Penetrant 8

Immersion Tests in Dye Penetrant Components 8

Immersion Tests in Solvents 14

RESULTS AND DISCUSSION 14

Results from Immersion Tests in Dye Penetrant 14

Results from Immersion Tests in Dye Penetrant Components 20

Results from Immersion Tests in Solvents 20

CONCLUSIONS AND FUTURE WORK 24

REFERENCES 28

2. The Effect of Environmental Stress Cracking on High Performance Polymeric Composites 35

INTRODUCTION 35

LITERATURE REVIEW.....36

Environmental Stress Cracking of Polymeric Materials.....36

Microcracking Analysis Models.....39

EXPERIMENTAL PROGRAM.....41

Materials.....41

Specimen Preparation.....42

Test Procedures.....46

Stress-Free Temperature (SFT) Tests.....46

Immersion Tests.....51

Transverse Flexure Tests.....51

Solvent drop (SD).....51

Solvent vapor (SV).....54

Solvent Soak (SS).....54

Solvent soak-wet (SSW).....54

Solvent soak-dry (SSD).....54

ANALYSIS.....55

Classical Laminate Theory (CLT) analysis.....55

Variational mechanics analysis.....59

RESULTS AND DISCUSSION.....66

Immersion test results.....66

Transverse flexure test results.....82

Solvent drop (SD) test results.....85

Solvent vapor (SV) test results 85

Sovent soak (SS) test results.....93

Solvent soak-wet (SSW) test results.....97

Solvent soak-dry (SSD) test results.....97

CONCLUSIONS AND FUTURE WORK 97

REFERENCES..... 105

APPENDIX A 111

VITA..... 134

LIST OF FIGURES

Figure 1.1. The formation of thermal residual ply stresses in multi-directional composite laminates..... 4

Figure 1.2. Chemical structures of LaRC™ materials. 7

Figure 1.3. Cure cycles for LaRC™ materials..... 9

Figure 1.4. Illustration of composite test specimen design.....10

Figure 1.5. Photomicrograph of a specimen edge prior to testing showing 90° ply groupings in a portion of a $[0/90/0_2/90_2/0_2/90_2]_s$ laminate of LaRC™-IAX.....15

Figure 1.6. Comparison of the different polishing techniques of IM7/LaRC™-IAX specimens.....16

Figure 1.7. Comparison of the crack densities between IM7/LaRC™-IAX and IM7/LaRC™-8515. 18

Figure 1.8. Microcracking pattern of IM7/LaRC™-IAX2 specimen exposed to dye penetrant. 19

Figure 1.9. Edge view of an IM7/LaRC™-IAX specimen after soaking in Photoflo 200™ for 24 hours. 21

Figure 1.10. Photomicrograph of an IM7/LaRC™ specimen in acetone for 96 hours.....22

Figure 1.11. X-rays of microcracks in IM7/LaRC™-IAX diglyme and MEK specimens.23

Figure 1.12. X-ray of an IM7/LaRC™-8515 MEK specimen. 25

Figure 2.1. The formation of thermal residual ply stresses in multi-directional composite laminates.....38

Figure 2.2. Chemical structures of LaRC™ materials.....43

Figure 2.3. Cure cycles for LaRC™ materials.....44

Figure 2.4. Illustration of composite test specimen designs.....47

Figure 2.5. Experimental apparatus used to determine the stress free temperatures.....48

Figure 2.6. Change in the panel height plotted against temperature for $[0_2/90_6]$ laminates.49

Figure 2.7. Photomicrograph of a typical solvent-induced microcrack. 52

Figure 2.8. Schematic of three-point bend fixture and solvent bath.....53

1. Dye Penetrant Induced Microcracking in High Performance Thermoplastic Polyimide Composites

INTRODUCTION

Fiber-reinforced composite materials are rapidly entering into numerous applications where they encounter various environmental conditions. To design and utilize composite structures to their full potential, their response to the service environment must be understood. Research has shown that certain environments accelerate damage in composite materials.

Composite materials lose much of their structural integrity when damaged. Damage in composites usually initiates from stress concentrators such as holes, corners, joints, free edges, etc. or from pre-existing flaws which can occur during manufacturing or during operation [1,2]. There are four primary failure modes associated with laminated composites. These modes are matrix microcracking, fiber debonding, delamination, and fiber breakage [1-5].

The first form of failure in an angle-ply and/or cross-ply laminate is matrix microcracking in the angled ply or plies [5,6]. Matrix microcracking is well documented in the literature primarily because microcracking affects the performance of composite structures in their service environments [7-25]. For instance, matrix microcracks cause a reduction in the coefficients of thermal expansion and in the stiffness [4,11-15,18-25]. They also allow an increase in moisture uptake and act as nucleation sites for more critical forms of damage such as delamination and fiber breakage [2,3,6]. There are many factors responsible for the initiation and progression of matrix microcracks. Such factors include ply orientation, ply thickness, matrix strength and toughness, mismatch in coefficients of thermal expansion, processing conditions, and the service environment [2,3,26]. Included in the service environment of a composite structure are solvents encountered during cleaning, testing, repairing, painting, paint stripping, fueling, etc. The possibility of matrix cracks resulting from exposure to environmental solvents, commonly referred to as environmental stress cracking (ESC) or solvent stress cracking, has become a concern to both researchers and the aircraft industry [7,25,27-29].

The research presented in this paper investigates the effect of dye penetrant exposure on the matrix cracking of fiber-reinforced cross-ply composites. The first section of the paper will review the literature regarding environmental stress cracking of polymeric materials and composites. The second section describes the experimental program, and the remainder of the paper presents experimental observations. The purpose of this research is to characterize dye penetrant induced microcracking in high performance thermoplastic polyimide cross-ply composites.

LITERATURE REVIEW

Environmental stress cracking of polymers has interested researchers since the 1950's [30,31]. Researchers have found that many polymeric materials, both semi-crystalline and amorphous, are susceptible to damage by organic solvents while under stress. Failure by ESC occurs at a lower stress level than would ordinarily be necessary to induce failure in the absence of the solvents. The exact mechanisms of ESC are not completely understood, but it is generally accepted that absorption of the liquid and simultaneous Tg reduction are closely related to stress cracking behavior [32-35].

Kambour and co-workers have shown that when polyphenylene oxide [32], polysulfone [33], polystyrene [34], and polycarbonate [35] are exposed to a wide variety of liquid environments, a correlation exists between the critical strain and the liquid solubility parameter (δ_l). They have also reported in their study of polystyrene that organic liquids do not exercise a significant surface energy role in solvent crazing but that their only roles are associated with flow processes [34].

Vincent and Raha [36] examined polymethylmethacrylate, polyvinyl chloride, and polysulfone in the presence of liquid environments and concluded that a two-parameter representation including the solubility parameter, δ_l, and the hydrogen bonding parameter is more effective than solely using the solubility parameter in predicting the stress cracking characteristics. Henry [37] has used a three dimensional solubility parameter approach to evaluate critical strains of polycarbonate and polysulfone.

Hittmair and Ullman [29] studied the effects of molecular weight, temperature, and crystallinity on stress cracking of polyethylene. They confirmed previously reported results that stress cracking is more severe the lower the molecular weight of the material. As the temperature was increased, the breaking time decreased at a given load. They also

noticed an inverse relationship between stress cracking and material crystallinity. In a material with low crystallinity, stress cracking occurred rapidly; whereas, in a highly crystalline material, the stress cracking slowed down and eventually stopped.

Polymeric materials are often used as matrix resins in composite structures. Despite their toughness, some matrix resins are susceptible to solvent induced microcracking while under stress. The stress can be either mechanically induced or it can result from thermal residual ply stresses. Generally a tensile residual stress develops in the transverse-fiber directions of multi-directional laminates when the laminate is exposed to temperatures below its stress free temperature (SFT). Exposure to these temperatures generally occurs during the cool-down cycle of processing and often throughout the service life. During cool-down, plies want to shrink more in the transverse direction than in the fiber direction, but the fiber direction plies constrain shrinkage in the transverse direction plies resulting in tensile residual stresses in the transverse plies. The formation of thermal residual stresses is illustrated in Figure 1.1.

Rothschilds et al. [24] studied the influence of temperature, moisture content, and hygrothermal history on matrix cracking in several different fiber/matrix cross-ply composites. They primarily studied the critical mechanical strain at the onset of matrix cracking. Their temperature and moisture content results showed that the critical strain was dependent upon material type, environmental conditions and G_{Ic}. Resistance to matrix cracking was found to be greater in the materials where the transverse moduli was lower. Their results also suggest that thermal contributions to matrix cracking can be minimized by lowering the mismatch in the coefficients of thermal expansion.

Hsieh, Schneider, and Mandell [7] investigated the effect of solvent on Mode I delamination crack propagation in polyetherimide based materials. They observed that in the presence of o-xylene, crack propagation occurred at significantly lower G_I levels than the respective G_{IC} value needed to produce a crack in air. Hsieh et al. [7] also performed immersion tests, in which there was no externally applied mechanical load, on adhesively bonded composites in several solvents and observed adhesive cracks in the adhesive layer of the bonded composites. Thus, the thermal residual stresses from processing were sufficient to drive solvent stress cracks in the composite laminates.

The dye penetrant technique is heavily utilized in research to investigate damage in composites [38-45]. Finn and Springer took x-rays in conjunction with a dye penetrant to

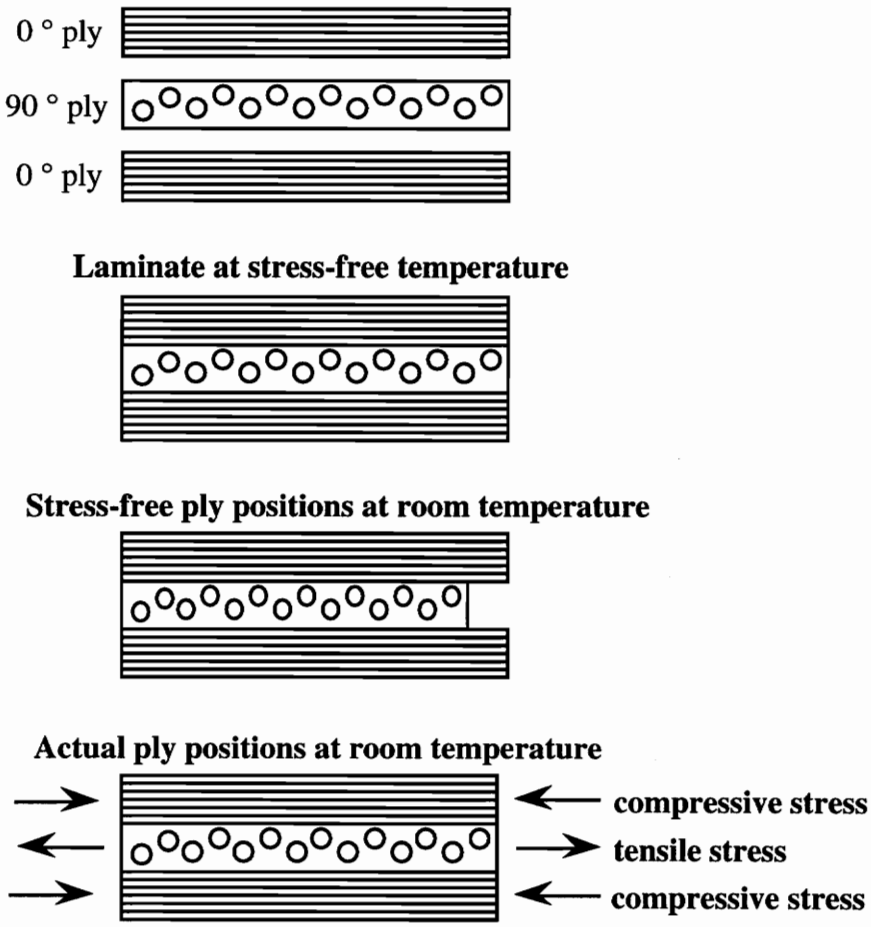

Figure 1.1. The formation of thermal residual ply stresses in multi-directional composite laminates.

show matrix cracks and delaminations in graphite-epoxy, graphite-toughened epoxy, and graphite-PEEK composite materials [38]. O'Brien utilized dye-penetrant-enhanced radiography to observe matrix cracking and delamination in T300/5208 graphite/epoxy laminates under quasi-static and cyclic loads [39]. Nelson studied thermal aging of Celion 6000/LaRC-160 and Celion 6000/PMR-15 graphite/polyimide composite materials. He used dye-penetrant-enhanced radiography to measure the crack depth along the specimen edges as a function of time and temperature [40]. Hitchen and Ogin quantified the damage in the form of transverse cracks in the core layer of a 50% by weight discontinuous glass fiber reinforced Nylon composite using a dye penetrant technique [41]. Jowitt reported on the techniques available to the aircraft inspector for use in non-destructive testing of aircraft. The most useful technique reported is the dye penetrant technique [42]. Rouillon and Gomina used a dye penetrant marking technique to monitor natural crack lengths in 2D C-SiC and 2D SiC-SiC fiber reinforced composite materials using three-point-bending tests [43]. Hitchen developed a milling/dye penetrant technique to quantify the cracking and average crack spacings associated with modulus reduction and damage accumulation during fatigue cycling of a long, discontinuous glass fiber reinforced nylon composite with a skin/core structure [44]. Sykes, Funk, and Slemp used an opaque penetrant to produce x-radiographs to observe cracking in C6000/P1700 thermoplastic composite specimens [45]. Razvan, Bakis, and Reifsnider used x-ray radiography to study the effect of cyclic load amplitudes on composite laminates [46]. Swain, Reifsnider, and Vittoser used x-radiographs to verify IST results [47].

EXPERIMENTAL PROCEDURE

Materials

The results presented in this paper are based on experiments and observations made on three polyimide material systems synthesized in the Composite and Polymers Branch (CPB) at NASA Langley Research Center. The material systems include IM7/ LaRC™-IAX, IM7/ LaRC™-IAX2, and IM7/ LaRC™-8515 (5.5%). The LaRC™-IAX, LaRC™-IAX2, and LaRC™-8515 (5.5%) resins were provided by IMITEC of Schenectady, New York. The fibers were 12k unsized IM7 carbon fibers supplied by Hercules.

LaRC™-IAX and LaRC™-IAX2 are matrix resins based on their predecessor LaRC™-IA (Langley Research Center-Improved Adhesive) [48,49]. LaRC™-IA is prepared from oxydiphthalic anhydride (ODPA) and 3,4'-oxydianiline (ODA) in *N*-methylpyrrolidone (NMP) as a 30% w/w solids solution [48,49]. The backbone of the LaRC™-IA polymers was altered by substituting the 3,4'-ODA with 1,4-phenylenediamine (*p*-PDA) at a 10% level to improve the solvent resistance. This new material was designated LaRC™-IAX [48,49]. In the case of LaRC™-IAX2, 20% of the ODPA in LaRC™-IA was replaced with 3,3',4,4'-benzophenonetetracarboxyl dianhydride (BTDA) to again improve solvent resistance [48,49]. These alterations in the LaRC™-IA polymers produced stiffer backbones, better mechanical properties and higher Tg's. LaRC™-8515 (5.5%) (Langley Research Center - 8515) is prepared from 3,3',4,4'-biphenyltetracarboxylic dianhydride (BPDA) and a ratio of 85:15 of 3,4'-oxydianiline (3,4'-ODA) and 1,3-bis(3-aminophenoxy)benzene (APB) [50,51]. The 5.5% refers to the stoichiometric offset of the polyimide [50,51]. The LaRC™-8515 material referred to herein corresponds to the 5.5% form. LaRC™-IAX, LaRC™-IAX2 and LaRC™-8515 are thermoplastic polyimides. Figure 1.2 illustrates the chemical structures of the polyimides.

Specimen Preparation

The NASA LaRC Multipurpose Prepreg Machine was used to make solution-coated prepreg tape for each material. The solution prepreg was then hand laid in the desired orientations in 6" square molds and processed into flat panels by press molding. A cross-ply orientation having a $[0/90/0_2/90_2/0_2/90_2]_s$ layup was chosen. This layup provided three stressed transverse ply groups each having a different thickness. The layup contained a 4 ply transverse group, a pair of 2 ply transverse groups and a pair of single ply transverse groups. This layup allowed the researcher to investigate the effects of thermal residual ply stresses and ply group thickness on matrix crack formation. The maximum transverse

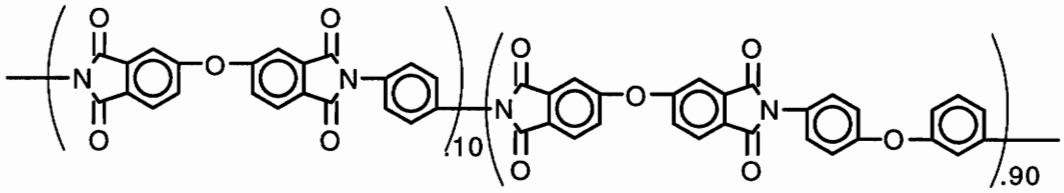

1.2a. Mer structure of LaRC™-IAX

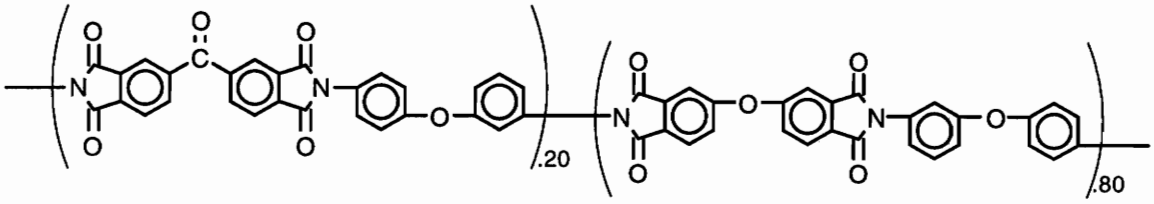

1.2b. Mer structure of LaRC™ -IAX2

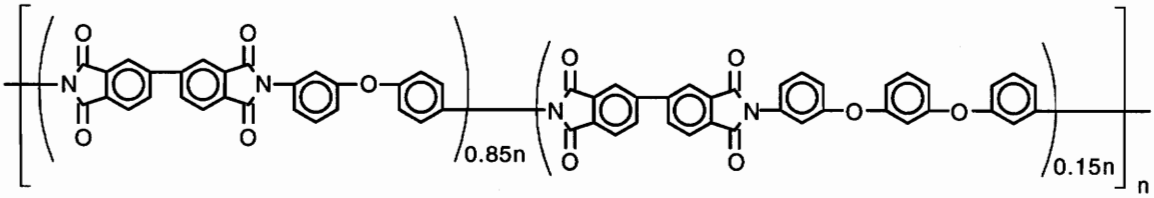

1.2c. Mer structure of LaRC™-8515

Figure 1.2. Chemical structures of LaRC™ materials.

thermal residual ply stresses associated with this layup have been calculated in Reference 2 using Classical Laminate Theory. The materials were processed using the cure cycles in Figure 1.3. The resultant composite panels were ultrasonically inspected and showed good consolidation.

A diamond saw, polisher, and microscope were used during the specimen preparation process. A K.O. Lee water cooled diamond saw was used to cut the panels into 25.4 mm by 25.4 mm specimens and were allowed to dry at room temperature and humidity for 24 hours. The specimen configuration used in this research showing the different transverse ply groupings is illustrated in Figure 1.4. The specimens were divided into twelve groups where each group contained one specimen per material. Table 1.1 describes the preparation of the specimens in each group, and indicates the solvents to which the specimens were exposed. The polished specimens were polished on an Ecomet 4 variable speed grinder-polisher with an Automet 2 power head. Four steps were involved in the polishing process. Table 1.2 describes the polishing process. An Olympus BH-2 optical microscope was used to examine the specimens.

Test Procedures

Immersion Tests in Dye Penetrant

The U-1-DP, S-1-DP, and B-1-DP groups were exposed to zinc iodine, a dye penetrant mixed in the Non-Destructive Evaluation Section (NDES) of the Models, Materials and Technology Branch (MMTB) at NASA Langley, for 18 hours. The specimens were x-rayed using a Faxitron 8050-310 Radiographic Inspection System. After the x-rays were taken, in order to examine the U-1-DP group under a microscope, one edge was polished parallel to the 0° direction with Struers polishing compounds. Then the x-radiographs were studied and the polished edges of each specimen were examined for microcracking using the microscope.

Immersion Tests in Dye Penetrant Components

Because microcracking was induced by the dye penetrant, other specimens were exposed to components of the dye penetrant to better understand the mechanisms involved.

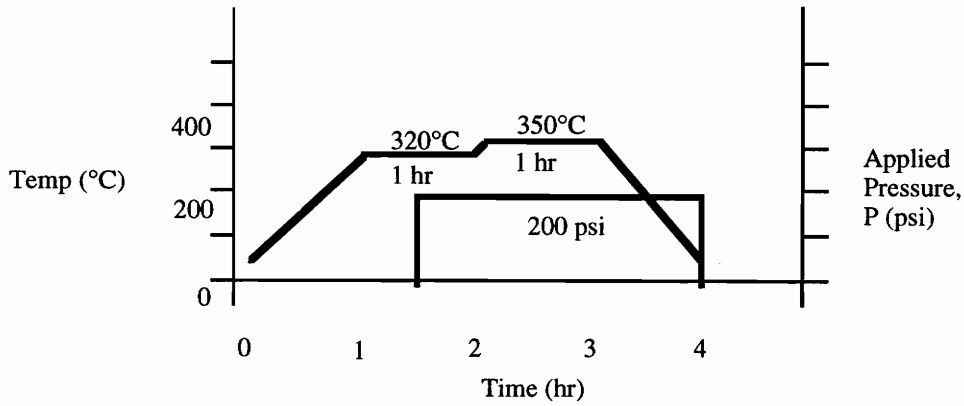

1.3a. LaRC™-IAX and LaRC™-IAX2 cure cycle.

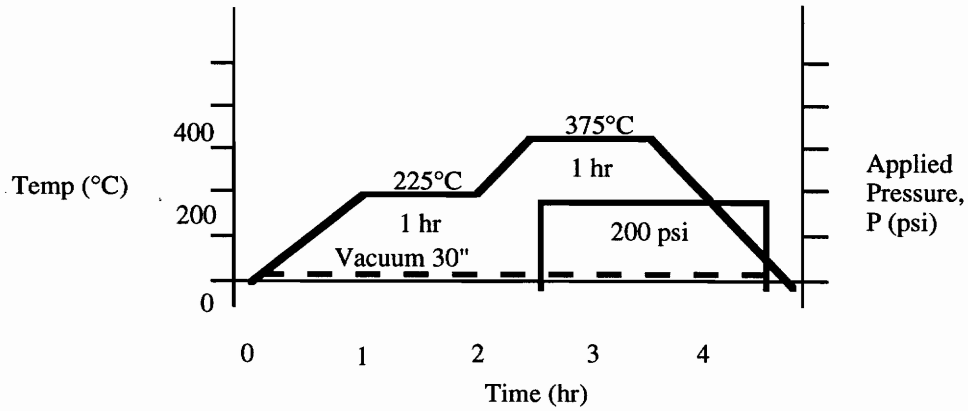

1.3b. LaRC™-8515 cure cycle.

Figure 1.3. Cure cycles for LaRC™ materials.

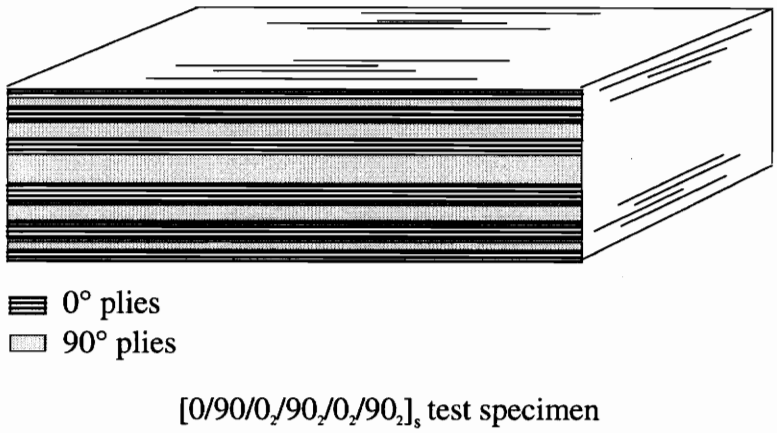

Figure 1.4. Illustration of composite test specimen design.

Table 1.1. Specimen preparation for each group.

Group	Materials in Group	Preparation	Solvent Exposure
U-1-DP	LaRC™-IAX LaRC™-IAX2 LaRC™-8515	unpolished specimens	zinc iodine
S-1-DP	LaRC™-IAX LaRC™-IAX2 LaRC™-8515	polished on one edge parallel to the 0° direction with Struers polishing compounds	zinc iodine
B-1-DP	LaRC™-IAX LaRC™-IAX2 LaRC™-8515	polished on one edge parallel to the 0° direction with Buehler polishing compounds	zinc iodine
S-2-DPC	LaRC™-IAX LaRC™-IAX2 LaRC™-8515	polished on one edge parallel to the 0° direction with Struers polishing compounds	n-propanol
S-3-DPC	LaRC™-IAX LaRC™-IAX2 LaRC™-8515	polished on one edge parallel to the 0° direction with Struers polishing compounds	iso-propanol
S-4-DPC	LaRC™-IAX LaRC™-IAX2 LaRC™-8515	polished on one edge parallel to the 0° direction with Struers polishing compounds	Photoflo 200™
S-5-Dig	LaRC™-IAX LaRC™-8515	polished on one edge parallel to the 0° direction with Struers polishing compounds	Diglyme zinc iodine

S-6-MEK	LaRC™-IAX LaRC™-8515	polished on one edge parallel to the 0° direction with Struers polishing compounds	MEK zinc iodine
S-7-Ace	LaRC™-IAX LaRC™-8515	polished on one edge parallel to the 0° direction with Struers polishing compounds	Acetone zinc iodine
S-8-Tol	LaRC™-IAX LaRC™-8515	polished on one edge parallel to the 0° direction with Struers polishing compounds	Toluene zinc iodine
S-9-TCE	LaRC™-IAX LaRC™-8515	polished on one edge parallel to the 0° direction with Struers polishing compounds	TCE 1,1,1 zinc iodine
S-10-Hyj	LaRC™-IAX LaRC™-8515	polished on one edge parallel to the 0° direction with Struers polishing compounds	Hyjet IV zinc iodine

Table 1.2. Polishing process used to polish composite specimens.

Steps	Time (min)	Force (lbs)	Polishing surface	Fluid	Direction	Speed (rpm)
1	1	25	320 grit sandpaper	water	CW***	120
2	3	25	#6 tin platen	15 micron*	CCW***	60
3	3	25	#10 ceramic platen	6 micron*	CCW***	60
4	4	50	Texmet	3 micron**	CW***	120

* diamond slurry

** alumina suspension

*** CW - clockwise; CCW - counterclockwise

The components of the zinc iodine dye penetrant are 1750g of zinc iodide, 300mL of water, 300mL of propanol, and 300mL of Photoflo 200™, an Eastman Kodak product. The S-2-DPC group was exposed to n-propanol for 24 hours. The S-3-DPC group was exposed to iso-propanol for 24 hours, and the S-4-DPC group was exposed to Photoflo 200™ for 24 hours. The polished edges of each specimen were examined under the microscope for microcracking.

Immersion Tests in Solvents

The S-5-Dig, S-6-MEK, S-7-Ace, S-8-Tol, S-9-TCE, and S-10-Hyj groups were initially immersed in solvents for 4 days (96 hours). Each group and its respective solvent are listed in Table 1.1. Following the solvent exposure, the specimens were examined for microcracking using the microscope. The specimens were then exposed to zinc iodine for 18 hours and x-rayed so that the depth of the crack could be measured.

RESULTS AND DISCUSSION

Prior to testing, all of the specimens were examined for microcracks. One of the IM7/LaRC™-IAX specimens polished with the Struers compounds revealed a microcrack in a 2 ply transverse grouping prior to solvent exposure, which was most likely the result of a defect. No microcracks were observed in the remaining specimens prior to testing. Figure 1.5 illustrates a typical specimen edge having no microcracks prior to testing.

Results from Immersion Tests in Dye Penetrant

For specimens immersed in dye penetrant for 18 hours, the x-radiographs revealed numerous through-the-width microcracks in all of the specimens. Figure 1.6 compares the three different polishing techniques of the IM7/LaRC™-IAX specimens in the U-1-DP, S-1-DP, and B-1-DP groups. The x-radiographs of the IM7/LaRC™-8515 and IM7/LaRC™-IAX2 were quite similar to those in Figure 1.6. There was no noticeable

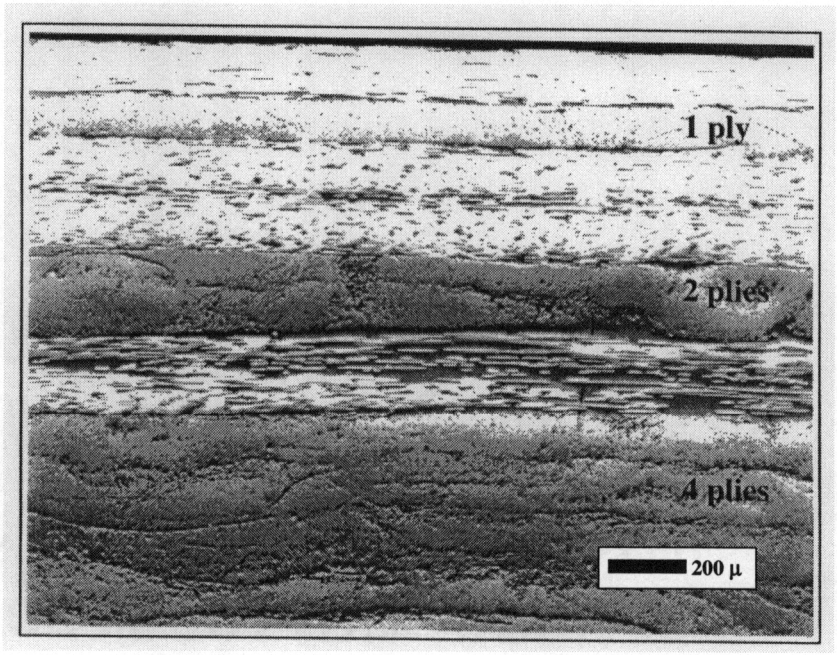

Figure 1.5. Photomicrograph of a specimen edge prior to testing showing 90° ply groupings in a portion of a $[0/90/0_2/90_2/0_2/90_2]_s$ laminate of LaRC^{TM}-IAX.

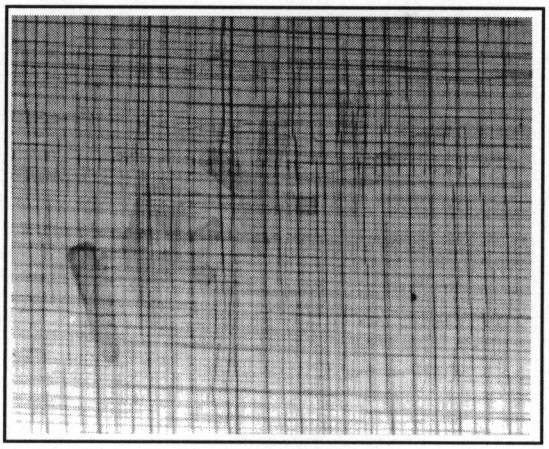

Unpolished

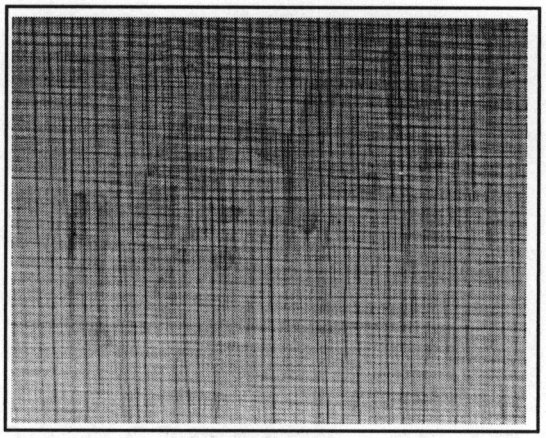

Buehler

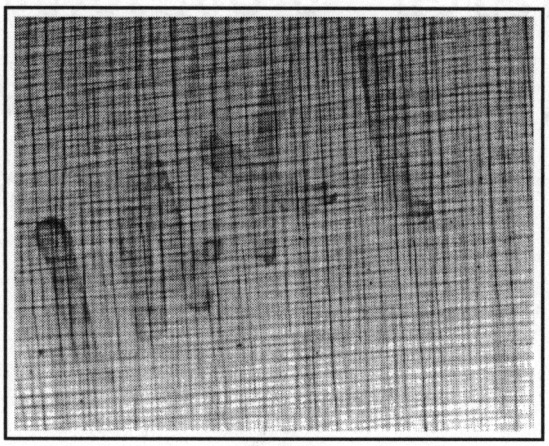

Struers

Figure 1.6. Comparison of the different polishing techniques of IM7/LaRC^{TM}-IAX specimens

difference between the unpolished and polished specimens; nor was there any difference in the cracking patterns as a result of the different polishing methods. These different polishing methods were tested to determine whether or not the polishing process had an effect on the degree of microcracking seen in these specimens. There was a concern that the polishing methods may have affected the amount of dye penetrant that traveled into the specimens. The two different polishing compounds were tested because one compound, Struers, contained ethanol, whereas the other one did not. There was also a concern that the ethanol may have had a detrimental effect on the specimens which interfered with the dye penetrant induced microcracking process.

IM7/LaRC™-IAX was the least resistant to the dye penetrant. Numerous large, distinct cracks were observed in each of the transverse ply groups. Large, clear microcracks were also observed in all three transverse ply groups of the IM7/LaRC™-8515 specimens. Although the cracks in the IM7/LaRC™-IAX and IM7/LaRC™-8515 specimens appeared to be equivalent in size, the crack density in the IM7/LaRC™-IAX specimens was greater; thus making it the less resistant material. Figure 1.7 illustrates this higher crack density in the IM7/LaRC™-IAX specimens. The crack spacing in the LaRC™-IAX specimens is approximately half of that in the LaRC™-8515 specimens.

Figure 1.8 illustrates the cracking pattern of IM7/LaRC™-IAX2. Large, definite matrix microcracks were observed in the 4 ply and 2 ply transverse groups of the IM7/LaRC™-IAX2 specimens. However, thinner, hairline microcracks were present in the single ply transverse group as opposed to larger, more distinct microcracks. There were also fewer microcracks in the single ply transverse group as compared to the LaRC™-IAX and LaRC™-8515 specimens. The crack spacings in the 4 and 2 ply transverse groups of the LaRC™-IAX2 specimen are very similar to that seen in the LaRC™-8515 specimen (Figure 1.7); however, the crack spacing in the single ply transverse group of the LaRC™-IAX2 specimen is almost double that of the LaRC™-8515 specimen, indicating fewer cracks.

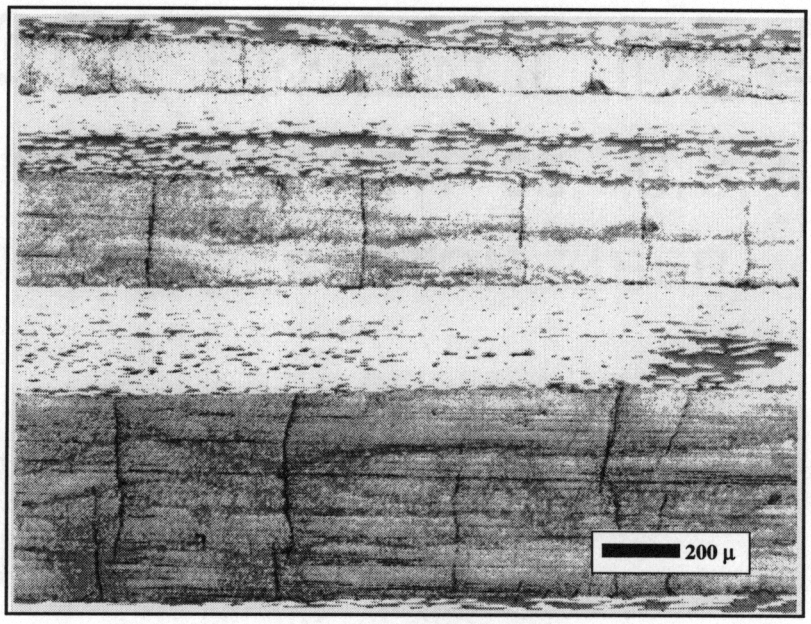

IM7/LaRC^{TM}-IAX

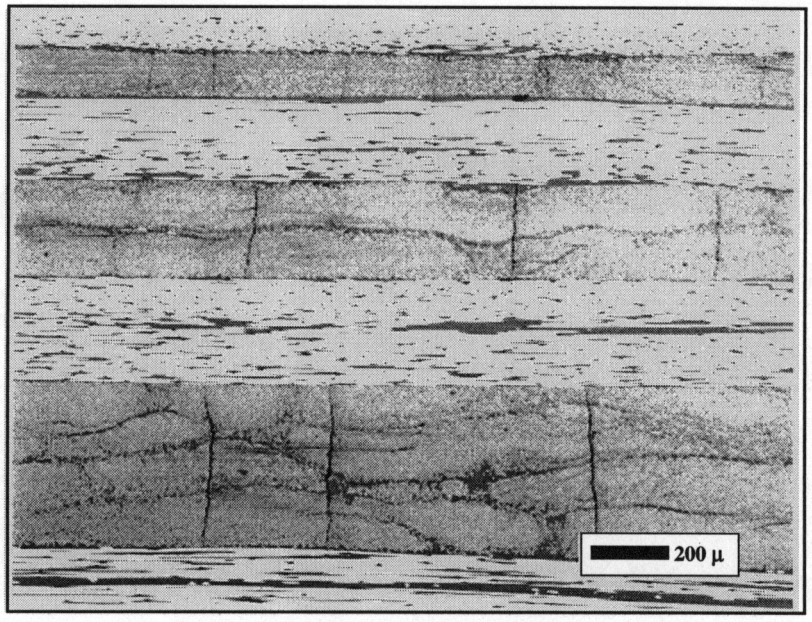

IM7/LaRC^{TM}-8515

Figure 1.7. Comparison of the crack densities between IM7/LaRC^{TM}-IAX and IM7/LaRC^{TM}-8515.

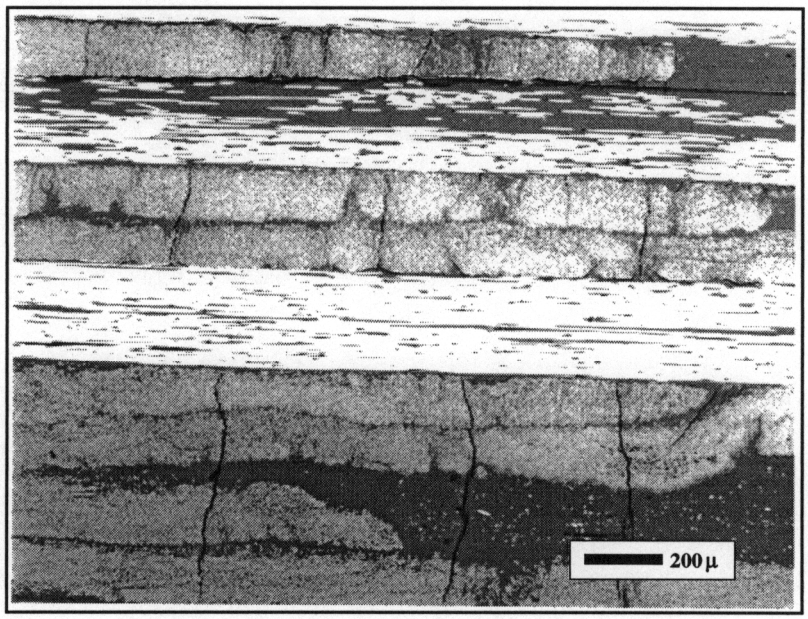

Figure 1.8. Microcracking pattern of IM7/LaRC^{TM}-IAX2 specimen exposed to dye penetrant.

Results from Immersion Tests in Dye Penetrant Components

In order to determine which dye penetrant components induced the microcracking, specimens were tested in n-propanol, isopropanol, and Photoflo 200™. A solution of zinc iodide with each individual component was not tested; however this is an area which can be studied in future work to determine the exact combination of these liquids which induces microcracking. Figure 1.9 shows an edge view of an IM7/LaRC™-IAX specimen after soaking in Photoflo 200™ for 24 hours. Figure 1.9 is representative of all the specimens. Observations showed that the individual components did not produce microcracking in the specimens. Hence, some combination of these fluids was responsible for microcracking the specimens.

Results from Immersion Tests in Solvents

Microcracks were observed on the polished edge of the solvent exposed specimens prior to dye penetrant exposure. Figure 1.10 is a representative photomicrograph of an IM7/LaRC™ specimen following a 96 hour soak in acetone. After observing the damage caused by the solvents, the specimens were placed in dye penetrant for 18 hours and then x-rayed. The IM7/LaRC™-IAX x-radiographs revealed numerous microcracks in all of the specimens except for the MEK exposed specimen. Figure 1.11 compares an IM7/LaRC™-IAX diglyme exposed specimen to the MEK exposed specimen. The diglyme exposed specimen is filled with through-the-width microcracks; whereas the MEK exposed specimen contains fewer microcracks and they do not span the width. The IM7/LaRC™-IAX diglyme exposed specimen looks very similar to the IM7/LaRC™-IAX dye penetrant exposed specimen, but there appears to be less in the IM7/LaRC™-IAX specimen when it is exposed to both MEK and dye penetrant than when it is exposed solely to dye penetrant. Other researchers have found that MEK causes plasticization in polyimide materials [52,53]. Therefore, it is possible that MEK was absorbed into the matrix at the crack tip and caused swelling and plasticization which resulted in a lowering of the Tg, and the thermal stresses within the specimen were sufficient to promote flow of the glassy material

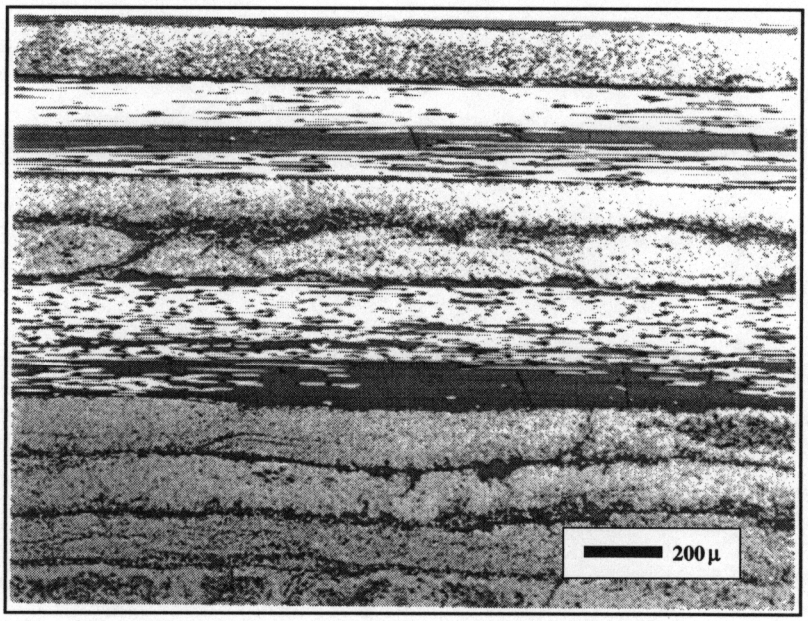

Figure 1.9. Edge view of an IM7/LaRC™-IAX specimen after soaking in Photoflo 200™ for 24 hours.

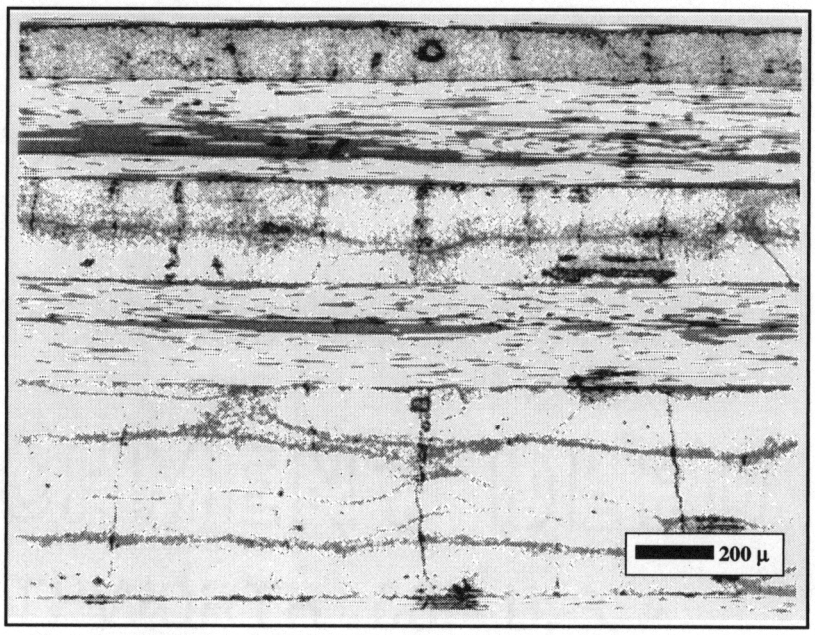

Figure 1.10. Photomicrograph of an IM7/LaRC^{TM} specimen in acetone for 96 hours.

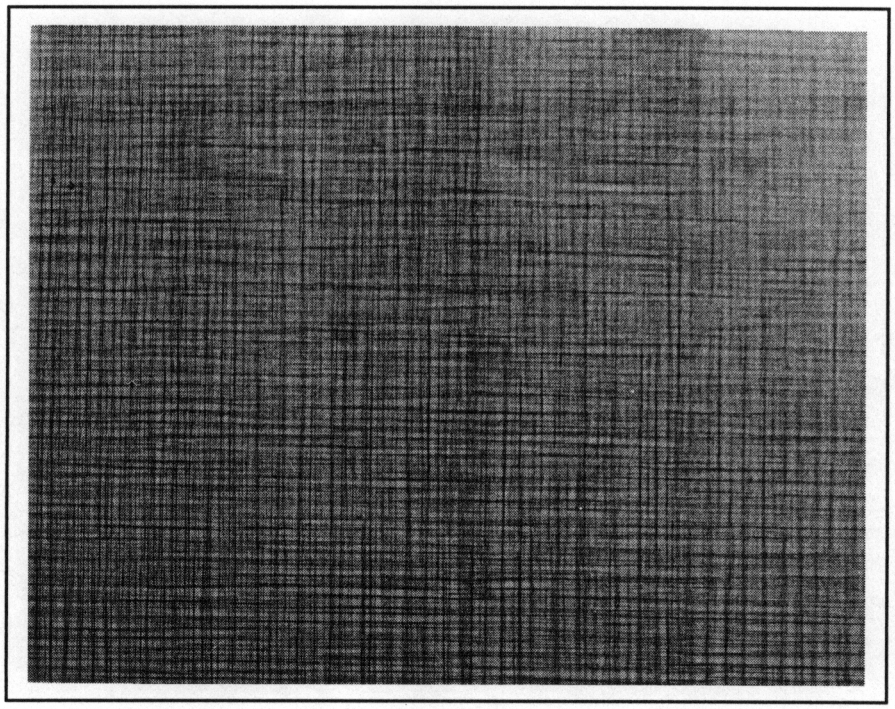

Diglyme specimen

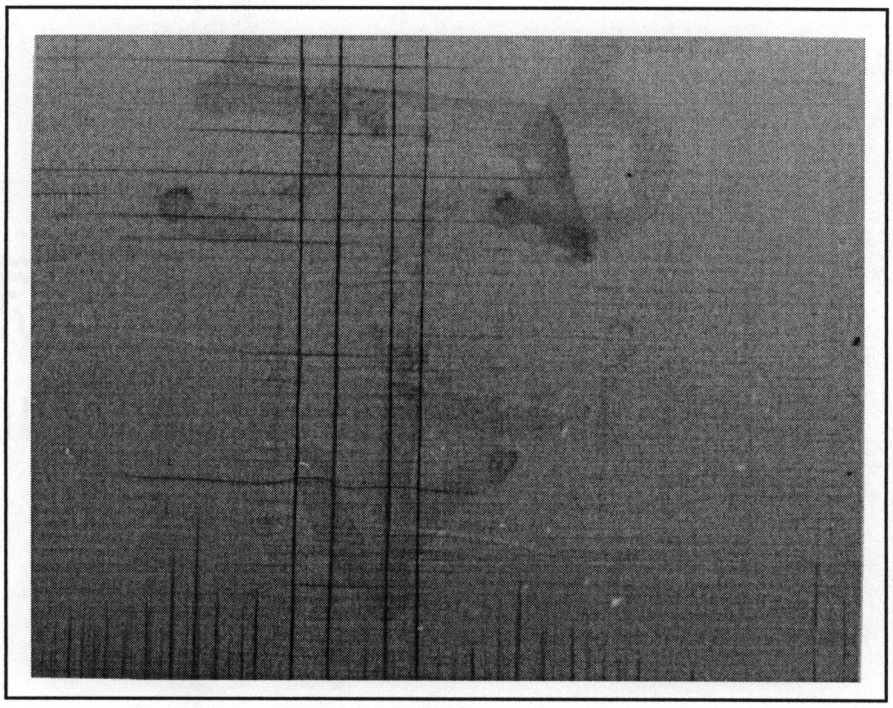

MEK specimen

Figure 1.11. X-rays of microcracks in IM7/LaRC^{TM}-IAX diglyme and MEK specimens.

in the stress direction. Hence, when the MEK exposed specimen was soaked in the dye penetrant, the available stress was insufficient to continue the microcracking process. The majority of the microcracks in the MEK exposed specimen emanate from the polished edge indicating that polishing may have affected the microcracking process. The cracks seen along the polished edge are much sharper and clearer than those originating from the three unpolished edges. This behavior is not understood, although a possible cause may include microdamage along the polished edge caused from the polishing process. The polishing process may have opened paths that were unattainable prior to polishing along which the solvents could easily travel.

A similar effect was seen in the IM7/LaRC™-8515 x-radiographs. However, none of the IM7/LaRC™-8515 specimens contained numerous through-the-width microcracks. Clear, sharp microcracks extended from the polished edge of each specimen. The polished edge microcracks did not span the width. Very faint microcracks could be seen along the remaining edges. Figure 1.12 illustrates this unique cracking pattern.

This phenomenon did not occur when the specimens were exposed solely to dye penetrant. The dye penetrant specimens had numerous through-the-width microcracks. It is possible that the residual thermal stresses were adequately relieved by the solvent induced microcracks thus the critical stress needed to initiate another microcrack during the dye penetrant soak was not available.

CONCLUSIONS AND FUTURE WORK

Immersion tests were conducted on IM7/LaRC™-IAX, IM7/LaRC™-IAX2, and IM7/LaRC™-8515 cross-ply composite specimens. Three groups, each containing one specimen per material, with different polishing methods were exposed to zinc iodine dye penetrant for 18 hours and then x-rayed. The x-radiographs revealed through-the-width microcracking in all of the specimens, thus the thermal residual stresses due to processing in the specimens were sufficient to drive microcracking in the presence of dye penetrant. The cracking patterns observed in each group were very similar, indicating that polishing does not have an effect on dye penetrant induced microcracking. However, the crack density associated with the different material specimens revealed that IM7/LaRC™-IAX

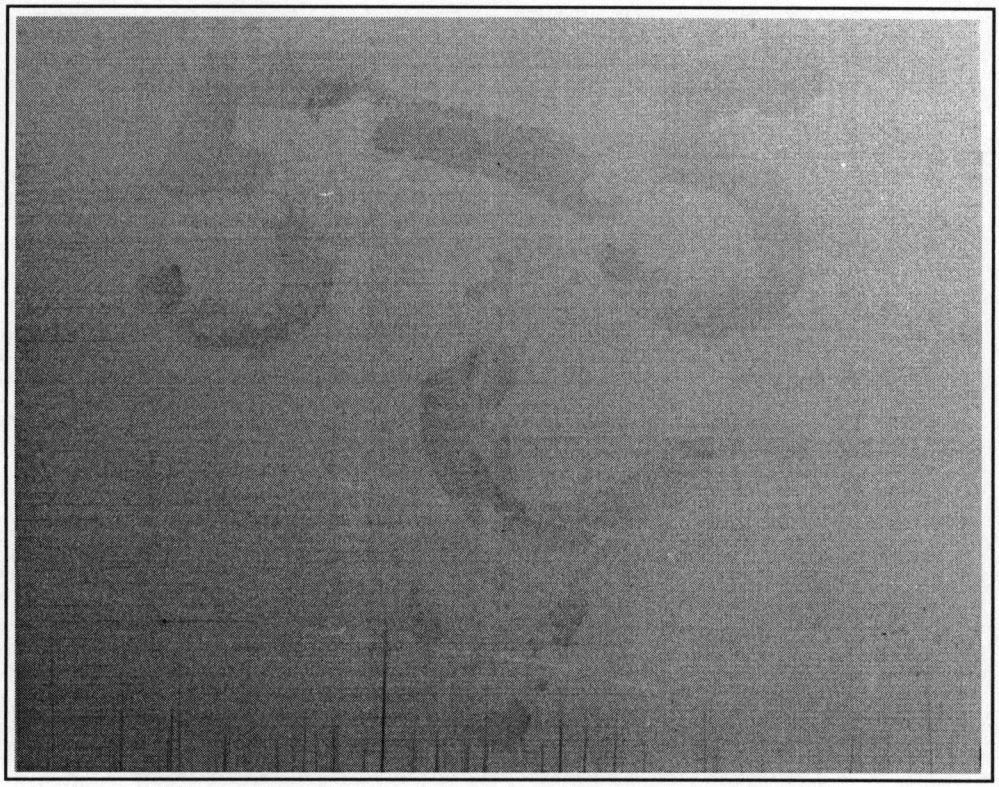

Figure 1.12. X-ray of an IM7/LaRC™-8515 MEK specimen.

was the least resistant to dye penetrant. This is followed by IM7/LaRC™-8515 and IM7/LaRC™-IAX2 respectively. Dye penetrant is not recommended for use with thermoplastic composites having substantial thermal residual stresses.

Immersion tests were performed on IM7/LaRC™-IAX, IM7/LaRC™-IAX2, and IM7/LaRC™-8515 cross-ply composite specimens. The specimens were exposed to several of the dye penetrant components which included n-propanol, isopropanol, and Photoflo 200™. These individual components did not induce microcracking in any of the materials. It is some combination of these materials which causes microcracking.

IM7/LaRC™-IAX and IM7/LaRC™-8515 cross-ply composite specimens were initially exposed to solvents for 4 days (96 hours). Following the solvent exposure, the specimens were immersed in zinc iodine dye penetrant and then x-rayed. Microcracking was observed along the polished edges of the specimens after solvent exposure using a microscope. Numerous through-the-width microcracks were observed in all of the solvent exposed IM7/LaRC™-IAX x-radiographs except for the MEK exposed specimen. The MEK exposed specimen contained fewer microcracks which did not span the width. The x-radiographs of the IM7/LaRC™-8515 solvent exposed specimens revealed that the microcracks in the IM7/LaRC™-8515 specimens did not span the width. However, the cracks observed growing along the polished edges in the x-radiographs of the IM7/LaRC™-IAX MEK exposed specimen and the IM7/LaRC™-8515 specimens were much sharper and clearer than those emanating from the unpolished edges. In these tests, the polishing method appears to have an effect on the microcracking process. This anomaly due to polishing is not understood.

Some areas of future work would include conducting further experiments to characterize the effects of polishing on composite specimens. Also, the combination of zinc iodine dye penetrant components should be studied more extensively to determine what combination causes the microcracking in specimens. Other dye penetrants should also be tested to determine if they also induce microcracking in composite specimens. The critical stress level associated with dye penetrant microcracking is an area of interest. If the critical stress level at which the dye penetrant induced microcracking occurred were known,

then researchers would know if their specimens were susceptible to microcracking due to dye penetrant exposure.

REFERENCES

1. Garg, A. C., "Environmental Stress Cracking Behavior of Delamination in Laminated Composites," Composite Materials and Structures; Proceedings of the International Conference, Madras, India, Jan. 6-9, 1988.

2. Clifton, A. Paige, Dillard, David A., St. Clair, Terry L. and Hinkley, Jeffrey, "The Effect of Environmental Stress Cracking on High Performance Polymeric Composites," *Journal of Composite Materials*, to be submitted in February 1996.

3. Moore, Robert H. and Dillard, David A., "Elastic and Time Dependent Matrix Cracking in Cross-Ply Laminates," Masters Thesis, College of Engineering, Virginia Polytechnic Institute and State University, Blacksburg, VA, April 1988.

4. Highsmith, A. L. and Reifsnider, K. L., "Stiffness-Reduction Mechanisms in Composite Laminates," *Damage in Composite Materials, ASTM STP 775,* K. L. Reifsnider, Ed., American Society for Testing and Materials, 1982, p. 103.

5. Reifsnider, K. L., Henneke, E. G., Stinchcomb W. W. and Duke, J. C., "Damage Mechanics and NDE of Composite Laminates," *Mechanics of Composite Materials, Recent Advances,* Z. Hashin and C. T. Herakovich, Eds., New York, Perganon, 1983, p. 399.

6. Nairn, John A., "Microcracking, Microcrack-Induced Delamination, and Longitudinal Splitting of Advanced Composite Structures," NASA Contractor Report 4472, November 1992.

7. Hsieh, Alex J. , Schneider, Nathaniel S. and Mandell, John F., "Solvent Stress cracking and Failure Mechanisms in Polyetherimide composites," *Polymer Composites*, **11** (4), August 1990, p. 240.

8. Hashin, Zvi, "The Effect of Microcracking on Thermal Expansion and Cyclic Stress-Strain Relations of Composites," in G. J. Dvorak and D. C. Lagoudas (ed.), *Microcracking-Induced Damage in Composites*, 1990, p. 35.

9. Allen, David H. and Lee, Jong-Won, "Matrix Cracking in Laminated Composites Under Monotonic and Cyclic Loadings," in G. J. Dvorak and D. C. Lagoudas (ed.), *Microcracking-Induced Damage in Composites*, 1990, p. 65.

10. Nairn, J. A. and Hu, S., "The Initiation and Growth of Delaminations Induced by Matrix Microcracks in Laminated Composites," *International Journal of Fracture*, **57**, 1992, p. 1.

11. Nairn, John A., "The Initiation of Microcracking in Cross-Ply Laminates: A Variational Mechanics Approach," American Society for Composites, Technical Conference, 3rd., Seattle, WA, Sept. 25-29, 1988.

12. Nairn, John A., "The Strain Energy Release Rate of Composite Microcracking: A Variation Approach," *Journal of Composite Materials*, **23**, 1989, p. 1106.

13. Gudmundson, Peter and Ostlund, Soren, "Numerical Verification of a Procedure for Calculation of Elastic Constants in Microcracking Composite Laminates," *Journal of Composite Materials*, **26** (17), 1992, p. 2480.

14. Gudmundson, Peter and Ostlund, Soren, "Prediction of Thermoelastic Properties of Composite Laminates with Matrix Cracks," *Composites Science and Technology*, **44**, 1992, p. 95.

15. Garrett, K. W. and Bailey, J. E., "Multiple Transverse Fracture in 90° Cross-Ply Laminates of a Glass Fibre-Reinforced Polyester" *Journal of Materials Science*, **12**, 1977, p.157.

16. Bailey, J. E., Curtis, P. T. and Parvizi, A., "On the Transverse Cracking and Longitudinal Splitting Behaviour of Glass and Carbon Fibre Reinforced Epoxy Cross Ply Laminates and the Effect of Poisson and Thermally Generated Strain" *Proc. R. Soc. Lond. A.*, 1979, p. 599.

17. Lim, S. G. and Hong, C. S., "Prediction of Transverse Cracking and Stiffness Reduction in Cross-Ply Laminated Composites," *Journal of Composite Materials*, **23**, 1989, p. 695.

18. Lee, J.-W. and Daniel, I. M., "Progressive Transverse Cracking of Crossply Composite Laminates," *Journal of Composite Materials*, **24**, 1990, p. 1225.

19. Bowles, David E., "Effect of Microcracks on the Thermal Expansion of Composite Laminates," *Journal of Composite Materials*, **17**, 1984, p. 173.

20. Laws, N. and Dvorak, G. J., "Transverse Matrix Cracking in Composite Laminates," Composite Material Response: Constitutive Relations and Damage Mechanisms; Proceedings of the Workshop, Glasgow, Scotland, July 30, 31, 1987.

21. Moore, Robert H. and Dillard, David A., "Time-dependent Matrix Cracking in Cross-ply Laminates," *Composites Science and Technology*, **39**, 1990, p. 1.

22. Talreja, Ramesh, Yalvac, Selim, Yats, Larry D. and Wetters, Derrick G., "Transverse Cracking and Stiffness Reduction in Cross Ply Laminates of Different Matrix Toughness," *Journal of Composite Materials*, **26** (11), 1992, p. 1644.

23. Swanson, S. R., "On the Mechanics of Microcracking in Fiber Composite Laminates Under Combined Stress," ASME, Winter Annual Meeting, Anaheim, CA, Dec. 7-12, 1986.

24. Rothschild, R. J., Ilcewicz, L. B., Nordin, P., and Applegate, S. J., " The Effect of Hygrothermal Histories on Matrix Cracking in Fiber Reinforced Laminates," *Journal of Engineering Materials and Technology*, **110**, 1988, p. 158.

25. Hsieh, Alex J. and Vanselow, Janice J., "Environmental Stress Crazing and Cracking of Transparent Polymers," U.S. Army Technology Laboratory, MTL TR 89-12, February 1989.

26. Reifsnider, Kenneth L. and Giacco, Alexander, "The Use of Microcrack Analysis in Performance Simulation for Composite Material Systems," ASME, AMD Volume III, Presented in Dallas, Texas, November 25-30, 1990.

27. Petrie, S. P., Dibenedetto, A. T., and Miltz, J., "The Effects of Stress Cracking on the Fracture Toughness of Polycarbonate," *Polymer Engineering and Science*, **20** (6), 1980, p. 385.

28. Henry, L. F. III, "Environmental Stress Cracking of Thermoplastics: A New Approach to Testing," *Journal of Testing and Evaluation*, JTEVA, **4** (4), July 1976, p. 263.

29. Hittmair, P. and Ullman, Robert, "Environmental Stress Cracking of Polyethylene," *Journal of Applied Polymer Science*, **6** (19), 1962, p. 1.

30. Lustiger, A. *Failure of Plastics*, edited by W. Brostow and R. D. Corneliussen, Chapter 16, Hanser Publications, 1986, p. 305.

31. Howard, J. B., *Soc. Plas. Eng. J.*, **6**, 1959, p. 397.

32. Bernier, G. A. and Kambour, R. P., "The Role of Organic Agents in the Stress Crazing and Cracking of Poly (2,6-dimethyl-1,4-phenylene oxide), *Macromolecules*, **1** (5), 1968, p. 393.

33. Kambour, R. P., Romagosa, E. E., and Gruner, C. L., "Swelling, Crazing, and Cracking of an Aromatic Copolyether-Sulphone in Organic Media," *Macromolecules*, **5** (4), 1972, p. 335.

34. Kambour, R. P., Gruner, C. L. and Romagosa, E. E., "Solvent Crazing of "Dry" Polystyrene and "Dry" Crazing of Plasticized Polystyrene," *Journal of Polymer Science*, **11**, 1973, p. 1879.

35. Kambour, R. P., Gruner, C. L. and Romagosa, E. E., "Bisphenol-A Polycarbonate Immersed in Organic Media. Swelling and Response to Stress," *Macromolecules*, **7** (2), 1974, p. 248.

36. Vincent, P. I. and Raha, S., "Influence of Hydrogen Bonding on Crazing and Cracking of Amorphous Thermoplastics," *Polymer*, **13**, 1972, p. 283.

37. Henry, L. F., "Prediction and Evaluation of Susceptibilities of Glassy Thermoplastics to Environmental Stress Cracking," *Polymer Engineering Science*, **14**, 1974, p. 167.

38. Finn, Scott R. and Springer, George S., *Comosite Plates Impact Damage - An Atlas*, Technomic Publishing Co., Lancaster, PA, 1991.

39. O'Brien, T. K., "Tension Fatigue Behavior of Quasi-isotropic, Graphite/Epoxy Laminates," Fatigue and Creep of Composite Materials; Proceedings of the Third Riso International Symposium on Metallurgy and Materials Science, Roskilde, Denmark, September 6-10, 1982.

40. Nelson, J. B., "Edge Crack Growth of Thermally Aged Graphite/Polyimide Composites," NASA Report Number NASA-TM-85763, March, 1984.

41. Hitchen, S. A. and Ogin, S. L., "Matrix Cracking and Modulus Reduction During the fatigue of an Injection-Moulded Glass/Nylon Composite," *Composites Science and Technology*, **47** (3), 1993, p. 239.

42. Jowitt, P., "Non-Destructive Testing," *Shell Aviation News*, n 372, 1969, p. 19.

43. Rouillon, M. H. and Gomina, M., "Natural Crack Lengths and Crack Growth Resistance Curves in Fiber-Reinforced Composite Materials," Strength Seminar on Ceramic Composite Materials, Stuttgart, Germany, Mar. 28-29, 1990.

44. Hitchen, S. A., "Modulus Reduction and Damage Accumulation During the Fatigue of a Glass/Nylon Composite," Dissertation Abstracts International, **52** (11), May, 1992, p. 205.

45. Sykes, George F., Funk, Joan G., and Slemp, Wayne, S., "Assessment of Space Environment Induced Microdamage in Toughened Composite Materials," 18th International SAMPE Conference, October 7-9, 1986.

46. Razvan, A., Bakis, C. E. and Reifsnider, K. L., "Influence of Load Levels on Damage Growth Mechanisms of Notched Composite Materials," Composite Materials: Testing and Design. Volume 9; Proceedings of the Ninth Symposium, Sparks, NV, April 27-29, 1988.

47. Swain, R. E., Reifsnider, K. L. and Vittoser, J., "Investigation of Damage in Composite Laminates Using the Incremental Strain Tests," Composite Materials: Testing and Design. Volume 9; Proceedings of the Ninth Symposium, Sparks, NV, April 27-29, 1988.

48. Hou, T. H., Johnston, N. J., and St. Clair, T. L., "IM7/LaRC™-IA Polyimide Composites," *High Performance Polymers*, **7**, 1995, p. 105.

49. Hou, T. H., "Processing and Properties of IM7/LaRC™-IA Polyimide Composites," 39th International SAMPE Symposium and Exhibition, Anaheim, California, April 11-14, 1994.

50. Hou, T. H., Wilkinson, S. P., and Jensen, B. J., "Processing and Properties of IM7/LaRC™-8515 Composites," *Polyimides: Synthesis, Characterization, and Applications*, edited by C. Feger, Plenum Press, New York, 1995.

51. Jensen, Brian J., Hou, Tan H., and Wilkinson, Steven P., "Adhesive and Composite Properties of LaRC™-8515 Polyimide," 40th SAMPE International Symposium and Exhibition, May 8-11, 1995.

52. Parvatareddy, H., Pasricha, A., Dillard, D. A., Holmes, B., and Dillard, J. G., "High Temperature and Environmental Effects on the Durability of TI-6AL-4V/LaRC-PETI-5 Adhesive Bonded System," ASTM Second Symposium on High Temperature and Environmental Effects on Polymeric Composites, November 13-14, 1995, Hampton, VA, STP 1274.

53. Atkins, A. G. and Mai, Y-W., *Elastic and Plastic Fracture*, John Wiley & Sons, New York, 1985.

2. The Effect of Environmental Stress Cracking on High Performance Polymeric Composites

INTRODUCTION

Fiber-reinforced composite materials are being used in numerous applications in which they encounter various environmental conditions. To design and utilize composite structures to their full potential, their response to the service environment must be understood. Research has shown that certain environments accelerate damage in composite materials.

Composite materials may lose much of their structural integrity when damaged. Damage in composites usually initiates from stress concentrators such as holes, corners, joints, free edges, etc. or from pre-existing flaws such as fiber matrix debonds which can occur during manufacturing [1,2,3,4,5]. There are four primary failure modes associated with tensile loaded laminated composites. These modes are matrix microcracking, fiber debonding, delamination, and fiber breakage [1,4,6-8]. Numerous observations have revealed that multi-directional laminate damage initiates with microcracks in the transverse plies running parallel to the fiber direction [2,3,4,9-12]. Although microcracks are not usually critical in terms of structural failure since the failure load is generally larger than the microcrack initiation load, their presence is considered undesirable [2-5,9-11,13]. Microcracks reduce the composite stiffness [2-4,6,7,9-11,14-21] and they change the thermal expansion coefficients [2-4,6,9-11,16,18]. The latter effect is an important consideration when designing structures that must maintain dimensional stability. Thermal and electrical properties such as conductance and resistance are affected by the accumulation of microcracks [22]. Moisture sorption is altered due to the increase in laminate surface area due to microcracks in piping [22]. Microcracks influence damage in surface layers such as paints and conductive surfaces [22]. In certain applications, where composite structures are important, the presence of microcracks may have to be interpreted as failure. Such applications include the walls of pressure or liquid containers or in wet or corrosive environments where microcracks would result in leakage and/or accelerated corrosion [2,3,11,13,23]. Microcracks often act as nucleation sites for more severe damage mechanisms including delamination, fiber/matrix debonding and fiber failure [6,9-11,14,18]. There are many factors responsible for the initiation and progression of

matrix microcracks. Such factors include ply orientation, ply thickness, matrix strength and toughness, mismatch in coefficients of thermal expansion, processing conditions, and the service environment [6,15,24]. Included in the service environment of a composite structure are solvents encountered during cleaning, testing, repairing, painting, paint stripping, fueling, etc. These microcracks induced by environmental solvents while the structure is under load, commonly referred to as environmental stress cracking (ESC), have become an important concern to the composites industry.

The research presented in this paper investigates the effect of environmental solvent exposure on the matrix cracking and strength of fiber-reinforced cross-ply composites. The first section of the paper will review the literature regarding environmental stress cracking of polymeric materials and composites, matrix cracking, and theoretical models that have been used for predicting various properties affected by matrix cracking. The second section discusses stress and microcracking analyses used in this study. The remainder of the paper presents solvent induced microcracking and strength reduction data. The purpose of this study was to evaluate the solvent resistance of polyimide materials and assess the damage induced by the presence of these solvents.

LITERATURE REVIEW

Environmental Stress Cracking of Polymeric Materials

Environmental stress cracking (ESC) of polymers has interested researchers since the 1950's [25,26]. Researchers have found that many polymeric materials, both semi-crystalline and amorphous, are susceptible to damage by organic solvents while under stress. Failure by ESC occurs at a lower stress level than would ordinarily be necessary in the absence of the solvents. The exact mechanisms of ESC are not completely understood, but it is generally accepted that absorption of the liquid and simultaneous Tg reduction are closely related to stress cracking behavior.

Kambour and co-workers have shown that when polyphenylene oxide [27], polysulfone [28], polystyrene [29], and polycarbonate [30] are exposed to a wide variety of liquid environments, a correlation exists between the critical strain and the liquid solubility parameter (δ_l). They have also reported in their study of polystyrene that organic

liquids do not exercise a significant surface energy role in solvent crazing but that their only roles are associated with flow processes [29].

Vincent and Raha [31] examined polymethylmethacrylate, polyvinyl chloride, and polysulfone in the presence of liquid environments and concluded that a two-parameter representation including the solubility parameter, δ_l, and the hydrogen bonding parameter is more effective than solely using the solubility parameter in predicting the stress cracking characteristics. Henry [32] has used a three dimensional solubility parameter approach to evaluate critical strains of polycarbonate and polysulfone.

Hittmair and Ullman [33] studied the effects of molecular weight, temperature, and crystallinity on stress cracking of polyethylene. They confirmed previously reported results that stress cracking is more severe the lower the molecular weight of the material. As the temperature was increased, the breaking time decreased at a given load. They also noticed an inverse relationship between stress cracking and material crystallinity. In a material with low crystallinity, stress cracking occurred rapidly; whereas, in a highly crystalline material, the stress cracking slowed down and eventually stopped.

Polymeric materials are often used as matrix resins in composite structures. Despite their toughness, some matrix resins are susceptible to solvent induced microcracking while under stress. The stress can be either mechanically induced or it can result from thermal residual ply stresses. Generally a tensile residual stress develops in the transverse-fiber directions of multi-directional laminates when the laminate is exposed to temperatures below its stress free temperature (SFT). Exposure to these temperatures generally occurs during the cool-down cycle of processing and often throughout the service life. During cool-down, transverse-fiber direction plies want to shrink more than the fiber direction plies, but the fiber direction plies constrain shrinkage in the transverse plies resulting in tensile residual stresses. The formation of thermal residual stresses is illustrated in Figure 2.1.

Rothschilds et al. [22] studied the influence of temperature, moisuture content, and hygrothermal history on matrix cracking in several different fiber/matrix cross-ply composites. They primarily studied the critical mechanical strain at the onset of matrix cracking. Their temperature and moisture content results showed that the critical strain was dependent upon material type, environmental conditions and G_{Ic}. Resistance to matrix cracking was found to be greater in the materials where the transverse moduli was lower. Their results also suggest that thermal contributions to matrix cracking can be minimized by lowering the mismatch in the coefficients of thermal expansion.

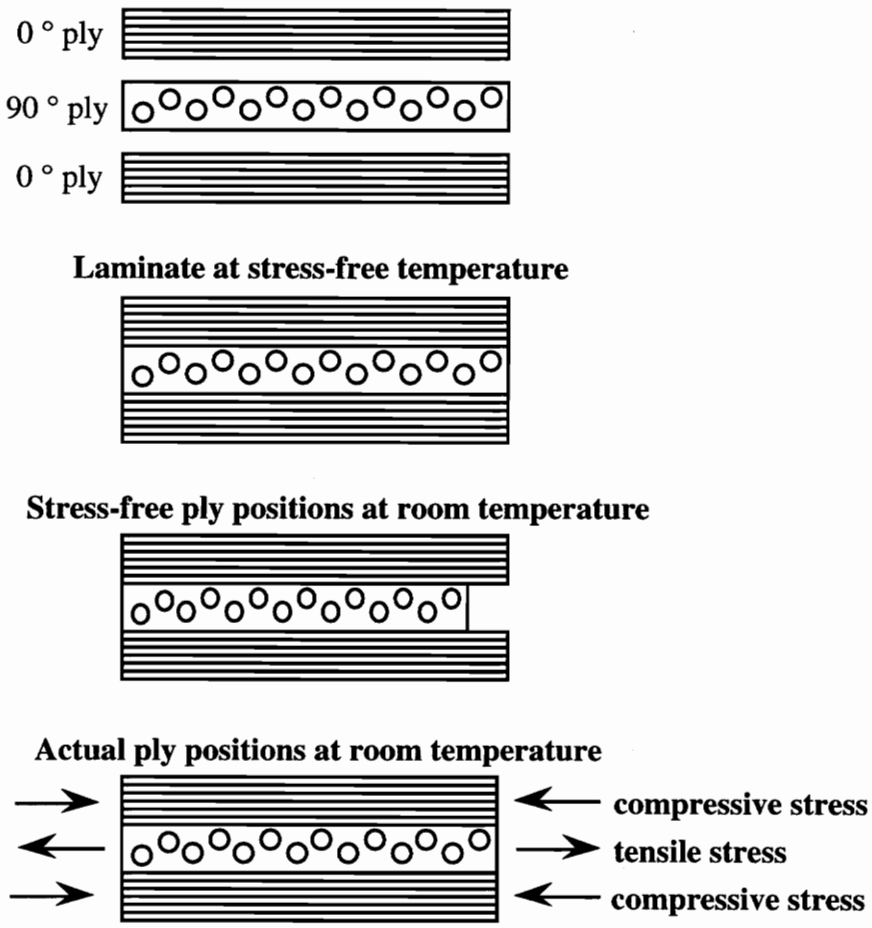

Figure 2.1. The formation of thermal residual ply stresses in multi-directional composite laminates.

Hsieh, Schneider, and Mandell [5] investigated the effect of solvent on Mode I delamination crack propagation in polyetherimide based materials. They observed that in the presence of o-xylene, crack propagation occurred at significantly lower G_I levels than the respective G_{IC} value needed to produce a crack in air. Hsieh et al. [5] also performed immersion tests, in which there was no externally applied mechanical load, on adhesively bonded composites in several solvents and observed adhesive cracks in the adhesive layer of the bonded composites. Thus, the thermal residual stresses from processing were sufficient to drive solvent stress cracks in the composite laminates.

Microcracking Analysis Models

In the past several researchers have developed mathematical models to predict several aspects associated with matrix microcracking which include reduction in stiffness and thermal expansion coefficients, stress levels associated with microcracking, microcrack density, and microcrack initiation [2,3,6,9-11,13-22]. These models have primarily been based on variational mechanics, shear-lag concepts, and finite element analyses.

Nairn [2,3,9] described a strain energy release rate method that builds on Hashin's variational mechanics approach. Hashin [34,35] used the variational mechanics approach to determine the effect of microcracks on the modulus of cross-ply composite laminates. Nairn used Hashin's variational approach to develop a new variational solution to calculate the strain energy release rate due to the initiation of microcracking in cross-ply laminates. This new energy criterion assumed that the first microcrack formed when the total energy associated with the formation of that crack exceeded some critical value. According to this energy failure criterion, a microcrack forms when the the energy release rate associated with the formation of a complete, through-the-width microcrack, G_m, equals or exceeds the microcracking fracture toughness of the composite material system. The new variational solution also yields the thermal expansion coefficient of the microcracked composite.

Laws and Dvorak [17,36] developed a progressive damage analysis based on statistical fracture mechanics for transverse cracking in cross-ply composite laminates based on a simple one-dimensional shear lag analysis. The stiffness reduction as a function of crack density and the crack density as a function of applied load can be determined using expressions developed in this model. The progressive analysis model introduces the probability density function for the site of the next crack. A drawback to this model is that

the shear lag parameter must be determined from the first ply failure stress and the energy release rate of the lamina which must be determined through another test.

Lee and Daniel [15] developed a progressive damage scheme for cross-ply composite laminates using a simplified shear lag analysis. The shear lag parameter is determined as a function of the shear moduli of the lamina and geometry of the specimen. The analysis gave expressions for the transverse crack density and for the stress distributions and reduced stiffnesses of the damaged plies and the whole laminate as a function of applied load and ply properties. The progressive cracking scheme incorporated by Lee and Daniel [15] assumed that the next crack or set of cracks in the transverse plies occurred when the maximum axial stress in the transverse plies was equivalent to the transverse strength of the layer. The analysis does not assume uniform crack spacing.

Lim and Hong [14] investigated the initiation of transverse matrix cracking and the stiffness reduction resulting from the presence of multiple tranverse matrix cracking in cross-ply composite laminates. They employed a simplified shear lag analysis that utilized the concept of an interlaminar shear layer. The energy concept was utilized to evaluate the effect of the transverse layer thickness and the contraining effect of the adjacent 0° layer on transverse cracking behavior of cross-ply composite laminates. The boundary conditions in this analysis were satisfied for any transverse crack spacing. The thermal residual stresses and Poisson's effects were also considered. They found that thermal residual stresses significantly influence transverse cracking in graphite/epoxy composite laminates. Poisson's effects are negligible in both graphite/epoxy and glass/epoxy systems. The results show reasonable agreement with existing models and experimental results.

Swanson [20] used a shear lag model in conjuction with a Weibull failure criterion to calculate stress distributions around microcracks and the reduction in stiffness associated with microcracking. His analysis considers both shear loading of the cracked plies along with the familiar case of transverse tension. The stiffness reduction results are consistent with existing calculations and experiments. The results also show that increasing loads are necessary to increase transverse microcracking.

Gudmundson and Ostlund [10,11] presented a new method for predicting the changes in all coefficients of the elastic compliance and thermal expansion tensor resulting from transverse matrix cracking. The method includes two thoeries: the dilute theory and the thoery for infinite microcrack densities. The dilute matrix crack density yields analytical expressions for the complementary strain energy, the compliance tensor, the reduction in thermal expansion coefficients and predictions of average strains due to the release of

residual stresses. The dilute theory is valid up to a crack density of about on crack per unit ply thickness, depending on the laminate layup. Laminate with crack densities greater than this must be analyzed using the theory for infinite microcrack densities. Together the two theories give reliable results for thermoelastic properties over the whole range of crack densities in cross-ply and angly-ply glass fiber reinforced epoxy laminates.

Bowles [16] quantitatively related the changes in the coefficient of thermal expansion of graphite/epoxy composite laminates with the number of microcracks. A finite element analysis was used to predict the effect of transverse microcracks on the coefficient of thermal expansion in the 0° direction in cross-ply and quasi-isotropic laminates. He found that the presence of microcracks reduced the effective stiffness of the transverse plies. This caused the laminate thermal response to behave like that of a unidirectional laminate. The change in the 0° CTE depended on lamina material properties, the microcrack density, laminate configuration, and the stacking sequence.

EXPERIMENTAL PROGRAM

Materials

The results presented in this paper are based on experiments and observations made on four polyimide material systems sythesized in the Composite and Polymers Branch (CPB) at NASA Langley Research Center. The material systems include IM7/LaRC™-IAX, IM7/LaRC™-IAX2, IM7/LaRC™-8515 (5.5%), and IM7/LaRC™-PETI-5. The LaRC™-IAX, LaRC™-IAX2, LaRC™-8515 (5.5%) and LaRC™-PETI-5 resins were provided by IMITEC of Schenectady, New York. The fibers were 12k unsized IM7 carbon fibers supplied by Hercules.

LaRC™-IAX and LaRC™-IAX2 are matrix resins based on their predecessor LaRC™-IA (Langley Research Center-Improved Adhesive) [37,38]. LaRC™-IA is prepared from oxydiphthalic anhydride (ODPA) and 3,4'-oxydianiline (ODA) in *N*-methylpyrrolidone (NMP) as a 30% w/w solids solution [37,38]. The backbone of the LaRC™-IA polymers was altered by substituting the 3,4'-ODA with 1,4-phenylenediamine (*p*-PDA) at a 10% level to improve the solvent resistance. This new material was designated LaRC™-IAX [37,38]. In the case of LaRC™-IAX2, 20% of the ODPA in

LaRC™-IA was replaced with 3,3',4,4'-benzophenonetetracarboxyl dianhydride (BTDA) to again improve solvent resistance [37,38]. These alterations in the LaRC™-IA polymers produced stiffer backbones, better mechanical properties and higher Tg's. LaRC™-8515 (5.5%) (Langley Research Center - 8515) is prepared from 3,3',4,4'-biphenyltetracarboxylic dianhydride (BPDA) and a ratio of 85:15 of 3,4'-oxydianiline (3,4'-ODA) and 1,3-bis(3-aminophenoxy)benzene (APB) [39,40]. The 5.5% refers to the stoichiometric offset of the polyimide [39,40]. The LaRC™-8515 material referred to herein corresponds to the 5.5% form. LaRC™-PETI-5 (Langley Research Center - Phenylethynyl Terminated Imide Oligomers) is based on BPDA and 85/15 mole percent ratio of 3,4'-ODA/APB and has phenylethynyl endcappers [41-45]. The phenylethynyl endcappers provide the material with more chemical and thermal stability [41-45]. LaRC™-IAX, LaRC™-IAX2 and LaRC™-8515 are thermoplastic polyimides. LaRC™-PETI-5 is a lightly-crosslinked thermoset polyimide [41-45]. Figure 2.2 illustrates the chemical structures of the polyimides.

Specimen Preparation

The NASA LaRC Multipurpose Prepreg Machine was used to make solution-coated prepreg tape for each material. The solution prepreg was then hand laid in the desired orientations in 6" square molds and processed into flat panels by press molding. The materials were processed using the cure cycles in Figure 2.3. The resultant composite panels were ultrasonically inspected and showed good consolidation.

A diamond saw, polisher, and microscope were used during the specimen preparation process. A K.O. Lee water cooled diamond saw was used to cut the panels into specimens. The specimens were polished on an Ecomet 4 variable speed grinder-polisher with an Automet 2 power head. Four steps were involved in the polishing process. Table 2.1 describes the polishing process. An Olympus BH-2 optical microscope was used to examine the specimens.

Three different layups were used in this study. $[0_2/90_6]$, $[0/90/0_2/90_2/0_2/90_2]_s$ and $[90_8]$ panels were prepared for each material. The $[0_2/90_6]$ panels were used as prepared. The $[0/90/0_2/90_2/0_2/90_2]_s$ panels were cut into 25.4 mm by 25.4 mm specimens. The specimens were allowed to dry at room temperature and humidity for 24 hours. One edge parallel to the 0° direction of each specimen was polished. After polishing, the specimens

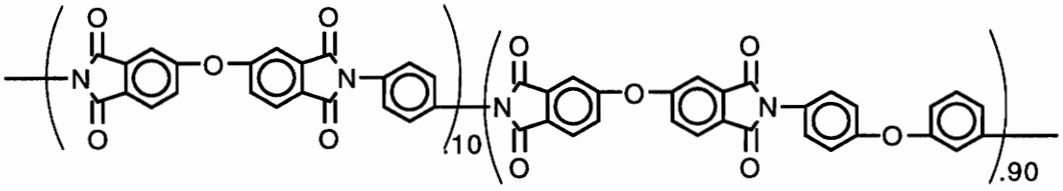

2.2a. Mer structure of LaRC™-IAX

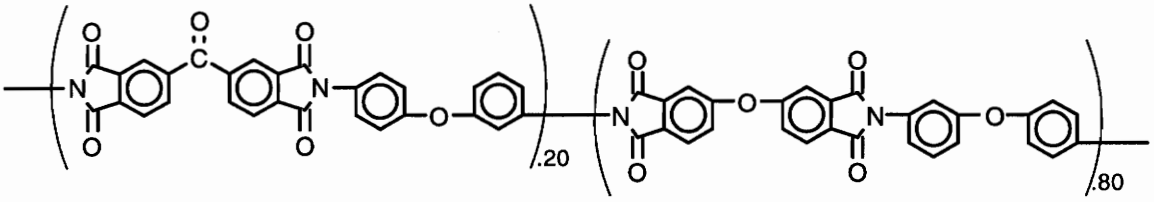

2.2b. Mer structure of LaRC™-IAX2

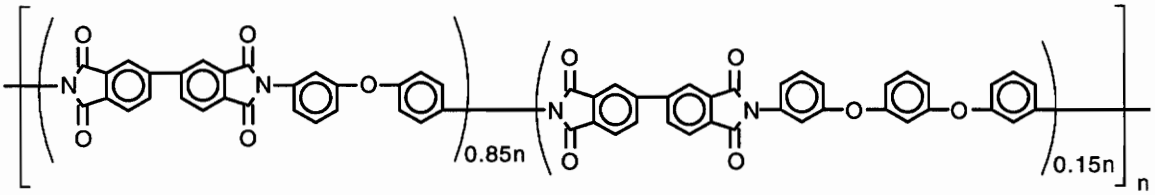

2.2c. Mer structure of LaRC™-8515

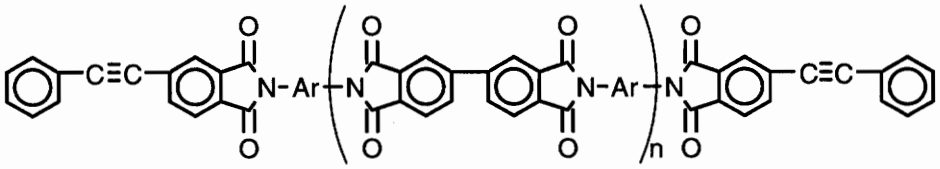

2.2d. Mer structure of LaRC™-PETI5

Figure 2.2. Chemical structures of LaRC™ materials.

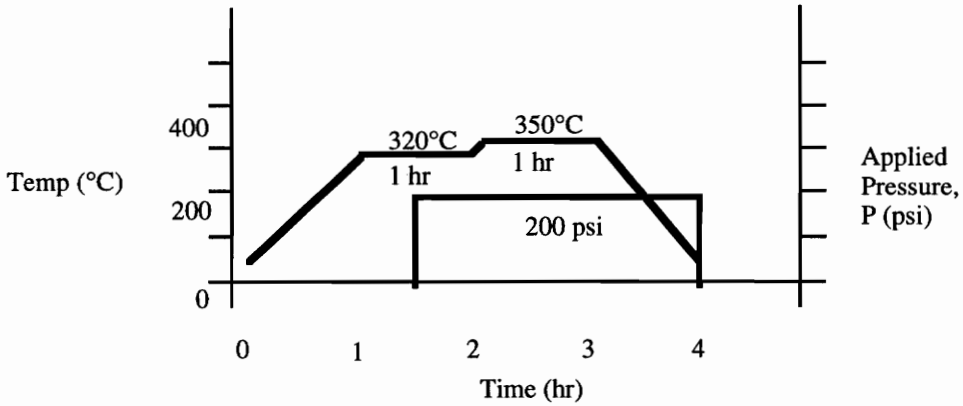

2.3a. LaRC™-IAX and LaRC™-IAX2 cure cycle.

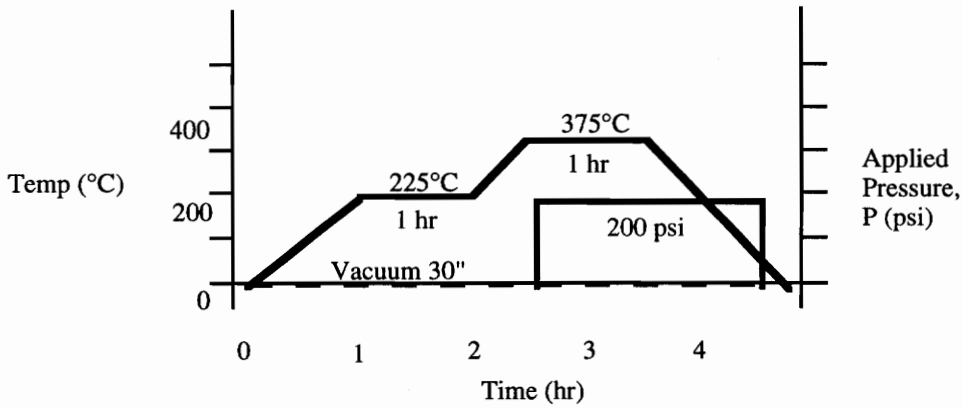

2.3b. LaRC™-8515 cure cycle.

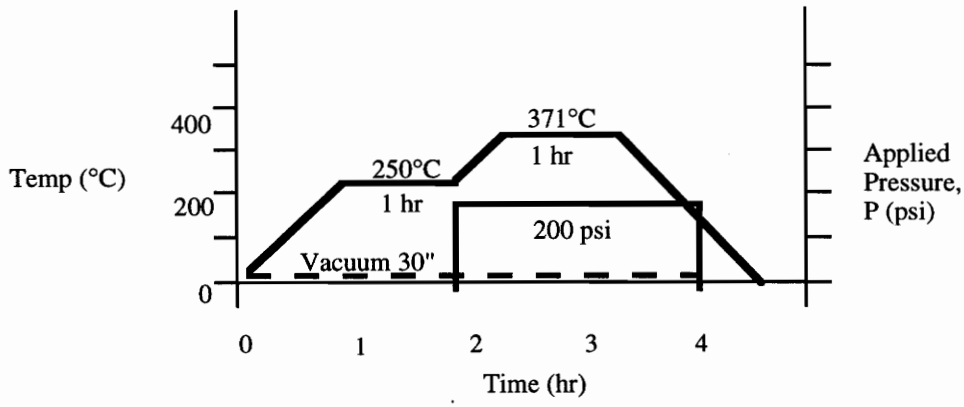

2.3c. LaRC™-PETI5 cure cycle

Figure 2.3. Cure cycles for LaRC™ materials.

Table 2.1. Polishing process used to polish composite specimens.

Steps	Time (min)	Force (lbs)	Polishing surface	Fluid	Direction	Speed (rpm)
1	1	25	320 grit sandpaper	water	CW***	120
2	3	25	#6 tin platen	15 micron*	CCW***	60
3	3	25	#10 ceramic platen	6 micron*	CCW***	60
4	4	50	Texmet	3 micron**	CW***	120

* diamond slurry

** alumina suspension

*** CW - clockwise; CCW - counterclockwise

were examined for microcracking. The $[90_8]$ panels were cut into 50.8 mm by 12.7 mm by 1.1 mm transverse (90°) flexure specimens. The specimens were allowed to dry at room temperature and humidity for 24 hours. The specimen configurations used in this research are illustrated in Figure 2.4. The curved $[0_2/90_6]$ panels were chosen so that the change in curvature could be monitored as the panels were heated in order to determine the stress-free temperature of each panel corresponding to zero curvature. The cross-ply orientation of the $[0/90/0_2/90_2/0_2/90_2]_s$ layup was chosen because the layup provided three stressed transverse ply groups each having a different thickness. The layup contained a 4 ply transverse group, a pair of 2 ply transverse groups and a pair of single ply transverse groups.
This layup allowed us to investigate the effects of residual thermal ply stresses and ply group thickness on matrix crack formation. The $[90_8]$ laminates were selected for use in flexure tests. Transverse flexure specimens were used to determine solvent effects on the matrix material.

Test Procedures

Stress-Free Temperature (SFT) Tests

The $[0_2/90_6]$ panels were used to determine the SFT of each material. A panel was placed in a Blue M Stabil-Therm Gravity Oven. The panel was heated at approximately 3°C/min and the height of the arc was monitored with a DCDT. The experimental apparatus is shown in Figure 2.5. The panel height versus temperature was plotted for each material (Figure 2.6). A linear curve was fitted to the data and the SFT was calculated. The temperature of the flat plate was taken as the SFT. Table 2.2 lists the materials, the stress-free temperatures, and the matrix resin glass transition temperatures, T_g, which were determined by DSC analysis. As expected, the stress-free temperatures of the IAX and IAX2 panels closely matched the glass transition temperatures of the respective matrix resins [46]. On the other hand, the stress-free temperatures of the 8515 and PETI-5 panels were approximately 50°C higher than the glass transition temperatures of the matrix resins. This difference may be a result of thermally induced crystallinity in the matrix resins during processing which would increase both the stress-free temperatures and the glass transition temperatures [39,43].

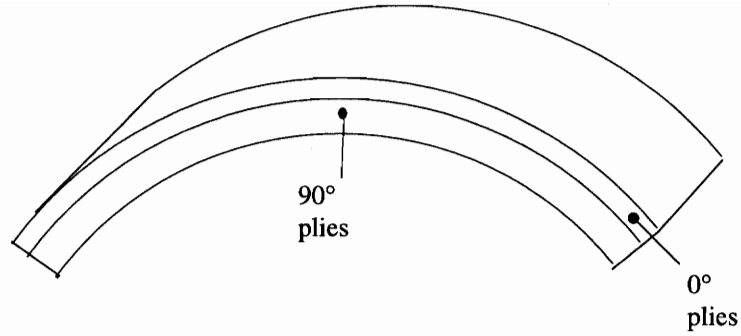

$[0_2/90_6]$ test panel

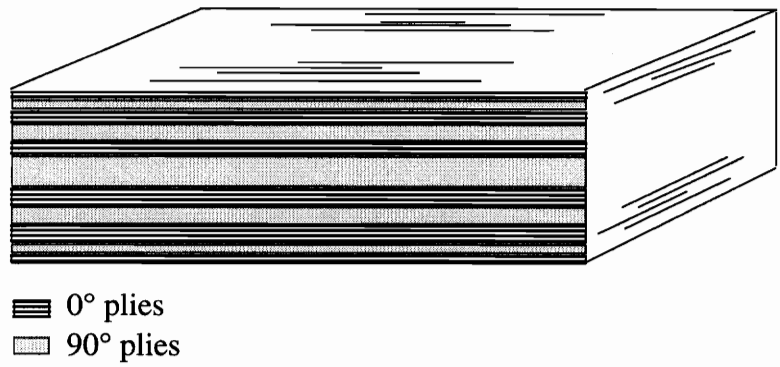

$[0/90/0_2/90_2/0_2/90_2]_s$ test specimen

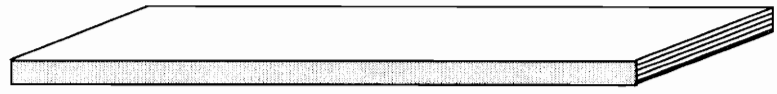

$[90_8]$ specimen

Figure 2.4. Illustration of composite test specimen designs.

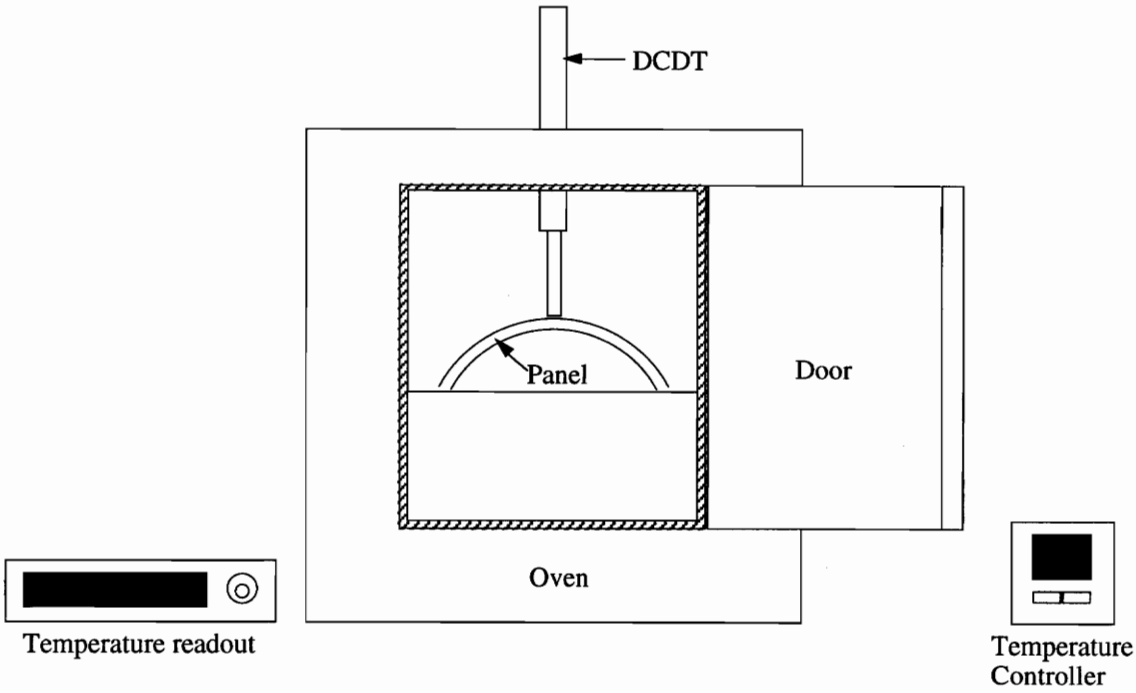

Figure 2.5. Experimental apparatus used to determine the stress free temperatures.

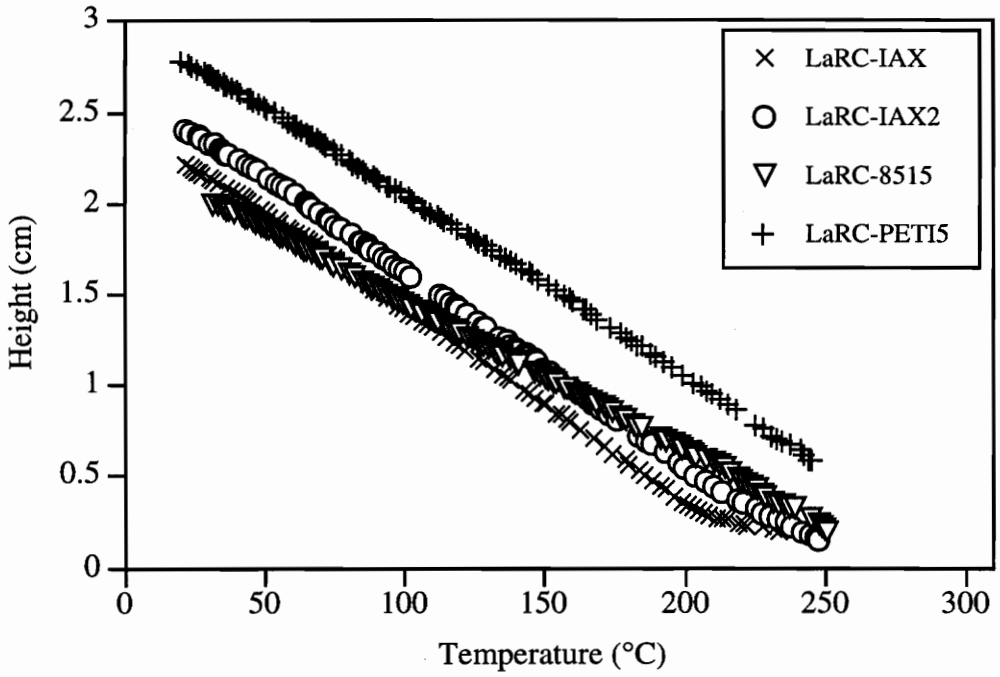

Figure 2.6. Change in the panel height plotted against temperature for $[0_2/90_6]$ laminates.

Table 2.2. Stress free and glass transition temperatures of materials used.

MATERIALS	SFT (°C)	T_g (°C)
LaRC™-IAX	237	246
LaRC™-IAX2	255	239
LaRC™-8515	289	240
LaRC™-PETI5	306	252

Immersion Tests

The $[0/90/0_2/90_2/0_2/90_2]_s$ specimens were used in the immersion tests. The polished specimens were immersed in seven solvents anticipated in various cleaning fluids, deicing fluids, brake fluids, and fuels which are likely to be used with advanced aircraft. The solvents were runway deicer, aircraft deicer, JP5 (jet fuel), diglyme (adhesion promoter), MEK (paint stripper), acetone (degreaser), and Hyjet IV (hydraulic fluid). Two laboratory solvents were also used because of their availability. These were toluene and TCE 1,1,1. The specimens were immersed in the solvents for a total of 96 hours. During the 96 hours, the specimens were removed from the solvents at specific time intervals and were allowed to dry at room temperature and humidity. Upon drying, the polished edges of the specimens were examined for solvent induced microcracking under the microscope. The crack densities was recorded for each of the three different transverse ply groups at each time interval. After recording the crack densities, the specimens were placed back into the solvents. A photomicrograph of typical solvent-induced microcracking is shown in Figure 2.7.

Transverse Flexure Tests

Transverse flexure tests were performed on the $[0_8]$ specimens. Mechanical tests were performed on a Sintec model 2W screw-driven machine. There were five transverse flexure test methods involved in this study. A three-point bend fixture and a solvent bath were designed to meet the needs of the five different methods. A schematic of the fixture and the bath are in Figure 2.8. The five test methods were solvent drop (SD), solvent vapor (SV), solvent soak (SS), solvent soak-dry (SSD), and solvent soak-wet (SSW).

Solvent drop (SD)

A specimen was placed on the fixture and a glass dropper was used to drop 2 to 4 drops of solvent onto the center of the specimen. The specimen was then immediately loaded to failure. A representative five specimens of each material were tested per solvent. The solvents used in this test were runway deicer, aircraft deicer, JP-5, diglyme, MEK, acetone, toluene, TCE 1,1,1, and Hyjet IV.

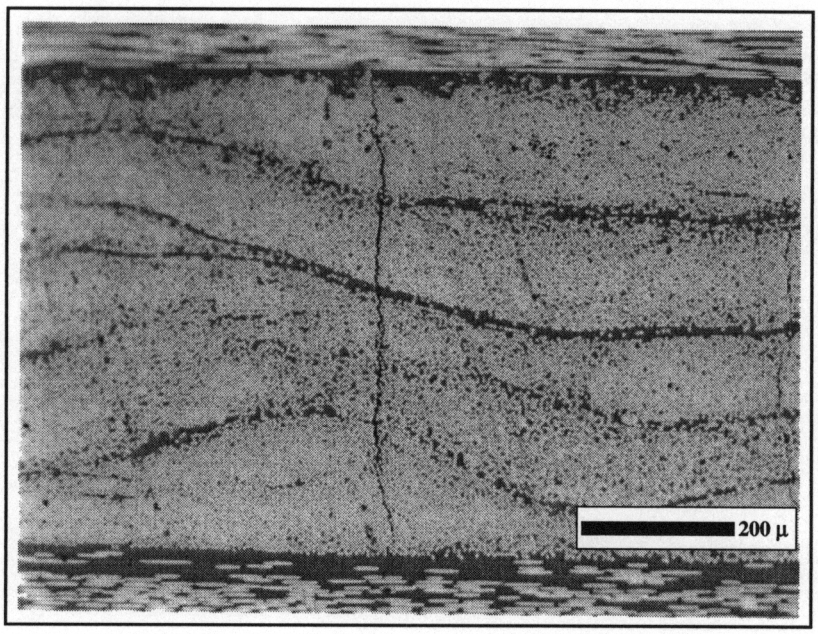

Figure 2.7. Photomicrograph of a typical solvent-induced microcrack.

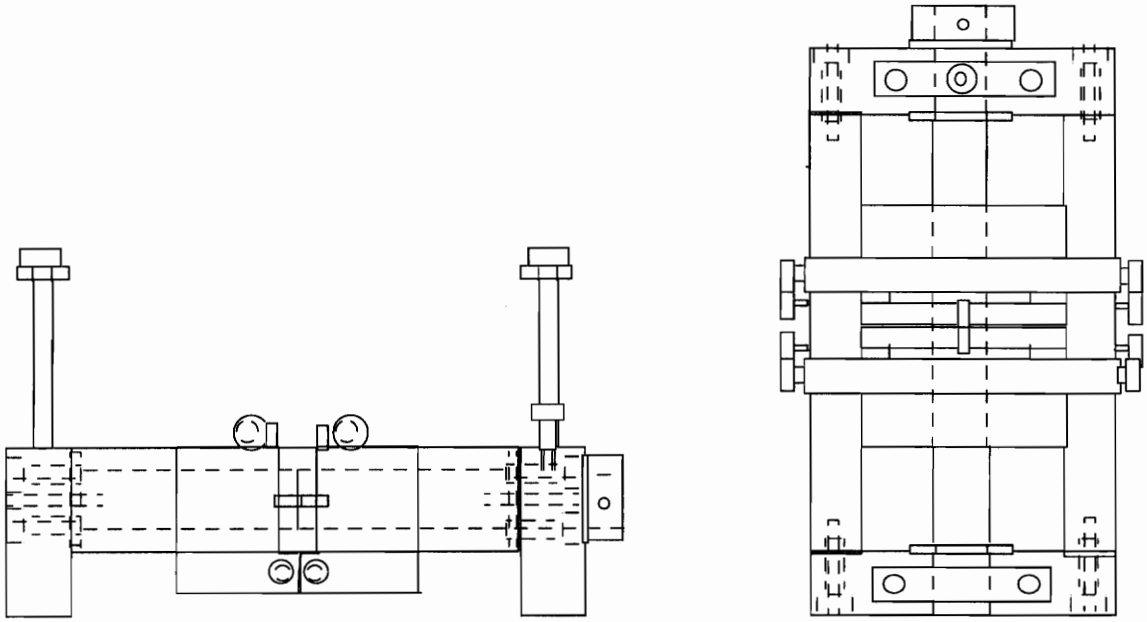

Three-point bend fixture

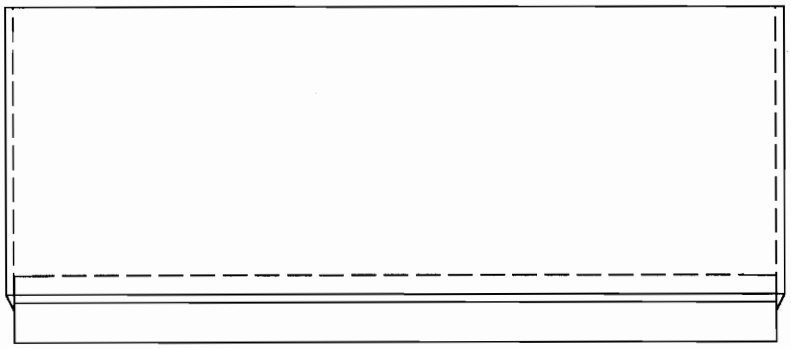

Solvent bath

Figure 2.8. Schematic of three-point bend fixture and solvent bath.

Solvent vapor (SV)

The fixture was placed in the solvent bath. Solvent was poured into the bath to a depth of approximately 6 mm. A specimen was placed on the fixture and mylar was placed over both the fixture and the bath in order to capture the solvent vapor. After approximately 1 minute, the specimen was loaded to failure. A representative five specimens of each material were tested per solvent. The solvents used in this test were runway deicer, aircraft deicer, JP-5, diglyme, MEK, acetone, toluene, TCE 1,1,1, and Hyjet IV.

Solvent Soak (SS)

The fixture was placed in the solvent bath. Solvent was poured into the bath until the fixture was submerged. A specimen was placed on the fixture and Mylar™ was placed over both the fixture and the bath to prevent the solvent from evaporating. The specimen was then immediately loaded to failure. A representative five specimens of each material were tested per solvent. The solvents used in this test were runway deicer, JP-5, diglyme, MEK, acetone, toluene, TCE 1,1,1, and Hyjet IV.

Solvent soak-wet (SSW)

IAX, IAX2, and PETI-5 specimens were soaked in diglyme, MEK, and acetone for two weeks. 8515 specimens were soaked in dilgyme and MEK for two weeks. The specimens were removed from the solvents and placed directly onto the fixture. They were immediately loaded to failure. Four to six specimens of each material were tested per solvent.

Solvent soak-dry (SSD)

IAX, IAX2, and PETI-5 specimens were soaked in diglyme, MEK, and acetone for two weeks. 8515 specimens were soaked in dilgyme and MEK for two weeks. The specimens were then removed from the solvents and allowed to dry at room temperature

and humidity for two weeks. The dry specimens were placed on the fixture and loaded to failure. Four to six specimens of each material were tested per solvent.

ANALYSIS

Classical Laminate Theory (CLT) analysis

The ply stresses in the $[0/90/0_2/90_2/0_2/90_2]_s$ specimens resulting solely from thermal loads during processing were calculated using a CLT code written in MathCAD 3.0. Appendix A contains a hardcopy of the program along with a user's guide. The program inputs include the number of plies, laminate layup, material properties of each lamina, ply thicknesses, resultant force and moment vectors, coefficients of thermal expansion, SFT, and moisture coefficients. The outputs include the A, B, and D matrices, laminate properties, midplane strains and curvatures, ply strains in the x-y and 1-2 coordinate systems, residual ply stresses in the x-y and 1-2 coordinate systems, and interlaminar stresses. The CLT inputs for the materials in the present study are listed in Table 2.3.

All of the necessary inputs were known except the stress-free temperatures and the coefficients of thermal expansion. The stress-free temperatures were experimentally determined as described in the test procedures section using the $[0_2/90_6]$ layups. A mechanics of composites approach was used to calculate the coefficients of thermal expansion. The CTE's were calculated using the $[0_2/90_6]$ laminates and then applied to the $[0/90/0_2/90_2/0_2/90_2]_s$ panels [47]. The thermal forces and moments equations were considered. The thermal forces equations are

$$\begin{Bmatrix} N_x^T \\ N_y^T \\ N_{xy}^T \end{Bmatrix} = \int \begin{bmatrix} \overline{Q}_{11} & \overline{Q}_{12} & \overline{Q}_{16} \\ \overline{Q}_{12} & \overline{Q}_{22} & \overline{Q}_{26} \\ \overline{Q}_{16} & \overline{Q}_{26} & \overline{Q}_{66} \end{bmatrix}_k \begin{Bmatrix} \alpha_x \\ \alpha_y \\ \alpha_{xy} \end{Bmatrix}_k \Delta T dz \qquad (1)$$

and

Table 2.3. Material properties used in the CLT analysis.

MATERIAL TYPE		ENVIRONMENT	ELASTIC MODULI				CTE			COMMENTS
Fiber Type	Matrix Type	Temp (°C)	E_{11} (GPa)	E_{22} (GPa)	ν_{12}	G_{12} (GPa)	α_{11}	α_{22}	SFT (°C)	
Carbon IM-7 unsized	LaRC™-IAX	22.2	193.8	8.4	0.33*	4.4*	0.0*	26.7×10^{-6}	237.5	Cure temperature = 350 °C Tg = 246 °C
Carbon IM-7 unsized	LaRC™-IAX2	22.2	208.5	10.0	0.33*	4.4*	0.0*	23.1×10^{-6}	255.4	Cure temperature = 350 °C Tg = 239 °C
Carbon IM-7 unsized	LaRC™-8515	22.2	199.8	10.0	0.33*	4.4*	0.0*	20.3×10^{-6}	289.2	Cure temperature = 375 °C Tg = 240 °C
Carbon IM-7 unsized	LaRC™-PETI5	22.2	187.9	8.3	0.33*	4.4*	0.0*	15×10^{-6}	306.9	Cure temperature = 371 °C Tg = 252 °C

* They values were taken as estimates for the composites being analyzed [22].

$$\begin{Bmatrix} N_x^T \\ N_y^T \\ N_{xy}^T \end{Bmatrix} = \begin{bmatrix} A_{11} & A_{12} & A_{16} \\ A_{12} & A_{22} & A_{26} \\ A_{16} & A_{26} & A_{66} \end{bmatrix} \begin{Bmatrix} \varepsilon_x^o \\ \varepsilon_y^o \\ \gamma_{xy}^o \end{Bmatrix} + \begin{bmatrix} B_{11} & B_{12} & B_{16} \\ B_{12} & B_{22} & B_{26} \\ B_{16} & B_{26} & B_{66} \end{bmatrix} \begin{Bmatrix} \kappa_x^o \\ \kappa_y^o \\ \kappa_{xy}^o \end{Bmatrix} \tag{2}$$

where N_i^T represents the thermal forces at room temperature,

$\overline{Q}_{ij}$ are the transformed reduced stiffnesses,

α represents the coefficients of thermal expansion,

ΔT is the room temperature minus the SFT,

A_{ij} are the extensional stiffnesses,

B_{ij} are the coupling stiffnesses,

ε are the strains,

and κ are the curvatures.

The thermal moments equations are

$$\begin{Bmatrix} M_x^T \\ M_y^T \\ M_{xy}^T \end{Bmatrix} = \int \begin{bmatrix} \overline{Q}_{11} & \overline{Q}_{12} & \overline{Q}_{16} \\ \overline{Q}_{12} & \overline{Q}_{22} & \overline{Q}_{26} \\ \overline{Q}_{16} & \overline{Q}_{26} & \overline{Q}_{66} \end{bmatrix}_k \begin{Bmatrix} \alpha_x \\ \alpha_y \\ \alpha_{xy} \end{Bmatrix}_k \Delta T z dz \tag{3}$$

and

$$\begin{Bmatrix} M_x^T \\ M_y^T \\ M_{xy}^T \end{Bmatrix} = \begin{bmatrix} A_{11} & A_{12} & A_{16} \\ A_{12} & A_{22} & A_{26} \\ A_{16} & A_{26} & A_{66} \end{bmatrix} \begin{Bmatrix} \varepsilon_x^o \\ \varepsilon_y^o \\ \gamma_{xy}^o \end{Bmatrix} + \begin{bmatrix} D_{11} & D_{12} & D_{16} \\ D_{12} & D_{22} & D_{26} \\ D_{16} & D_{26} & D_{66} \end{bmatrix} \begin{Bmatrix} \kappa_x^o \\ \kappa_y^o \\ \kappa_{xy}^o \end{Bmatrix} \tag{4}$$

where M_i^T are the thermal moments,

z is the ply thickness,

and D_{ij} are the bending stiffnesses.

In equations (1) through (4), the A, B, and D matrices are known from the CLT analysis. Assumptions are made that the shear thermal force, the shear thermal moment, the shear strain, the shear curvature, and the fiber direction α are zero. Expanding equations (1) through (4) for the $[0_2/90_6]$ laminates and substituting the zero terms yields four equations and four unknowns:

$$A_{11}\varepsilon_x^o + A_{12}\varepsilon_y^o + B_{11}\kappa_x = \begin{bmatrix} \overline{Q}_{12}^1 z_1 + \overline{Q}_{12}^2 z_2 + \overline{Q}_{11}^3 z_3 + \overline{Q}_{11}^4 z_4 + \\ \overline{Q}_{11}^5 z_5 + \overline{Q}_{11}^6 z_6 + \overline{Q}_{11}^7 z_7 + \overline{Q}_{11}^8 z_8 \end{bmatrix} \alpha\Delta T \tag{5}$$

$$A_{12}\varepsilon_x^o + A_{22}\varepsilon_y^o + B_{22}\kappa_y = \begin{bmatrix} \overline{Q}_{22}^1 z_1 + \overline{Q}_{22}^2 z_2 + \overline{Q}_{12}^3 z_3 + \overline{Q}_{12}^4 z_4 + \\ \overline{Q}_{12}^5 z_5 + \overline{Q}_{12}^6 z_6 + \overline{Q}_{12}^7 z_7 + \overline{Q}_{12}^8 z_8 \end{bmatrix} \alpha\Delta T \tag{6}$$

$$B_{12}\varepsilon_x^o + B_{12}\varepsilon_y^o + D_{11}\kappa_x + D_{12}\kappa_y = \begin{bmatrix} \overline{Q}_{12}^1 \frac{z_1^2}{2} + \overline{Q}_{12}^2 \frac{z_2^2}{2} + \overline{Q}_{11}^3 \frac{z_3^2}{2} + \overline{Q}_{11}^4 \frac{z_4^2}{2} + \\ \overline{Q}_{11}^5 \frac{z_5^2}{2} + \overline{Q}_{11}^6 \frac{z_6^2}{2} + \overline{Q}_{11}^7 \frac{z_7^2}{2} + \overline{Q}_{11}^8 \frac{z_8^2}{2} \end{bmatrix} \alpha\Delta T \tag{7}$$

$$B_{22}\varepsilon_y^o + D_{12}\kappa_x + D_{22}\kappa_y = \begin{bmatrix} \overline{Q}_{22}^1 \frac{z_1^2}{2} + \overline{Q}_{22}^2 \frac{z_2^2}{2} + \overline{Q}_{12}^3 \frac{z_3^2}{2} + \overline{Q}_{12}^4 \frac{z_4^2}{2} + \\ \overline{Q}_{12}^5 \frac{z_5^2}{2} + \overline{Q}_{12}^6 \frac{z_6^2}{2} + \overline{Q}_{12}^7 \frac{z_7^2}{2} + \overline{Q}_{12}^8 \frac{z_8^2}{2} \end{bmatrix} \alpha\Delta T \tag{8}$$

The unknowns are ε_x^o, ε_y^o, κ_y, and α. The curvature, κ_x, of the $[0_2/90_6]$ panels was determined from the maximum arc height:

$$\rho = \frac{L^2}{8 * h} \tag{9}$$

where L is the length of the curved panel and h is the maximum height of the arc. Equation (9) is an approximation from a Taylor Series expansion of the following equation:

$$\cos\left(\frac{\theta}{2}\right) = 1 - \frac{h}{\rho} \qquad (10)$$

The maximum heights and corresponding curvatures for each material are listed in Table 2.4. The thermal expanison coefficient of each material was determined by solving equations (4) through (8). The α values are included in Table 2.4.

Nine layups were analyzed using CLT. The layups included the 20 ply research panel, three miscellaneous panel designs, and five Boeing aircraft panels [48]. The layups are given in Table 2.5. The maximum transverse tensile residual thermal stresses of the miscellaneous and Boeing panels were compared to that of the 20 ply research panel. The comparison showed a maximum difference of 8.5%; thus, the stresses in the 20 ply composite specimens used in this study are comparable to the stresses found in composite panels being considered for use in the air and space industries. Figure 2.9 compares the maximum transverse tensile residual thermal stresses in the LaRC™-8515 analyzed panels. Table 2.6 summarizes the CLT stress analysis.

Variational mechanics analysis

A two-dimensional, variational mechanics analysis using an energy release rate criterion was used to determine G_m, the energy release rate associated with the formation of a complete, through-the-width microcrack [2,3,9,49,50]. According to the energy failure criterion, the next microcrack will form when the energy release associated with the formation of that microcrack reaches or exceeds the critical energy release rate, G_{mc}. G_{mc} is also referred to as the microcracking fracture toughess of the material system. Because microcracks are matrix cracks confined to one ply or to a ply group, G_{mc} can also be interpretted as the intralaminar fracture toughness. The photomicrograph shown in Figure 2.7 is representative of the intralaminar cracks in this study. According to the variational mechanics analysis for microcrack initiation, G_m is [2,3,9,49,50]:

$$G_m = \sigma_{xo}^{(1)^2} t_1 \sqrt{C_1(C_4 - C_2 + 2\sqrt{C_1 C_3})} \qquad (11)$$

Table 2.4. The maximum height and curvature of the $[0_2/90_6]$ tested panels.

Material	height, h (mm)	curvature, ρ (mm)	CTE, α (°C^{-1})
LaRC™-IAX	22	132	28×10^{-6}
LaRC™-IAX2	24	121	23×10^{-6}
LaRC™-8515	20	145	20×10^{-6}
LaRC™-PETI5	28	104	15×10^{-6}

Table 2.5. CLT analysis panel layups.

	Layups
Research panel	20 ply: $[0/90/0_2/90_2/0_2/90_2]_s$
Miscellaneous panels	$[0/0/45/-45]_s$
	$[0/90/45/-45]_s$
	$[0/60/-60]_s$
Boeing panels [48]	Wing: $[\pm45/0_2/90/\pm45/0_3]_s$
	Fuselage 1: $[45/90/-45/45/0/-45]_s$
	Fuselage 2: $[\pm45/90/0/\pm60/\pm30/0/90/\pm30/\pm60/0/90/\pm45]$
	Fuselage 3: $[\pm45/90/0/\pm60/90/\pm60/0/90/\pm45]$
	Fuselage 4: $[\pm45/90/0/\pm60/15/90/-15/\pm60/0/90/\pm45]$

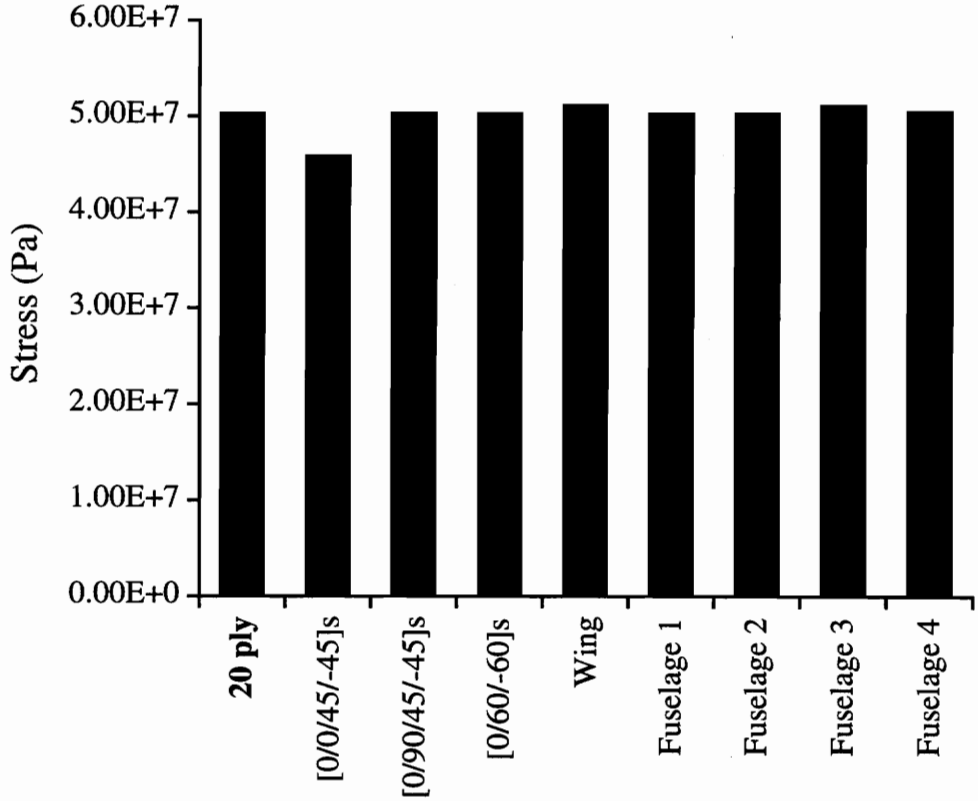

Figure 2.9. Maximum transverse tensile residual thermal stresses in LaRC™-8515 panels.

Table 2.6. Maximum transverse tensile residual thermal stresses determined using CLT analysis.

Layups	IAX	% difference	IAX2	% difference	8515	% difference	PETI-5	% difference
20 ply	**45.05**		**49.68**		**50.08**		**33.05**	
[0/0/45/-45]s	41.63	- 7.6	45.57	- 8.3	45.83	- 8.5	30.51	- 7.7
[0/90/45/-45]s	45.05	0	49.68	0	50.08	0	33.05	0
[0/60/-60]s	45.05	0	49.68	0	50.08	0	33.05	0
Wing	45.65	+ 1.3	50.43	+ 1.5	50.88	+ 1.6	33.50	+ 1.4
Fuselage 1	45.05	0	49.68	0	50.08	0	33.05	0
Fuselage 2	45.15	+ 0.2	49.81	+ 0.3	50.13	+ 0.1	33.12	+ 0.2
Fuselage 3	45.80	+ 1.7	49.05	+ 1.3	51.06	+ 2.0	33.61	+ 1.7
Fuselage 4	45.38	+ 0.7	50.09	+ 0.8	50.51	+ 0.9	33.29	+ 0.7

Note: All stresses are in MPa.

where $\sigma_{xo}^{(1)}$ is the total residual thermal stress due to processing in the x direction in the transverse ply group, t_1 is half the thickness of the transverse ply group, and C_1, C_2, C_3, and C_4 are constants defined as [2,3,9,49,50]:

$$C_1 = \frac{1}{E_{22}} + \frac{1}{\lambda E_{11}} \tag{12}$$

$$C_2 = \frac{\upsilon_{21}}{E_{22}}\left(\lambda + \frac{2}{3}\right) - \frac{\lambda \upsilon_{12}}{3E_{11}} \tag{13}$$

$$C_3 = \frac{\lambda + 1}{60E_{22}}(3\lambda^2 + 12\lambda + 8) \tag{14}$$

$$C_4 = \frac{1}{3}\left(\frac{1}{G_{21}} + \frac{\lambda}{G_{12}}\right) \tag{15}$$

where E_{22}, E_{11}, G_{21}, G_{12}, ν_{21}, and ν_{12} are the transverse and axial Young's moduli, shear moduli, and Poisson's ratio, respectively, and $\lambda = t_2/t_1$, where t_2 is the thickness of each 0° ply. According to modulus data from bending tests, the solvents do not lower the stiffnesses of the materials; therefore, Equations (12) through (14) remain valid. The G_m results for each transverse ply group of each material are summaried in Table 2.7.

G_{mc} measures a materials resistance to microcracking. In this study, it was assumed that $G_{mc} \approx G_{Ic}$. The values of G_{mc} are qualitatively similar to G_{Ic}, the delamination fracture energy, since both microcracks and delamination are primarily mode I crack growth through the matrix. The difference between G_{mc} and G_{Ic} is that G_{mc} is measuring an **intralaminar** crack growth process whereas G_{Ic} is measuring an **interlaminar** process [2,3,9,49,50]. The G_{Ic} values for each material are listed in Table 2.7 [37,38,40,42].

Table 2.7. Material G_m and G_{Ic} values.

Materials	G_m (J/m^2) 4 ply	2 ply	1 ply	G_{Ic} (J/m^2)
LaRC™-IAX	96	54	33	≈ 1820
LaRC™-IAX2	103	58	35	≈ 1820
LaRC™-8515	93	52	32	≈ 438
LaRC™-PETI-5	51	28	17	≈ 4790

RESULTS AND DISCUSSION

Immersion test results

The crack densities in the center transverse ply group (4 plies) of each material are shown in Figures 2.10 through 2.13. Observations were made over a gage length of 25.4 mm. In this study, a crack is counted if its spans a length one-half or greater than the ply group thickness. The results show that matrix microcracks were initially observed in the transverse plies of the specimens after only 1 minute of solvent exposure; thus, solvent induced microcracking can be a very rapid irreversible process. The material with the largest initial microcracking response was IAX. Observations showed that the crack density in the four ply transverse group of the IAX digylme specimen following a one minute soak was 22 cracks/cm. As seen in Figure 2.10, the majority of the damage caused by diglyme occured in the first minute of exposure. Toluene and acetone are two additional solvents which caused the maximum extent of their damage within the first minute. MEK produced only 3 cracks/cm during the first minute but after one hour the crack density of the MEK specimen was equivalent to that of the diglyme specimen. With increasing exposure time, Hyjet IV, TCE, 1,1,1, and runway deicer induced microcracking. It should be noted that the crack densities produced by the solvents in the IAX exposed specimens were within 8% of the maximum crack densities after an exposure time of only 1 hour. The crack densities of the affected IAX specimens are considered high [49]. However, when compared to the crack densities of the other tested materials, IAX has a low crack density (Figures 2.10 through 2.13). The size of the matrix cracks in each of the transverse groupings of the IAX solvent specimens were very distinct. All of the matrix cracks were clear and through the thickness. A photomicrograph of the cracks in each transverse ply grouping of an IAX specimen is shown in Figure 2.14. This definite crack size and rapid development of the majority of the cracks, which occurred during the first minute of solvent exposure, indicated that the solvents quickly travelled into the IAX material along growing cracks. According to the immersion tests, the solvents which affect IAX are runway deicer, diglyme, MEK, acetone, toluene, TCE 1,1,1, and Hyjet IV. The worst of these solvents would be diglyme, MEK, and acetone.

Observations showed that IAX2 had a very high crack density after 96 hours of exposure (Figure 2.11). Matrix cracking in IAX2 began within the first minute of

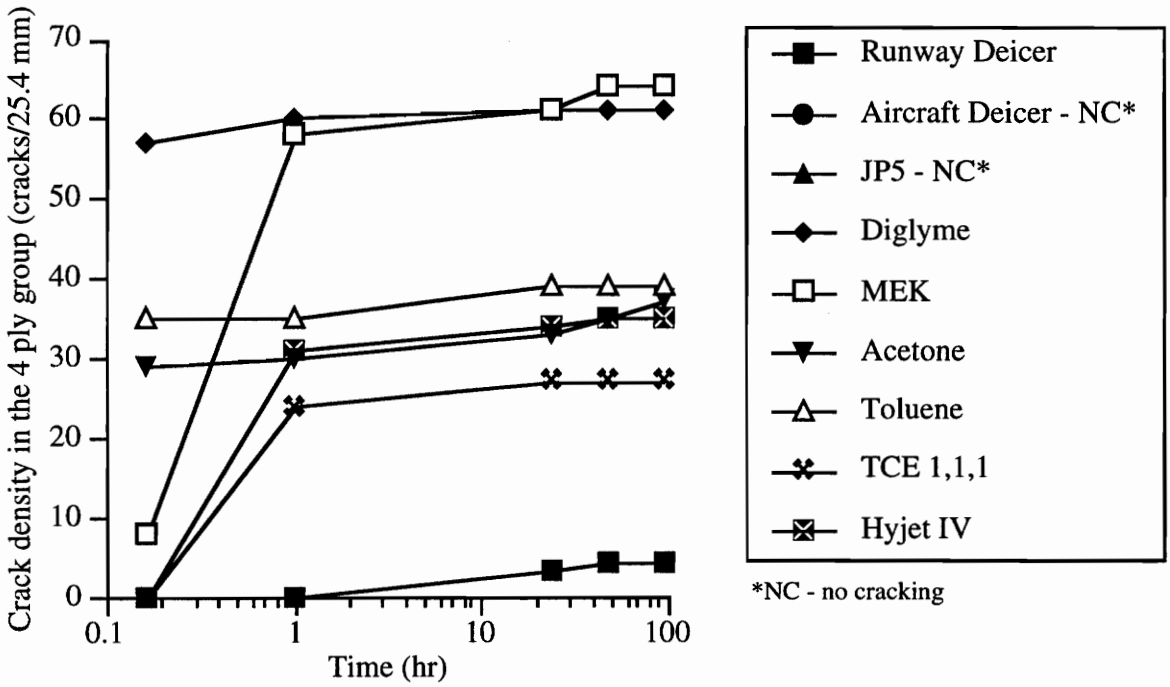

Figure 2.10. Time dependent matrix microcracking in the center transverse 4-ply group of a $[0/90/0_2/90_2/0_2/90_2]_s$ LaRC™-IAX specimen.

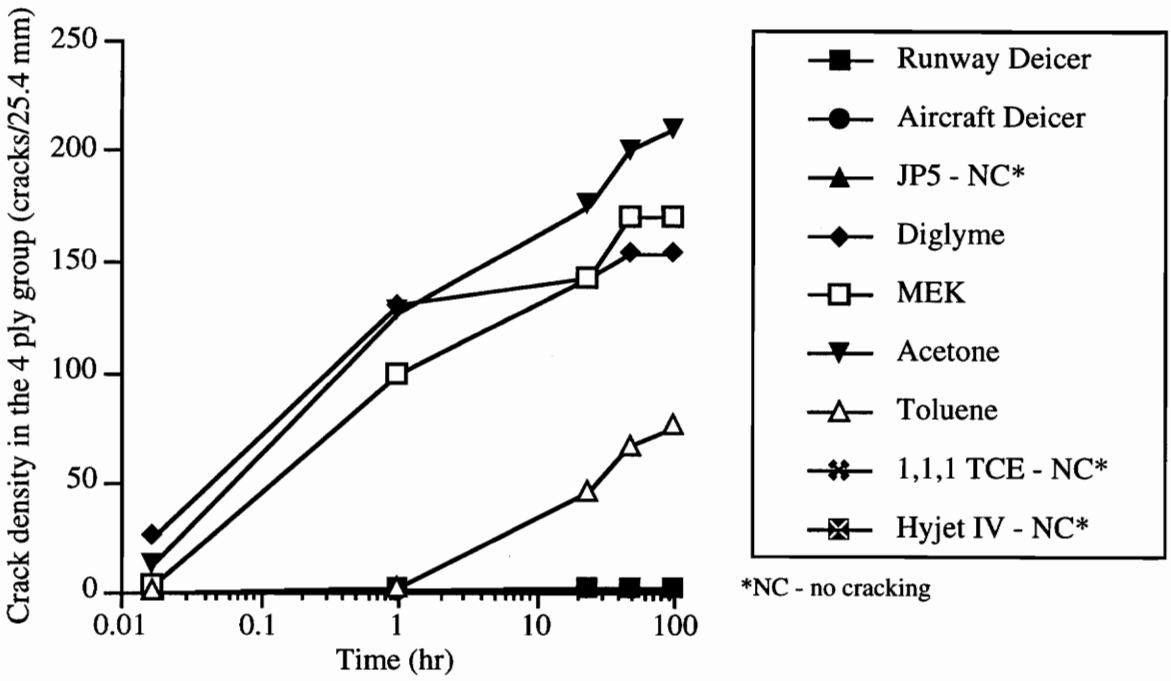

Figure 2.11. Time dependent matrix microcracking in the center transverse 4-ply group of a $[0/90/0_2/90_2/0_2/90_2]_s$ LaRC™-IAX2 specimen.

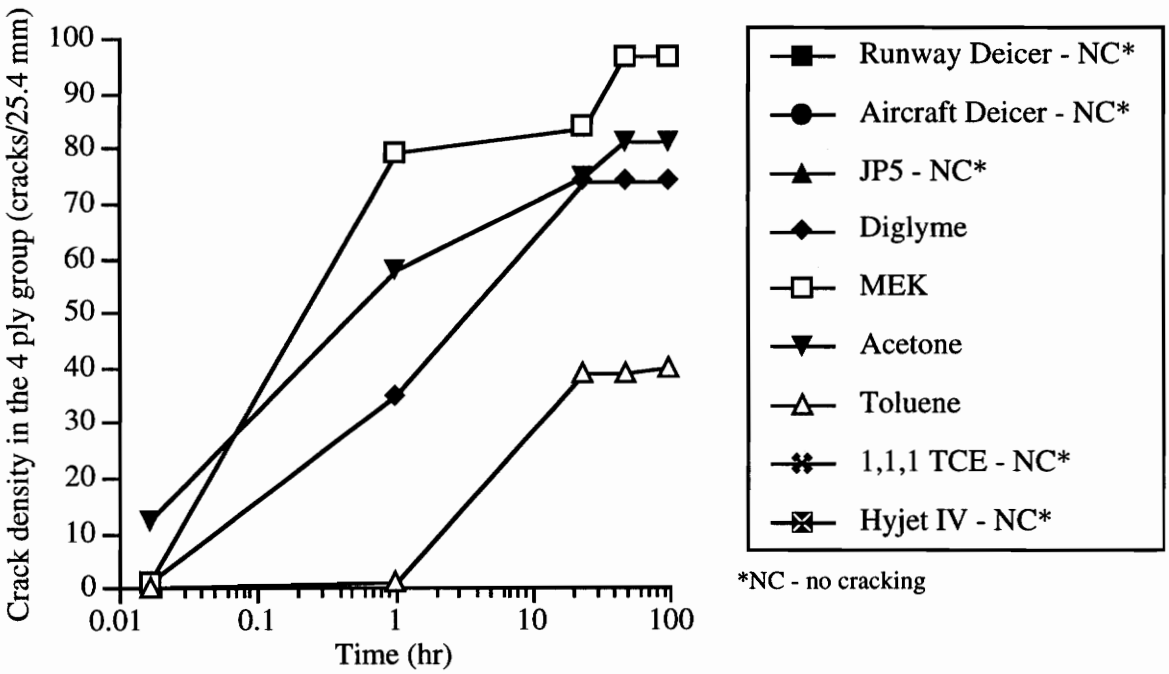

Figure 2.12. Time dependent matrix microcracking in the center transverse 4-ply group of a $[0/90/0_2/90_2/0_2/90_2]_s$ LaRC™-8515 specimen.

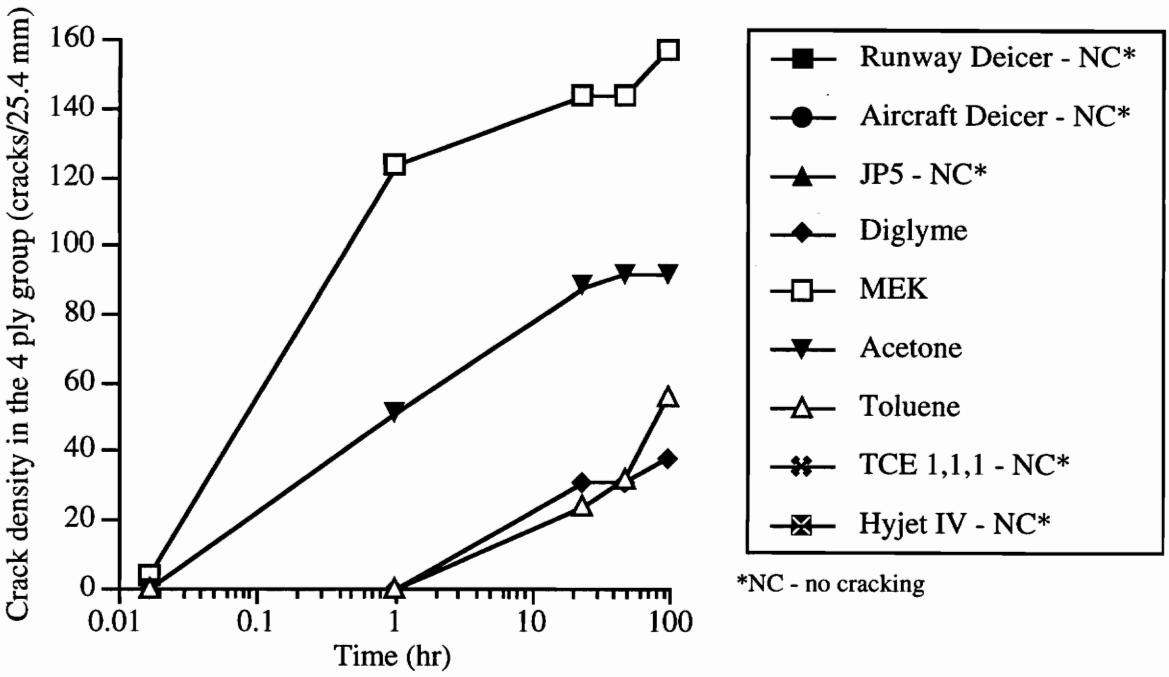

Figure 2.13. Time dependent matrix microcracking in the center transverse 4-ply group of a $[0/90/0_2/90_2/0_2/90_2]_s$ LaRC™-PETI-5 specimen.

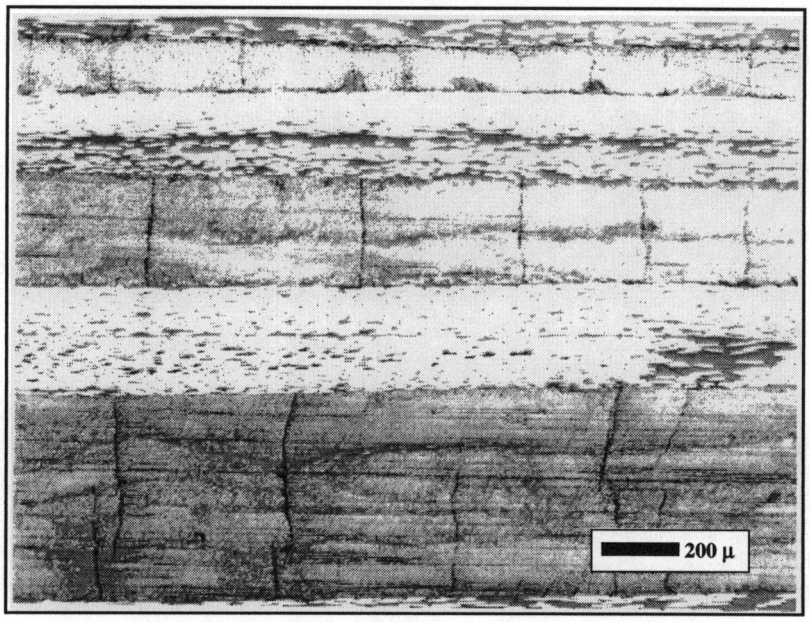

Figure 2.14. Photomicrograph of microcracks in each transverse ply grouping of a $[0/90/0_2/90_2/0_2/90_2]_s$ IAX specimen.

exposure. Diglyme, acetone, and MEK were the first solvents to affect IAX2 with diglyme being the most significant. Toluene, runway deicer, and aircraft deicer began to induce microcracking after 1 hour. Toluene had a significant effect after 96 hours of exposure. Runway deicer and aircraft deicer produced several cracks in each of the transverse ply groups following 96 hours of exposure, but all of the cracks originated from voids. It is possible that the cracks may not have been direct results of the solvents. Exposure to the solvents may have lowered the strength of the material enough to allow the voids to develop cracks. However, this same strength reduction may not have been sufficient to develop a crack in the absence of the voids. In studies involving stress induced microcracking of cross-ply composites, the initial cracks have also been observed to be located at macroscopic flaws [49]. The cracks observed in each of the transverse groups of the diglyme, MEK, acetone, and toluene exposed specimens were very thin, especially in the single ply transverse group. Cracks in the single ply group were very hard to distinguish, even at a magnification of 80X. Very few of the matrix cracks were through-the-thickness and they were very randomly spaced. There were no evident patterns as there are in many of the stress induced microcracking experiments [2,3,9,49]. This type of cracking suggests that this material was more solvent resistant than IAX. Although the crack densities of the IAX2 solvent specimens were much higher than those of the IAX solvent specimens, the cracks in the IAX specimens were larger in width than the cracks in the IAX2 specimens. This suggests that the total surface area created by the cracks in each ply of the IAX2 specimens was small in comparison to that of the IAX specimens. Therefore, the available energy was released at a higher rate in the IAX specimens. When determining the solvent resistance of a material, one must consider both the crack density and the surface area created by the cracks. When taking this into account, IAX is the less solvent resistant of the two materials. A comparison of crack densities in the IAX and IAX2 specimens is shown in Figure 2.15.

The 8515 diglyme, MEK, and acetone exposed specimens developed cracks in each of the three transverse ply groups during the first minute of exposure. The highest crack density was initially seen in the single transverse ply. The cracks in the specimens were very thin and faint. As the exposure time increased, cracks were observed in the toluene exposed specimen. After 24 hours, the appearance of the cracks in the specimens began to take different forms. The microcracks observed in the 4 and 2 transverse ply groups of the diglyme specimen were medium in size. The single transverse ply contained very faint, thin microcracks. The microcracks seen in all of the transverse ply groups of the MEK

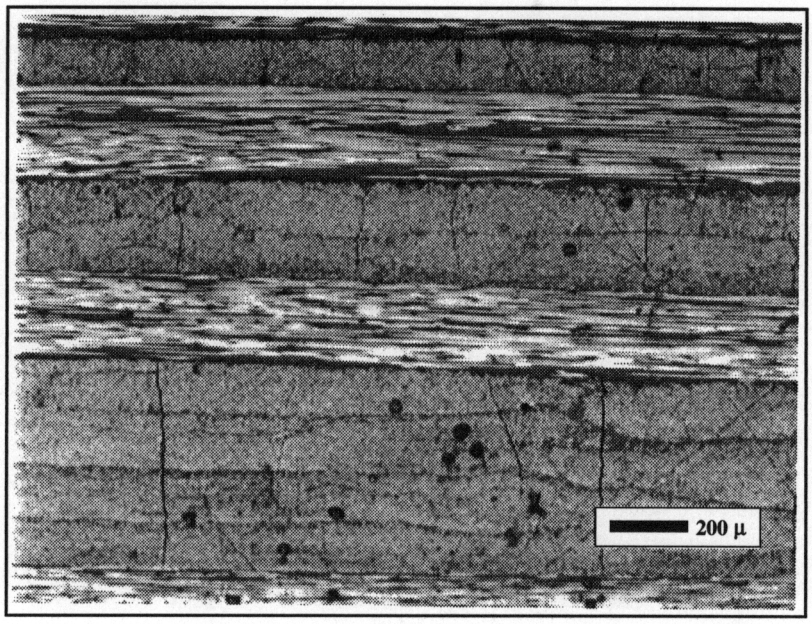

LaRC^{TM}-IAX

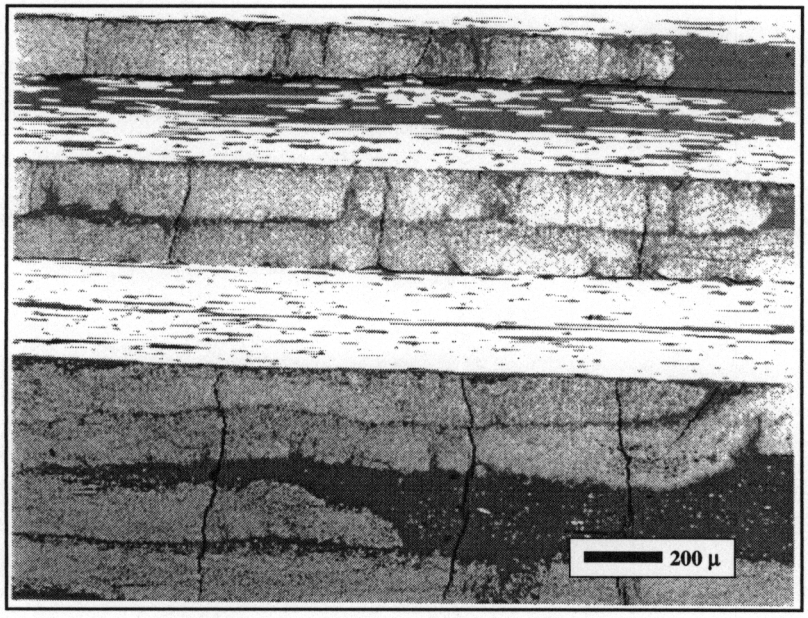

LaRC^{TM}-IAX2

Figure 2.15. Comparison of the crack densities between LaRC^{TM}-IAX and LaRC^{TM}-IAX2.

specimen were very thin. The cracks were notably scattered and very few were through-the-thickness. The microcracks in the acetone and toluene specimens were average in all of the transverse ply groups. Very little change occurred in the appearance of the cracks between 24 hours and 96 hours. However, the size of the cracks in the 4 and 2 ply transverse groups of the MEK specimen increased in width. The cracks remained scattered and did not span the thickness of the plies. As with IAX2, there was no specific cracking pattern. Figures 2.16 through 2.19 contain photomicrographs illustrating microcracking in the 8515 exposed specimens.

During the first minute of exposure, microcracks were observed in the PETI-5 MEK specimen. An insignificant number of cracks were seen in the 4 and 2 ply transverse groups, but there were 31 cracks/cm in the single transverse ply. The cracks were very faint and difficult to detect. With increasing exposure time, observations revealed microcracks in the diglyme, acetone, and toluene specimens. After 48 hours, the cracks in the diglyme, MEK, and toluene specimens were miniscule in size. The cracks in the acetone specimen were more defined and easier to identify. The appearance of the cracks in the diglyme specimen did not change following the full exposure period. The cracks in the MEK specimen developed into more noticeable cracks, however they were still only average in size. The cracks were not completely through-the-thickness either. They were very random. The cracks in the acetone specimen were also very scattered and not fully developed. The faint cracks in the toluene specimen grew into medium cracks in the 4 and 2 ply transverse ply groups. The cracks in the single transverse group remained thin. Again, there are no discernable cracking patterns. The cracking was similar to that observed in the 8515 specimens.

From a stress analysis of the tested specimens, one would expect to see the highest crack density in the thinnest transverse layer, and as the thickness of the transverse layers increased, the crack density would decrease. One would also expect the stress required to initiate a microcrack to increase as the thickness of the transverse plies decreased; thus, matrix cracks would form first in the transverse plies having the greatest thickness. This increase in stress may be attributed to a size affect. Statistically, thinner transverse ply groups have fewer flaws and therefore should have a higher effective strength [9]. Experimental observations indicated that the formation of matrix cracks originated in the 4 ply transverse group, which has the largest thickness of all the transverse groups. However, in many cases, the highest crack density was not seen in the thinnest transverse layer. The crack density increased between the 4 and 2 ply transverse groups, but it often

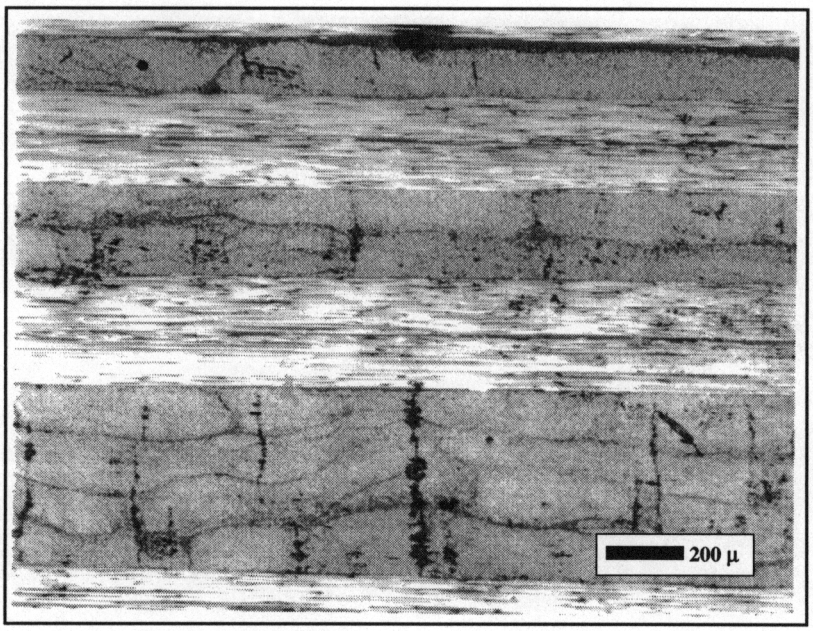

Figure 2.16. Photomicrograph of a $[0/90/0_2/90_2/0_2/90_2]_s$ LaRC^{TM}-8515 diglyme exposed specimen.

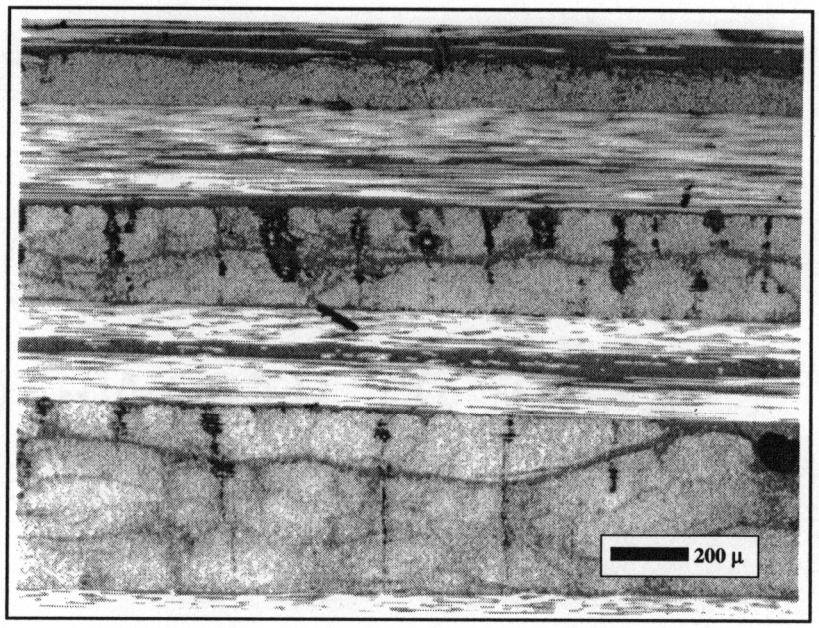

Figure 2.17. Photomicrograph of a $[0/90/0_2/90_2/0_2/90_2]_s$ LaRC^{TM}-8515 MEK exposed specimen.

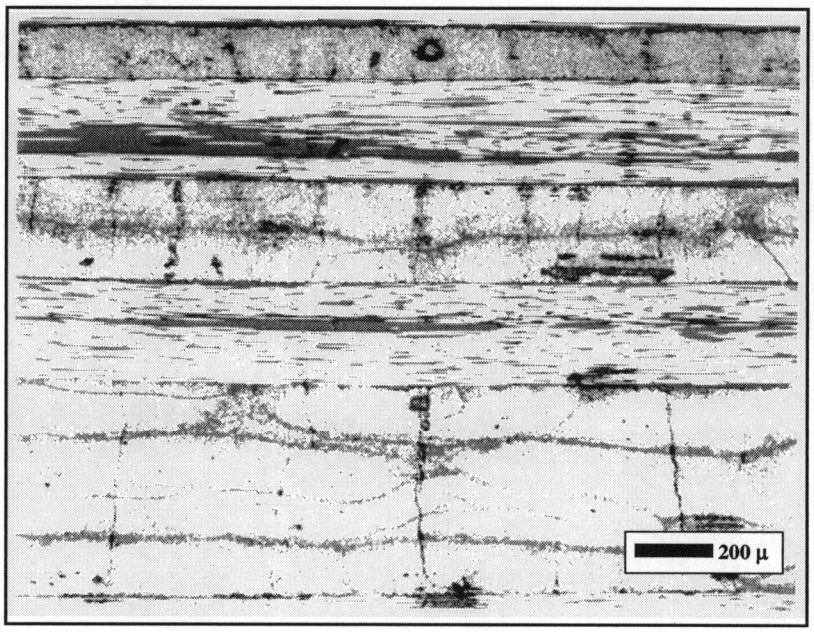

Figure 2.18. Photomicrograph of a $[0/90/0_2/90_2/0_2/90_2]_s$ LaRC™-8515 acetone exposed specimen.

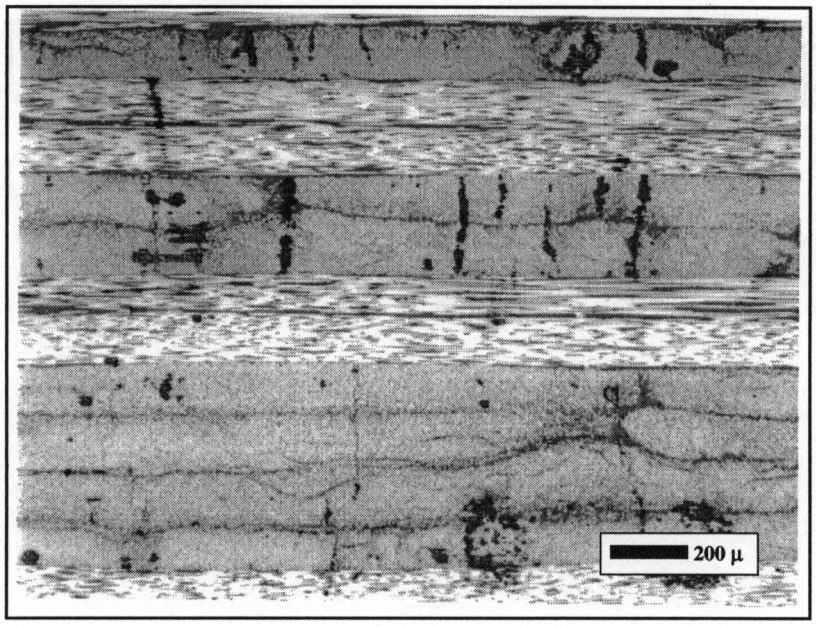

Figure 2.19. Photomicrograph of a $[0/90/0_2/90_2/0_2/90_2]_s$ LaRC^{TM}-8515 toluene exposed specimen.

decreased between the 2 ply and single transverse groups. This occurrence is particularly noticeable in IAX2 and PETI-5. Figures 2.20 and 2.21 respectively show the crack densities corresponding to each transverse ply group for these two materials.

In Figure 2.20, notice the slight increase in crack density between the 4 and 2 transverse ply groups for each of the solvent specimens except MEK. Instead, the crack density in the MEK specimen decreases as the thickness decreases. Then, as the thickness of the transverse groups decrease from 2 plies to a single ply, the crack density slightly decreases in each of the solvent specimens except MEK. The crack density in the single transverse ply of the MEK specimen increases. The behavior of the MEK specimen is unusual. It is possible that the recorded crack density in the 2 ply transverse group is not correct. Because the matrix cracks in the IAX2 specimens were so thin, some cracks may not have been detected during observation. The decrease in crack density between the 2 ply and single transverse groups is more pronounced in the PETI-5 specimens. Results in Figure 2.21 shows that the crack density in the single transverse ply is substantially lower than that in the 2 ply transverse group.

This phenomenon can be explained using the strain energy principle. As stated previously, a microcrack forms when $G_m \geq G_{mc}$. According to the values in Table 2.7, this statement is not met. However, observations reveal critical microcracking in many of the solvent exposed composite specimens. In the presence of air, these same specimens show no microcracking. Therefore, the application of solvents substantially lowers the material's G_{mc} values to allow the formation of microcracks. The energy available to form a microcrack, G_m, decreases as the ply group thickness decreases making cracking in thinner layers difficult to achieve. Therefore, the crack density in the single transverse ply groups never fully saturates because of the low available G_m, whereas the G_m in the 4 and 2 ply transverse groups is sufficient to completely develop the saturated crack density. According to equation (11),

$$\mathbf{G_m \propto t} \qquad \textbf{(16)}$$

If $G_{m\,1}$, $G_{m\,2}$, and $G_{m\,4}$ are the available energy release rates due to residual stresses corresponding to the 1, 2, and 4 ply transverse groups, then equation (11) states

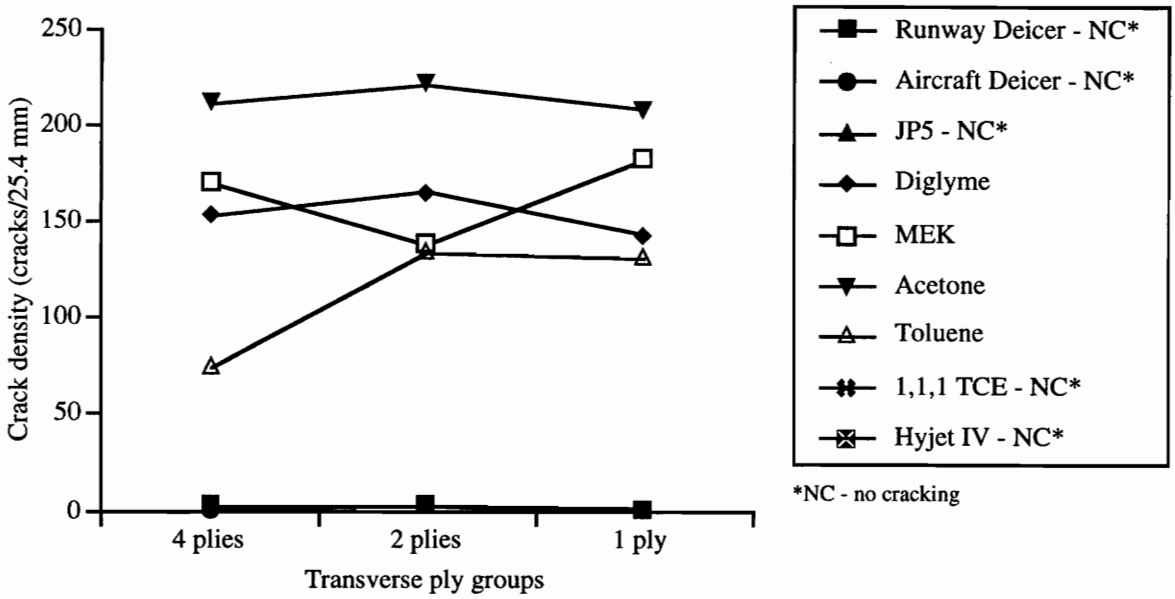

Figure 2.20. Crack density in each transverse ply group of LaRC™-IAX2 following a 96 hour immersion period.

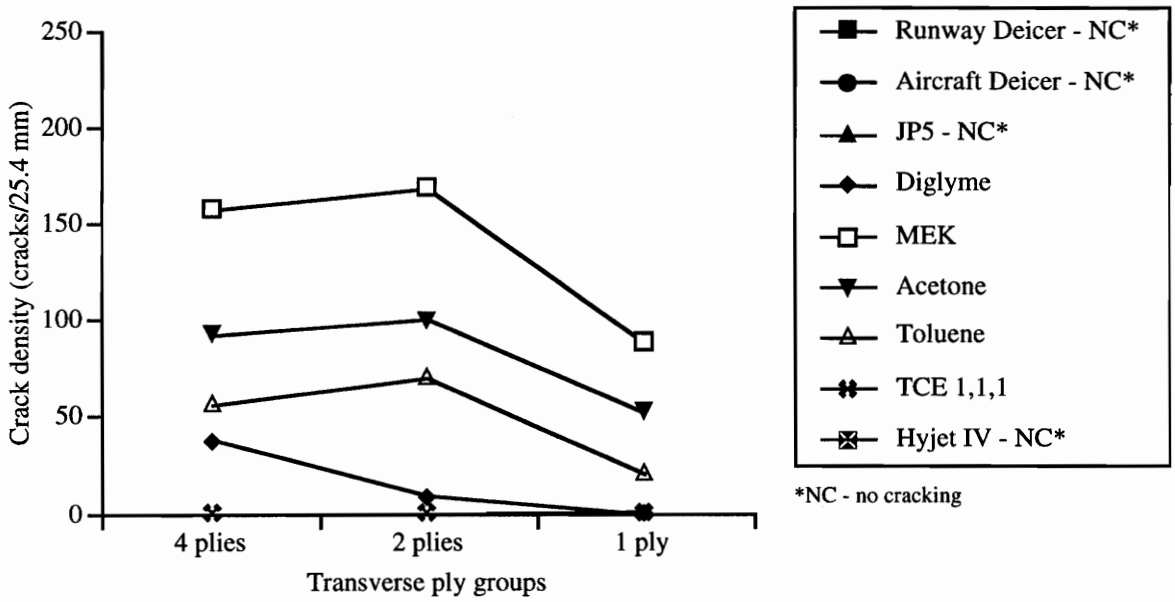

Figure 2.21. Crack density in each transverse ply group of LaRC™-PETI-5 following a 96 hour immersion period.

$$\frac{G_{m1}}{1} = \frac{G_{m2}}{2} = \frac{G_{m4}}{4} \tag{17}$$

If $G_{mc} < G_{m1} < G_{m2} < G_{m4}$, then each ply should develop characteristic spacing with the number of cracks in the single ply group being 4 times that of the 4 ply group. However, if $G_{m1} < G_{mc} < G_{m2} < G_{m4}$, then the cracks would not reach saturation spacing in the single ply group. This is quite consistent with the IAX2 and PETI-5 data. There is only one example where the available G_m was insufficient to generate the maximum possible crack density in the 2 ply transverse group. This occurred in the PETI-5 diglyme specimen.

The IAX and 8515 crack density results were as expected. The crack densities increased as the ply thickness decreased. The results are in Figures 2.22 and 2.23 respectively. The four solvents that induced microcracking in the 8515 specimens lowered the G_{mc} value of the material enough such that the G_m available in each transverse ply group was adequate to fully develop the crack densities in each group. All but two of the IAX solvent specimens developed saturated crack densities. These two were MEK and TCE 1,1,1.

Transverse flexure test results

An Analysis of Variance statistical procedure was used to analyze the transverse flexure test data. The statistical analysis was performed at Virginia Tech. The analysis was necessary to determine the relevance of certain tests due to the large amount of scatter in the data. The analysis arranged the mean break stress from highest to lowest for each material per method. It then divided the solvents into groups indicating the significant difference, if any, among the solvents. Other NASA researchers have reported scatter in 90° flexure tests ranging from 10% to 50% [51]. The 90° flexure tests are highly dependent on the quality of the specimens being tested. When testing composites, laminate consolidation is extremely important. The presence of voids can greatly affect 90° flexure test results. In this study, the application of solvents causes even more variation. The fiber volume, matrix volume, and void volume are different for each specimen. This affects how quickly the solvents migrate into the specimens. Therefore, when testing a representative 5 specimens per solvent, the results may vary immensely due to the microscopic differences within the specimens.

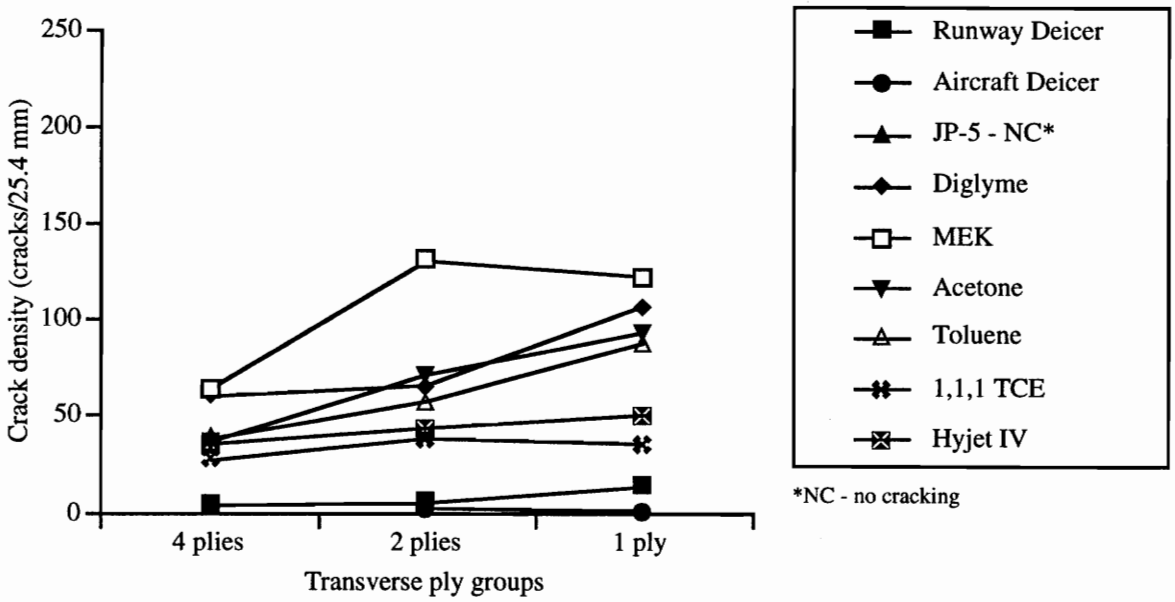

Figure 2.22. Crack density in each transverse ply group of LaRC™-IAX following a 96 hour immersion period.

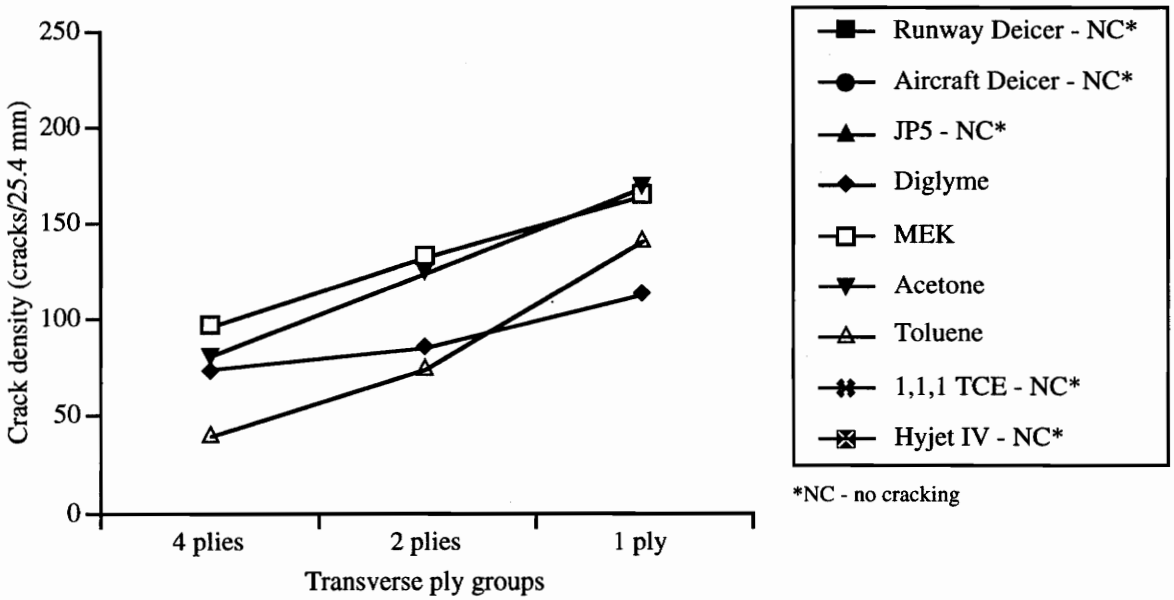

Figure 2.23. Crack density in each transverse ply group of LaRC™-8515 following a 96 hour immersion period.

Solvent drop (SD) test results

The SD test results are summarized in Table 2.8. The strength retention of the materials in each solvent are given in Table 2.9. The highest overall strength retention was seen in IAX2 and PETI-5. These two materials retained 70% of their original strength after being exposed to several drops of their most damaging solvents. According to the analysis, MEK was the most harmful to IAX2. The solvents causing little or no reduction were aircraft deicer, runway deicer, and Hyjet IV. The remaining solvents were not significantly different from one another and therefore were considered to produce similar degrees of strength reduction. MEK and acetone caused the largest strength reduction in PETI-5. The analysis showed that there was no significant difference between the effects of these two solvents. Runway deicer, aircraft deicer, JP-5, TCE 1,1,1, and Hyjet IV had the least effect on PETI-5. Diglyme and toluene caused an average strength reduction. 8515 retained 56% of its original strength after being exposed to acetone. Acetone caused the most reduction of all the solvents. Runway deicer was the least harmful. The remaining solvents showed no significant differences. Their effects on 8515 were similar. IAX retained 48% of its strength in diglyme. The mean break stress with diglyme was the lowest of all the solvents; however, there was no significant difference among diglyme, MEK, and TCE 1,1,1. These were the worst solvents for IAX in the SD test. The data showed that the average break stresses for IAX in aircraft deicer and JP-5 were greater than the average break stress of the control specimen. This may be due to the presence of flaws within the tested control specimens which resulted in a decrease in the mean break stress. It is also possible that the solvents plasticized the polymer causing it to toughen; thus increasing the strength. Significantly, however, there is no difference in the break stress of the control, aircraft deicer, and JP-5 specimens. The remaining solvents are considered to be average microcracking agents for IAX. Figure 2.24 shows the strength of each material in diglyme, MEK, and acetone.

Solvent vapor (SV) test results

Table 2.10 summarizes the SV test results and Table 2.11 contains strength retention data for the four materials in each solvent. According to the numerical data, a 77% retention in strength was seen in IAX and IAX2. The lowest mean break stress for IAX resulted from exposure to MEK. The data indicates that six of the IAX solvent

Table 2.8. Solvent drop test method break stress results.

LaRC™-IAX		LaRC™-IAX2		LaRC™-8515		LaRC™-PETI-5	
Solvent	Break stress, MPa	Solvent	Break Stress, MPa	Solvent	Break stress, MPa	Solvent	Break stress, MPa
JP5	117.3	Control	126.7	Control	136.6	Control	149.5
AD	115.2	Hyjet IV	117.6	RD	136.59	AD	145.7
Control	102.1	JP5	114.7	AD	124.1	RD	145
RD	99.3	AD	112.5	JP5	122.4	JP5	141.3
Acetone	76.4	RD	109.7	TCE 1,1,1	106.4	Hyjet IV	135.8
Toluene	72.4	Acetone	100.5	Hyjet IV	98.7	TCE 1,1,1	134.4
Hyjet IV	72.1	Toluene	96.6	Toluene	88.1	Diglyme	119.6
TCE 1,1,1	59.4	TCE 1,1,1	96.4	MEK	87.2	Toluene	119.5
MEK	54.6	Diglyme	96	Diglyme	82.4	MEK	104.6
Diglyme	48.5	MEK	88.5	Acetone	76.4	Acetone	104.3

Table 2.9. Percent strength retention of the solvent drop test specimens.

Solvents	LaRC™-IAX	LaRC™-IAX2	LaRC™-8515	LaRC™-PETI-5
Runway deicer	100.0	86.6	100.0	97.0
Aircraft deicer	112.8	88.8	90.8	97.4
JP5	114.9	90.5	89.6	94.5
Diglyme	47.5	75.7	60.3	80.0
MEK	53.5	69.9	63.8	70.0
Acetone	74.9	79.3	55.9	69.7
Toluene	70.9	76.2	64.5	79.9
TCE 1,1,1	58.2	76.1	77.9	89.9
Hyjet IV	70.6	92.8	72.3	90.8

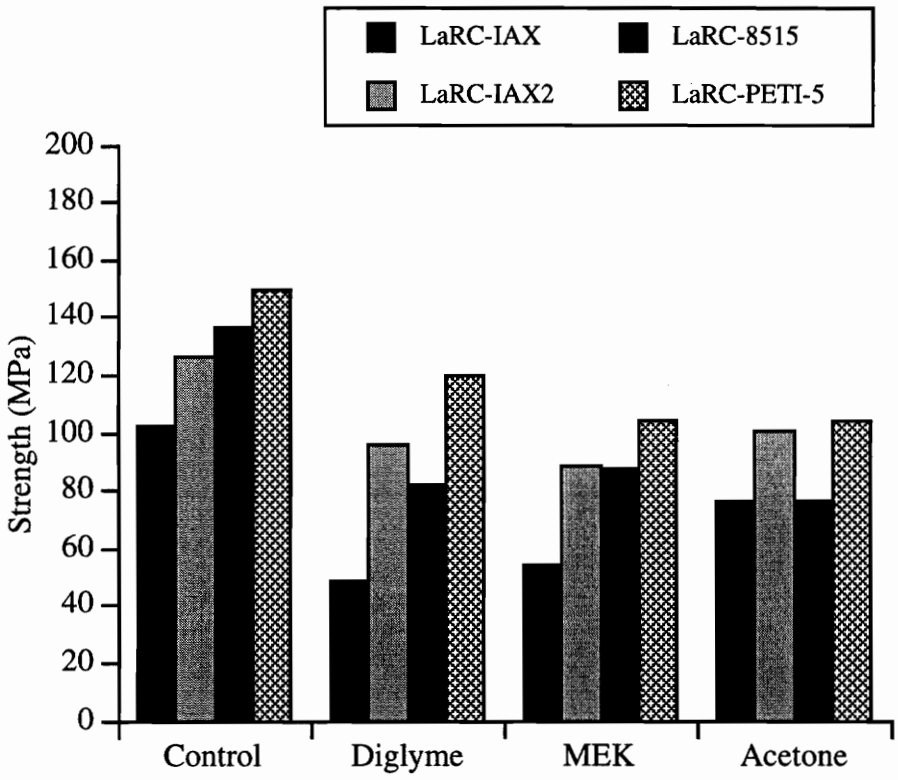

Figure 2.24. Strength retention of dilgyme, MEK, and acetone LaRC™ solvent drop specimens.

Table 2.10. Solvent vapor test method break stress results.

LaRC™-IAX		LaRC™-IAX2		LaRC™-8515		LaRC™-PETI-5	
Solvent	Break stress, MPa	Solvent	Break Stress, MPa	Solvent	Break stress, MPa	Solvent	Break stress, MPa
RD	120.2	Hyjet IV	149.0	Control	136.6	JP5	161.6
JP5	118.3	RD	127.1	JP5	125.9	RD	159.2
Hyjet IV	115.5	Diglyme	126.8	RD	121.5	Hyjet IV	158.0
Diglyme	110.0	Control	126.7	Diglyme	120.4	Control	149.5
TCE 1,1,1	105.1	JP5	126.2	TCE 1,1,1	118.6	Diglyme	149.5
AD	103.7	AD	117.6	AD	117.5	TCE 1,1,1	139.7
Control	102.1	TCE 1,1,1	108.2	Toluene	106.6	AD	132.8
Toluene	99.1	Toluene	107.4	MEK	93.5	Toluene	118.6
Acetone	87.0	MEK	101.6	Acetone	87.3	MEK	111.0
MEK	79.8	Acetone	96.9	Hyjet IV	86.9	Acetone	103.4

Table 2.11. Percent strength retention of the solvent vapor test specimens.

Solvents	LaRC™-IAX	LaRC™-IAX2	LaRC™-8515	LaRC™-PETI-5
Runway deicer	117.7	100.3	88.9	106.5
Aircraft deicer	101.6	92.8	86.0	88.8
JP5	115.9	99.6	92.2	108.1
Diglyme	107.8	100.0	88.1	100.0
MEK	78.2	80.1	68.4	74.3
Acetone	85.2	76.4	63.9	69.2
Toluene	97.1	84.7	78.0	79.3
TCE 1,1,1	103.0	85.4	86.8	93.5
Hyjet IV	113.2	117.6	63.6	105.7

specimens showed an increase in strength over the control specimen. The control specimen mean break stress is located near the lower end of the break stress interval (Table 2.10). As previously suggested, flaws may have been present in the control specimens which resulted in a reduced break stress. According to the statistical analysis there is little significant difference among the IAX solvent specimens. It is possible to conclude that MEK is more detrimental than runway deicer, JP-5, and Hyjet IV. The analysis also suggests that acetone is a more severe solvent than runway deicer. However, there is no significant difference between MEK and acetone. Numerically, though, runway deicer is the least harmful solvent while MEK is the most harmful solvent. Acetone caused the largest reduction in strength in IAX2. The Hyjet IV, runway deicer, and diglyme IAX2 vapor specimens showed higher strengths than the control specimen. However, statistically, there is no significant difference in the strength data of the Hyjet IV, runway deicer, diglyme, control, and JP-5 specimens. The vapor of these solvents exhibited little or no effect on IAX2. The remaining solvents, aircraft deicer, TCE 1,1,1, toluene, MEK, and acetone, had the largest effect on IAX2. PETI-5 was affected the most by acetone. The results showed a 69% retention in strength in PETI-5 after exposure to acetone vapors. MEK and toluene had similar effects on PETI-5. There is no significant difference in the strength data obtained for PETI-5 after exposure to acetone, MEK, and toluene vapors. It can be concluded that TCE 1,1,1, aircraft deicer, toluene, MEK, and acetone caused the most damage to PETI-5. The least damage was caused by JP-5, runway deicer, Hyjet IV, control, and diglyme due to their low volatility. The strength retention of 8515 in acetone was 64%. The data suggests that Hyjet IV caused the greatest damage in 8515. However, there were noticeable voids along the edges of the Hyjet IV specimens. Therefore, the experimental data is not an accurate measure of the strength of 8515 exposed to Hyjet IV vapors. The statistical results showed that acetone, MEK, and toluene were the most harmful to 8515. The least harmful solvents were JP-5, runway deicer, diglyme, TCE 1,1,1, and aircraft deicer.

Although the statistical analysis of the SV tests indicated that there was little significant difference between many of the solvents, there are noticeable trends associated with the solvent exposed materials. For all of the materials the three worst solvents were acetone, MEK, and toluene. This was expected because these were the most volatile solvents. Figure 2.25 shows the strength of the materials tested in these three solvents. Another finding was that Hyjet IV, runway deicer, diglyme, and JP-5 were the least harmful to the materials and aircraft deicer, TCE 1,1,1, toluene, MEK, and acetone were

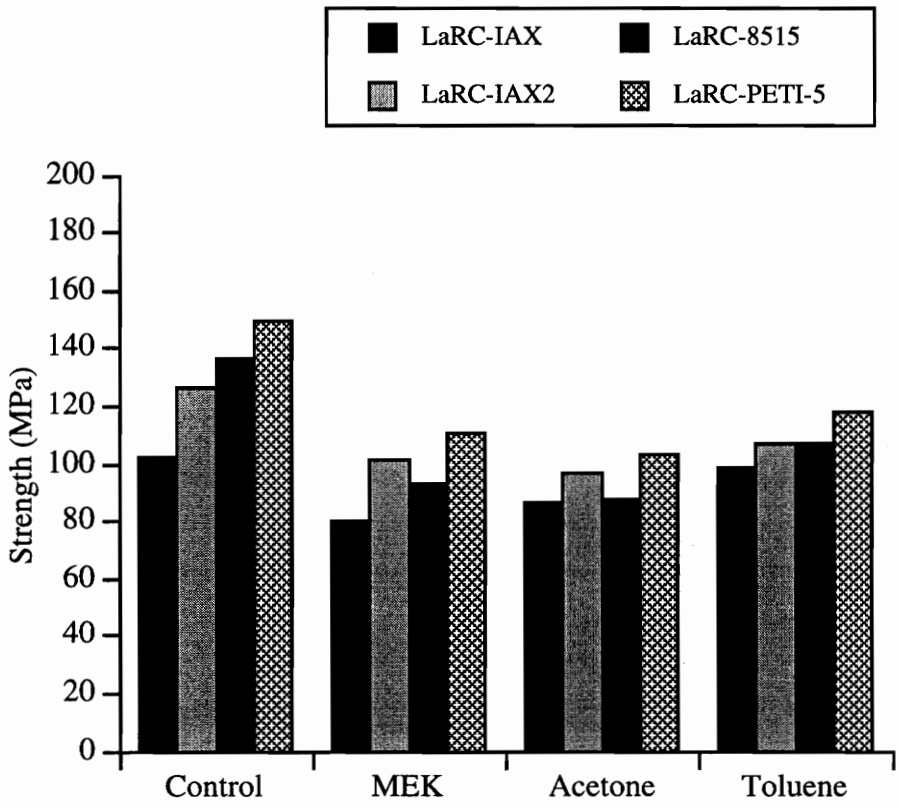

Figure 2.25. Strength retention of MEK, acetone, and toluene LaRC™ solvent vapor specimens.

the most harmful to the materials. There were a few exceptions, but these were the foremost observations.

Solvent soak (SS) test results

The SS test method had the most severe effect on the strength of the materials. Table 2.12 summarizes the SS test results. The strength retention of the materials in each solvent is given in Table 2.13. There is a considerable reduction in strength after exposure to certain solvents during the SS transverse flexure tests. The most detrimental solvent for all of the materials was acetone. Results showed that IAX retained only 10% of its original strength when tested in acetone. The IAX statistical analysis results divided the solvents into three groups. Acetone, diglyme, and MEK were the most detrimental to IAX. Hyjet IV, TCE 1,1,1, and toluene had an intermediate effect. Runway deicer and JP-5 were the least harmful. The IAX2 results were similar to the IAX results. IAX2 retained 24% of its original strength when exposed to acetone. The statistical analysis indicated that acetone was significantly the single most harmful solvent to IAX2. Diglyme and MEK also severely affected IAX2. The strength retention of IAX2 tested in these solvents was 53%and 54% respectively. Toluene and TCE 1,1,1 caused intermediate effects to IAX2; runway deicer, JP-5, and Hyjet IV had little or no effect. 8515 retained 47% of its strength when tested in acetone. PETI-5 was least affected by acetone exposure; however, a considerable reduction in strength was accomplished. PETI-5 retained 62% of its original strength when tested in acetone. Noticeable strength reductions to 8515 and PETI-5 were also induced by toluene, MEK, diglyme, TCE 1,1,1. PETI-5 and 8515 was least affected by runway deicer, JP-5, and Hyjet IV.

The SS test method yields information regarding the extent of damage associated with the different solvents for each material. For the tested materials, runway deicer, JP-5, and Hyjet IV are the least harmful. Diglyme, MEK, toluene, and TCE 1,1,1 cause considerable strength reductions and acetone is the most detrimental. Figure 2.26 shows the strength of the materials tested in diglyme, MEK, and acetone. This trend is dominant for all of the materials. This test method also most accurately predicts the solvent resistance of the materials. According to the SS test results, PETI-5 is the most solvent resistant. This is followed by 8515, IAX2, and IAX respectively. These results are consistent with the nature of the materials. PETI-5 is a thermoset while the remaining materials are thermoplastics. A thermoset is more solvent resistant than a thermoplastic because solvent

Table 2.12. Solvent soak test method break stress results.

LaRC™-IAX		LaRC™-IAX2		LaRC™-8515		LaRC™-PETI-5	
Solvent	Break stress, MPa	Solvent	Break Stress, MPa	Solvent	Break stress, MPa	Solvent	Break stress, MPa
JP5	106.8	Control	126.7	Control	136.6	Control	149.5
	102.1	RD	126.2	RD	105.4	Hyjet IV	147.6
RD	99.4	Hyjet IV	120.7	JP5	99.2	RD	147.0
Hyjet IV	77.5	JP5	105.8	Hyjet IV	87.0	JP5	140.5
TCE 1,1,1	67.8	TCE 1,1,1	92.6	TCE 1,1,1	85.5	TCE 1,1,1	119.1
Toluene	56.7	Toluene	80.0	Diglyme	74.7	Diglyme	115.2
MEK	33.6	MEK	68.2	Toluene	74.4	MEK	103.1
Diglyme	30.7	Diglyme	66.9	MEK	68.2	Toluene	100.6
Acetone	10.0	Acetone	30.7	Acetone	63.9	Acetone	92.9

Table 2.13. Percent strength retention of the solvent soak test specimens.

Solvents	LaRC™-IAX	LaRC™-IAX2	LaRC™-8515	LaRC™-PETI-5
Runway deicer	97.4	99.6	77.2	98.3
JP5	104.7	83.5	72.6	94.0
Diglyme	30.1	52.8	54.7	86.3
MEK	32.9	53.8	49.9	69.0
Acetone	9.8	24.2	46.8	62.1
Toluene	55.6	63.1	54.5	67.3
TCE 1,1,1	66.4	73.1	62.6	79.7
Hyjet IV	76.0	95.2	63.7	98.7

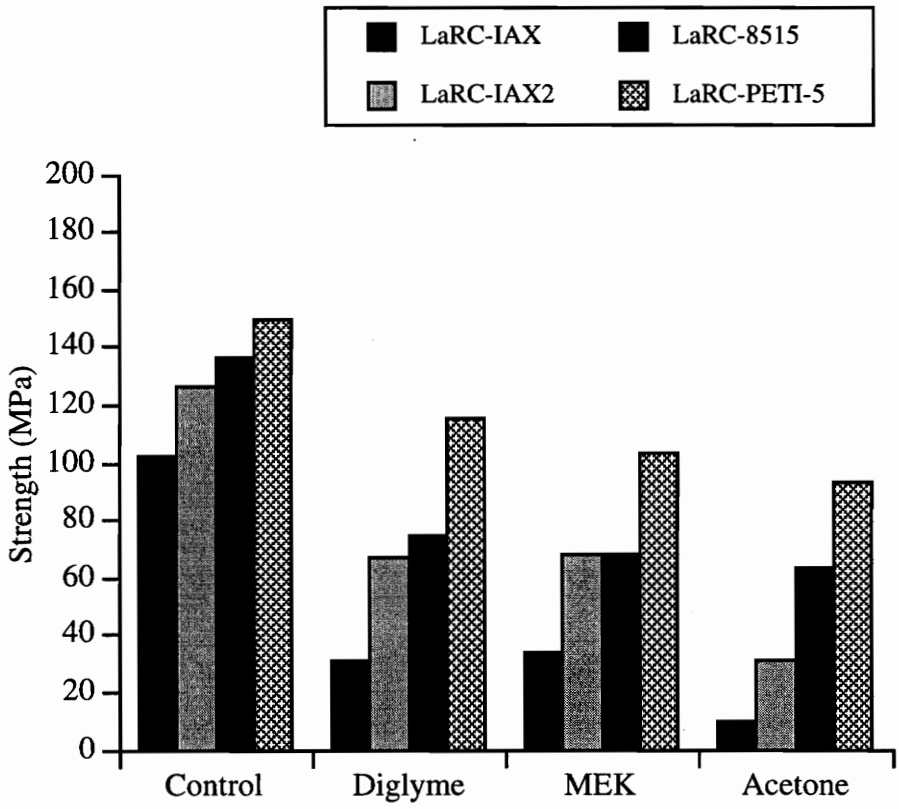

Figure 2.26. Strength retention of dilgyme, MEK, and acetone LaRC™ solvent soak specimens.

penetration is prohibited by both the crosslinks and the solvent resistance of the backbone structure; whereas the solvent resistance of a thermoplastic depends solely on the solvent resistance of the backbone structure.

Solvent soak-wet (SSW) test results

Table 2.14 summarizes the SSW test results. Diglyme had the greatest effect on all of the materials. The strength retention for each material tested in diglyme is given in Table 2.15. The results were as expected because acetone and MEK evaporate rapidly, whereas diglyme does not. Therefore, before the acetone and MEK specimens were completely tested, the solvents had evaporated leaving a dry specimen to be tested. Diglyme, on the other hand, remained in the specimens throughout the flexure test and induced significant reductions in strength. Figure 2.27 shows the strength of each material in diglyme, MEK, and acetone. The SSW test results justify that both stress and solvent must be present to reduce composite strength.

Solvent soak-dry (SSD) test results

The SSD test results are given in Table 2.16. The statistical analysis results indicated that the solvents did not cause any significant damage in any of the materials. Figure 2.28 illustrates this graphically. This test method also verifies that both stress and solvent must be present to reduce composite strength.

CONCLUSIONS AND FUTURE WORK

Solvent immersion tests were conducted on cross-ply composite specimens. IAX, IAX2, 8515, and PETI-5 polyimide composite specimens were exposed to nine organic liquids. The total duration of solvent exposure was 96 hours. During the tests, the specimens were examined for microcracking after 1 minute, 1 hour, 24 hours, 48 hours, and 96 hours.

Microcracking was observed in all of the materials. These observations confirm that thermal residual stresses combined with certain solvents are sufficient to induce microcracking. The initiation of damage resulting from the presence of solvents is very

Table 2.14. Solvent soak-wet test method break stress results.

LaRC™-IAX		LaRC™-IAX2		LaRC™-8515		LaRC™-PETI-5	
Solvent	Break stress, MPa	Solvent	Break Stress, MPa	Solvent	Break stress, MPa	Solvent	Break stress, MPa
Acetone	104.8	Control	126.7	Control	136.6	Acetone	164.0
Control	102.1	Acetone	123.7	MEK	113.7	Control	149.5
MEK	98.6	MEK	106.8	Diglyme	69.3	MEK	138.6
Diglyme	28.1	Diglyme	70.3	--	--	Diglyme	122.0

Table 2.15. Percent strength retention of the solvent soak-wet test specimens.

Solvents	LaRC™-IAX	LaRC™-IAX2	LaRC™-8515	LaRC™-PETI-5
Diglyme	27.5	55.5	50.7	81.6
MEK	96.6	84.3	83.2	92.7
Acetone	102.7	97.6	--	109.7

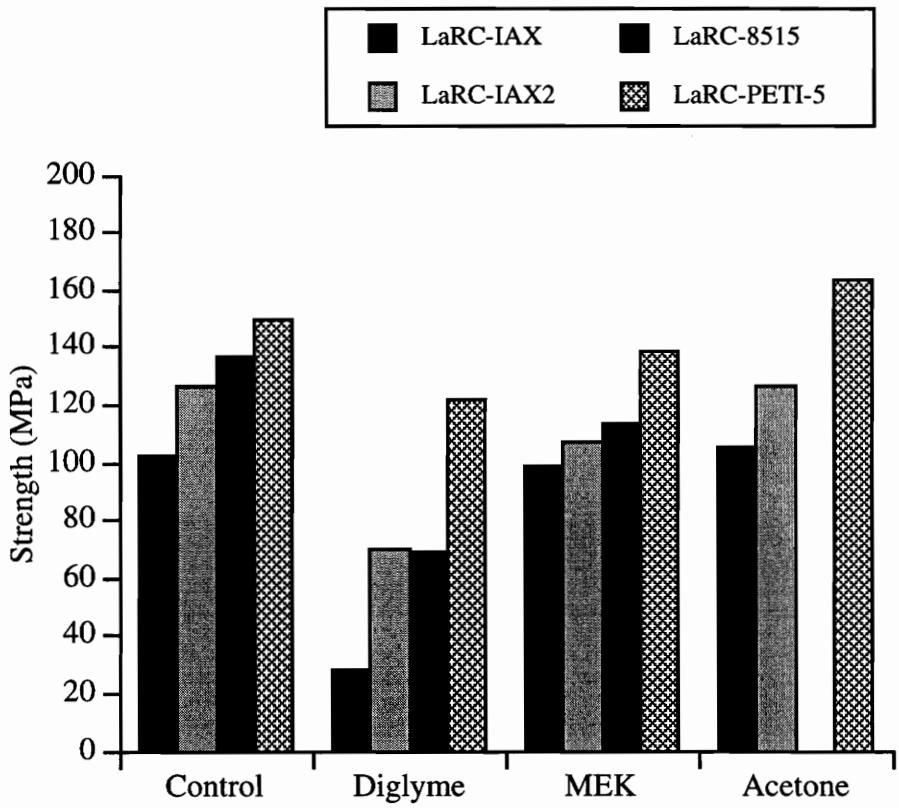

Figure 2.27. Strength retention of dilgyme, MEK, and acetone LaRC™ solvent-soak wet specimens.

Table 2.16. Solvent soak-dry test method break stress results.

LaRC™-IAX		LaRC™-IAX2		LaRC™-8515		LaRC™-PETI-5	
Solvent	Break stress, MPa	Solvent	Break Stress, MPa	Solvent	Break stress, MPa	Solvent	Break stress, MPa
MEK	122.4	MEK	148.9	Control	136.6	MEK	183.1
Diglyme	119.0	Acetone	135.2	Diglyme	136.1	Diglyme	161.2
Acetone	107.7	Diglyme	128.1	MEK	134.9	Acetone	152.9
Control	102.1	Control	126.7	--	--	Control	149.5

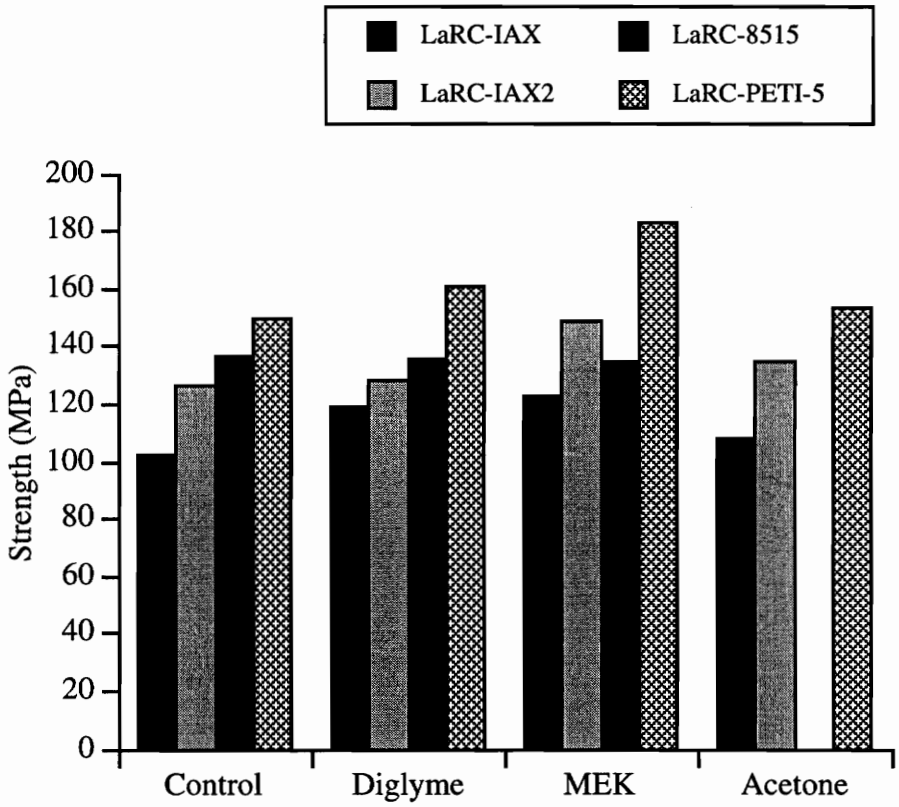

Figure 2.28. Strength retention of dilgyme, MEK, and acetone LaRC™ solvent-soak dry specimens.

rapid. All of the materials revealed some degree of damage within the first minute of exposure. Overall, diglyme, MEK, and acetone were the most harmful solvents. PETI-5 was the most solvent resistant polymer. The resistance of IAX2 and 8515 was similar. IAX was the least resistant of the materials. Many high performance composites may be susceptible to ESC. Organic solvents appear to be the most severe, but microcracking also occurs with everyday aircraft fluids.

Crack development in solvents for all four systems occurs at much lower G_{mc} values than the respective G_{mc} values needed to grow a crack in air. The presence of the solvents lowers the G_{mc} values such that the available strain energy, G_m, within the transverse ply groups is sufficient to initiate microcracking. However, G_m decreases as the transverse ply group thickness decreases making higher crack densities in thinner layers difficult to achieve. Therefore, the crack density in the single transverse ply groups never fully develops because of the low available G_m, whereas the G_m in the 4 and 2 ply transverse groups is sufficient to completely develop the saturation crack density.

Transverse flexure tests having different solvent application methods were conducted on IAX, IAX2, 8515, and PETI-5 unidirectional composites. Certain solvent application techniques severly reduced the strength of the materials. The solvent soak, solvent vapor, solvent drop, and solvent soak/wet methods affected the strengths of the materials. The solvent soak method produced the most severe effects while the solvent vapor tests were the least harmful. Results showed that IAX retained merely 10% of its original strength when tested in acetone. Diglyme, MEK, and acetone produced the most severe effects on the materials. Hyjet IV, runway deicer, aircraft deicer, and JP-5 were the least harmful. The solvent soak/wet and solvent soak/dry test methods verified that both stress and solvent must be present to reduce composite strength. The presence of one without the other does not result in material degradation. Results indicated that PETI-5 was the most resistant to solvents. This is followed by 8515, IAX2, and IAX in order of highest solvent resistance.

This study shows that thermosets are the most solvent resistant to certain organic solvents. Although matrix microcracking can not be prevented, the degree of microcracking can be reduced to some extent by the type of matrix material chosen, the layup of the laminate, and the type of solvent exposure. The worst type of solvent exposure a composite structure can be subjected to is solvent soaking.

Some areas of future work would include conducting solvent immersion tests on the same materials having different processing conditions and different layups since these

two factors strongly influence the amount of residual stress retained in the laminates. Another area of interest would be to determine if solvent induced microcracking lowered the fatigue life of materials.

REFERENCES

1. Garg, A. C., "Environmental Stress Cracking Behavior of Delamination in Laminated Composites," Composite Materials and Structures; Proceedings of the International Conference, Madras, India, Jan. 6-9, 1988.

2. Nairn, John A., "The Initiation of Microcracking in Cross-Ply Laminates: A Variational Mechanics Approach," American Society for Composites, Technical Conference, 3rd., Seattle, WA, Sept. 25-29, 1988.

3. Nairn, John A., "The Strain Energy Release Rate of Composite Microcracking: A Variation Approach," *Journal of Composite Materials*, **23**, November 1989, p. 1106.

4. Clifton, A. Paige, Dillard, David A., St. Clair, Terry L., and Hinkley, Jeffrey, "Dye Penetrant Induced Microcracking in High Performance Polymeric Thermoplastic Polyimide Composites," *Journal of Thermoplastic Composites*, to be submitted February 1996.

5. Hsieh, Alex J., Schneider, Nathaniel S. and Mandell, John F., "Solvent Stress Cracking and Failure Mechanisms in Polyetherimide Composites," *Polymer Composites*, **11**(4), August 1990, p. 240.

6. Moore, Robert H. and Dillard, David A., "Elastic and Time Dependent Matrix Cracking in Cross-Ply Laminates," Masters Thesis, College of Engineering, Virginia Polytechnic Institute University, April 1988.

7. Highsmith, A. L. and Reifsnider, K. L., "Stiffness-Reduction Mechanisms in Composite Laminates," *Damage in Composite Materials, ASTM STP 775,* K. L. Reifsnider, Ed., American Society for Testing and Materials, 1982, p. 103.

8. Reifsnider, K. L., Henneke, E. G., Stinchcomb W. W. and Duke, J. C., "Damage Mechanics and NDE of Composite Laminates," *Mechanics of Composite Materials, Recent Advances,* Z. Hashin and C. T. Herakovich, Eds., New York, Perganon, 1983, p. 399.

9. Nairn, John A., "Microcracking, Microcrack-Induced Delamination, and Longitudinal Splitting of Advanced Composite Structures," NASA Contractor Report 4472, November 1992.

10. Gudmundson, Peter and Ostlund, Soren, "Numerical Verification of a Procedure for Calculation of Elastic Constants in Microcracking Composite Laminates," *Journal of Composite Materials*, **26** (17), 1992, p. 2480.

11. Gudmundson, Peter and Ostlund, Soren, "Prediction of Thermoelastic Properties of Composite Laminates with Matrix Cracks," *Composites Science and Technology*, **44**, 1992, p. 95.

12. Reifsnider, Kenneth L. and Giacco, Alexander, "The Use of Microcrack Analysis in Performance Simulation for Composite Material Systems," in G. J. Dvorak and D. C. Lagoudas (ed.), *Microcracking-Induced Damage in Composites*, 1990, p. 19.

13. Garrett, K. W. and Bailey, J. E., "Multiple Transverse Fracture in 90° Cross-Ply Laminates of a Glass Fibre-Reinforced Polyester," *Journal of Materials Science*, **12**, 1977, p.157.

14. Lim, S. G. and Hong, C. S., "Prediction of Transverse Cracking and Stiffness Reduction in Cross-Ply Laminated Composites," *Journal of Composite Materials*, **23**, 1989, p. 695.

15. Lee, J.-W. and Daniel, I. M., "Progressive Transverse Cracking of Crossply Composite Laminates," *Journal of Composite Materials*, **24**, 1990, p. 1225.

16. Bowles, David E., "Effect of Microcracks on the Thermal Expansion of Composite Laminates," *Journal of Composite Materials*, **17**, 1984, p. 173.

17. Laws, N. and Dvorak, G. J., "Transverse Matrix Cracking in Composite Laminates," Composite Material Response: Constitutive Relations and Damage Mechanisms; Proceedings of the Workshop, Glasgow, Scotland, July 30, 31, 1987.

18. Moore, Robert H. and Dillard, David A., "Time-dependent Matrix Cracking in Cross-ply Laminates," *Composites Science and Technology*, **39**, 1990, p. 1.

19. Talreja, Ramesh, Yalvac, Selim, Yats, Larry D. and Wetters, Derrick G., "Transverse Cracking and Stiffness Reduction in Cross Ply Laminates of Different Matrix Toughness," *Journal of Composite Materials*, **26** (11), 1992, p. 1644.

20. Swanson, S. R., "On the Mechanics of Microcracking in Fiber Composite Laminates Under Combined Stress," ASME, Winter Annual Meeting, Anaheim, CA, Dec. 7-12, 1986.

21. Allen, David H. and Lee, Jong-Won, "Matrix Cracking in Laminated Composites Under Monotonic and Cyclic Loadings," in G. J. Dvorak and D. C. Lagoudas (ed.), *Microcracking-Induced Damage in Composites*, 1990, p. 65.

22. Rothschild, R. J., Ilcewicz, L. B., Nordin, P., and Applegate, S. J., " The Effect of Hygrothermal Histories on Matrix Cracking in Fiber Reinforced Laminates," *Journal of Engineering Materials and Technology*, **110**, 1988, p. 158.

23. Bailey, J. E., Curtis, P. T. and Parvizi, A., "On the Transverse Cracking and Longitudinal Splitting Behaviour of Glass and Carbon Fibre Reinforced Epoxy Cross-Ply Laminates and the Effect of Poisson and Thermally Generated Strain," *Proc. R. Soc. Lond. A.*, 1979, p. 599.

24. Reifsnider, Kenneth L. and Giacco, Alexander, "The Use of Microcrack Analysis in Performance Simulation for Composite Material Systems," ASME, AMD Volume III, Presented in Dallas, Texas, November 25-30, 1990.

25. Lustiger, A. *Failure of Plastics*, edited by W. Brostow and R. D. Corneliussen, Chapter 16, Hanser Publications, 1986, p. 305.

26. Howard, J. B., *Soc. Plas. Eng. J.*, **6**, 1959, p. 397.

27. Bernier, G. A. and Kambour, R. P., "The Role of Organic Agents in the Stress Crazing and Cracking of Poly (2,6-dimethyl-1,4-phenylene oxide)," *Macromolecules*, **1** (5), 1968, p. 393.

28. Kambour, R. P., Romagosa, E. E., and Gruner, C. L., "Swelling, Crazing, and Cracking of an Aromatic Copolyether-Sulphone in Organic Media," *Macromolecules*, **5** (4), 1972, p. 335.

29. Kambour, R. P., Gruner, C. L. and Romagosa, E. E., "Solvent Crazing of "Dry" Polystyrene and "Dry" Crazing of Plasticized Polystyrene," *Journal of Polymer Science*, **11**, 1973, p. 1879.

30. Kambour, R. P., Gruner, C. L. and Romagosa, E. E., "Bisphenol-A Polycarbonate Immersed in Organic Media. Swelling and Response to Stress," *Macromolecules*, **7** (2), 1974, p. 248.

31. Vincent, P. I. and Raha, S., "Influence of Hydrogen Bonding on Crazing and Cracking of Amorphous Thermoplastics," *Polymer*, **13**, 1972, p. 283.

32. Henry, L. F., "Prediction and Evaluation of Susceptibilities of Glassy Thermoplastics to Environmental Stress Cracking," *Polymer Engineering Science*, **14**, 1974, p. 167.

33. Hittmair, P. and Ullman, Robert, "Environmental Stress Cracking of Polyethylene," *Journal of Applied Polymer Science*, **VI** (19), 1962, p. 1.

34. Hashin, Z., "Analysis of cracked Laminates: A Variational Approach," *Mechanics of Materials*, **4**, 1985, p. 121.

35. Hashin, Z., "Analysis of Stiffness Reduction of Cracked Cross-Ply Laminates," *Engineering Fracture Mechanics*, **25**, 1986, p. 771.

36. Laws, N. and Dvorak, G. J., "Progressive Transverse Cracking in Composite Laminates," *Journal of Composite Materials*, **22**, 1988, p. 900.

37. Hou, T. H., Johnston, N. J., and St. Clair, T. L., "IM7/LaRC™-IA Polyimide Composites," *High Performance Polymers*, **7**, 1995, p. 105.

38. Hou, T. H., "Processing and Properties of IM7/LaRC™-IA Polyimide Composites," 39th International SAMPE Symposium and Exhibition, Anaheim, California, April 11-14, 1994.

39. Hou, T. H., Wilkinson, S. P., and Jensen, B. J., "Processing and Properties of IM7/LaRC™-8515 Composites," *Polyimides: Synthesis, Characterization, and Applications*, edited by C. Feger, Plenum Press, New York, 1995.

40. Jensen, Brian J., Hou, Tan H., and Wilkinson, Steven P., "Adhesive and Composite Properties of LaRC™-8515 Polyimide," 40th SAMPE International Symposium and Exhibition, May 8-11, 1995.

41. Jensen, B.J., Bryant, R. G., Smith, Jr., J. G., and Hergenrother, P. M., "Adhesive Properties of Cured Phenylethynyl-Terminated Imide Oligomers," *Journal of Adhesion*, **54** (1), 1995, p. 1.

42. Bryant, R. G., Jensen, B. J., Smith, Jr., J. G., and Hergenrother, P. M., "Adhesive Properties of Phynylethynyl Terminated Polyimides," 39th International SAMPE Symposium and Exhibition, Anaheim, California, April 11-14, 1994.

43. Hou, T. H., Jensen, B. J., and Hergenrother, P. M., "Processing and Properties of IM7/PETI Composites," *Journal of Composite Materials*, in publication.

44. Smith, Jr., J. G. and Hergenrother, P. M., *Polymer Prepr.*, **35**, 1994, p. 353.

45. Hergenrother, P. M., Bryant, R. G., Jensen, B. J., Smith, Jr., J. G., and Wilkinson, S. P., *Soc. Adv. Matl. Proc. Eng. Series*, **39**, 1994, p. 961.

46. Hinkley, J. A., Johnston, N. J., and O'Brien, T. K., "Interlaminar Fracture Toughness of Thermoplastic Composites," NASA Technical Memorandum 100532, US Army Aviation Systems Command Technical Memorandum 88-B-002, 1988.

47. Jones, Robert M., *Mechanics of Composite Materials*, Hemisphere Publishing Corporation, New York, NY, 1975.

48. Swanson, G. D., Wishart, R. E., and Eastland, C. C. M., "Compression Strength Results for Stiffened Composite Fuselage Structure," 4th NASA/DoD Advanced Composite Technical Conference, Salt Lake City, Utah, June 7-11, 1993, p. 125.

49. Liu, Siulie and Nairn, John A., "The Formation and Propagation of Matrix Microcracks in Cross-Ply Laminates during Static Loading," *Journal of Reinforced Plastics and Composites*, **11**, 1992, p. 158.

50. Nairn, John A., Hu, Shoufeng, and Bark, Jong Song, "Master Plot Analysis of Microcracking in Graphite/Epoxy and Graphite/PEEK Laminates," 3rd NASA Advanced Composite Tech. Conf., Long Beach, CA, June 1992.

51. Unpublished data from Trish McDaniel and Mia Siochi at NASA-Langley Research Center, 1995.

APPENDIX A

Appendix A contains a user's guide to the Classical Laminate Theory (CLT) code used in this research and a hardcopy of the actual code.

Table of Contents

I. **What is Classical Laminate Theory Code?** 113

- **Getting Started** 113
- **How to use this manual** 113

II. **Input Data** 114

III. **Equations**. 117

IV. **Outputs**. 117

V. **Laminate Strength and Ply Discount**. 118

VI. **Program Modifications**. 119

VII. **Program List**. 120

I. What is Classical Laminate Theory Code?

Classical Laminate Theory (CLT) code is a composite laminate analysis program which when given specific inputs calculates the following laminate information:

- the A, B, D matrices
- the laminate E_x, E_y, ν_{xy}, G_{xy}
- the global stresses and strains for N and M (mechanical forces and moments), T (thermal), and H (moisture) loadings
- the ply stresses and strains for N and M (mechanical forces and moments), T (thermal), and H (moisture) loadings
- the laminate strength using ply discount
- the approximate interlaminar stresses

The program was written using Mathcad 3.1 Macintosh version. It is designed to calculate the above information for 10 ply laminates. The code can be easily modified to account for additional plies. The modification process is explained in section VI.

• Getting Started

In order to use this code, the user must have some knowledge of Mathcad. If the user is not familiar with this application program then please refer to a Mathcad 3.1 user's guide at this time.

• How to use this manual

This manual is divided into the following sections:

II. Input Data: This section explains the input data and describes the format in which it must be entered into the program.

III. Equations: This section lists references which explain in more detail the equations used in this CLT program.

IV. Output Data: This section explains the output data and how it is interpreted.

V. Laminate Strength and Ply Discount: This section explains the steps which must be followed to determine first ply failure and rupture ofthe laminate.

VI. Program Modifications: This section explains how the program can be modified to include more plies.

VII. Program List: This section contains an output of the actual program.

II. Input Data

• **p:** number of plies in the laminate. The program is designed for a laminate with a maximum of 10 plies. It can be easily modified to include the desired number of plies (see section VI.).

• θ**:** rotation of principle material axes from arbitrary x-y axes. This is the offset angle of each ply.

•**E1:** Young's modulus of the fibers. This data is input in matrix form. The matrix consists of one row and 10 columns. Input **E1** into the matrix columns until the number of columns equals **p**. In the remaining columns enter 0.

Example 1: p = 6

E1 := (39 39 39 39 39 39 0 0 0 0) * 10^9

•**E2:** Young's modulus of the matrix. This data is input in matrix form. The matrix consists of one row and 10 columns. Input **E2** into the matrix columns until the number of columns equals **p**. In the remaining columns enter 0.

Example 2: $p = 6$

$E2 := (4.8\ 4.8\ 4.8\ 4.8\ 4.8\ 4.8\ 0\ 0\ 0\ 0) * 10^9$

•**ν12:** Poisson's ratio. This data is input in matrix form. The matrix consists of one row and 10 columns. Input **ν12** into the matrix columns until the number of columns equals **p**. In the remaining columns enter 0.

Example 3: $p = 6$

$\nu 12 := (0.3\ 0.3\ 0.3\ 0.3\ 0.3\ 0.3\ 0\ 0\ 0\ 0)$

•**G12:** the shear modulus. This data is input in matrix form. The matrix consists of one row and 10 columns. Input **G12** into the matrix columns until the number of columns equals **p**. In the remaining columns enter 0.

Example 4: $p = 6$

$G12 := (6.0\ 6.0\ 6.0\ 6.0\ 6.0\ 6.0\ 0\ 0\ 0\ 0) * 10^9$

•**tp:** ply thickness. This data is input in matrix form. The matrix consists of one row and 10 columns. Input **tp** into the matrix columns until the number of columns equals **p**. In the remaining columns enter 0.

Example 5: $p = 6$

$tp := (.125\ .125\ .125\ .125\ .125\ .125\ 0\ 0\ 0\ 0) *10^{-3}$

•**Nm:** mechanical forces. **Nm** is a vector consisting of Nx, Ny, and Nxy. These are forces applied to the laminate in the x-direction, y-direction, and xy-direction respectively. The units are N/m.

Example 6: $Nm := (100\ 200\ 0)$

•**Mm:** mechanical moments. **Mm** is a vector consisting of Mx, My, and Mxy. These are moments applied to the laminate in the x-direction, y-direction, and xy-direction respectively. The units are Nm.

Example 7: Mm := (10 20 0)

• $\alpha 12$: coefficient of thermal expansion vector. $\alpha 1$ is the coefficient of thermal expansion in the fiber direction. $\alpha 2$ is the coefficient of thermal expansion in the transverse fiber direction. $\alpha 12$ is the coefficient of thermal expansion in the 1-2 direction.

Example 8: $\alpha 12$:= (-1.8 27 0)

•**RT:** room temperature. This is the room temperature in degrees Celsius at which the laminate will be used.

•**SFT:** stress free temperature. This is the stress free temperature or cure temperature of the laminate in degrees Celsius.

• $\beta 12$: moisture coefficient vector. $\beta 1$ is the moisture coefficient in the fiber direction. $\beta 2$ is the moisture coefficient in the transverse fiber direction. $\beta 12$ is the moisture coefficient in the 1-2 direction.

Example 9: $\beta 12$:= (1 5 0)

•**M1:** the initial or reference moisture state.

•**M2:** the final moisture state.

III. Equations

The equations used in this CLT code are self explanatory within the program. If there are further questions, the user may refer to "Mechanics of Composite Materials" by Robert M. Jones.

IV. Outputs

•**A, B, and D matrices:** These matrices provide laminate information. The **A** matrix contains the extensional stiffnesses; the **B** matrix contains the coupling stiffnesses; the **D** matrix contains the bending stiffnesses.

•**Ex:** This is Young's modulus of the laminate in the global x-direction.

•**Ey:** This is Young's modulus of the laminate in the global y-direction.

•**Gxy:** This is the shear modulus of the laminate in the global x-y system.

• υ**xy:** This is poisson's ratio of the laminate in the global system.

• εmid**:** These are the midplane strains of the laminate. The output is in vector form. εmid_1 is the midplane strain in the global x-direction. εmid_2 is the midplane strain in the global y-direction. εmid_3 is the midplane strain in the global xy-direction.

•**K:** These are the curvatures of the laminate. The output is in vector form. $\mathbf{K_1}$ is the curvature in the global x-direction. $\mathbf{K_2}$ is the curvature in the global y-direction. $\mathbf{K_3}$ is the curvature in the global xy-direction.

• εxy**:** the ply strains in the x-y coordinate system. The output is in vectorform. There is an εxy output equivalent to the number of plies, **p**. εxy_1 is the ply strain in the x-direction. εxy_2 is the ply strain in the y direction. εxy_3 is the ply strain in the xy-direction.

• $\varepsilon 12$: the ply strains in the material coordinate system. The output is in vector form. There is an $\varepsilon 12$ output equivalent to the number of plies, **p**. $\varepsilon 12_1$ is the ply strain in the fiber direction. $\varepsilon 12_2$ is the plystrain in the transverse fiber direction. $\varepsilon 12_3$ is the ply strain in the 1-2 direction.

• σxy: the ply stresses in the global x-y coordinate system. The output is in vector form. There is an σxy output equivalent to the number of plies, **p**. σxy_1 is the ply stress in the x- direction. σxy_2 is the ply stress in the y- direction. σxy_3 is the ply stress in the x-y direction.

• $\sigma 12$: the ply stresses in the material coordinate system. The output is in vector form. There is an $\sigma 12$ output equivalent to the number of plies, **p**. $\sigma 12_1$ is the ply stress in the fiber direction. $\sigma 12_2$ is the ply stress in the transverse fiber direction. $\sigma 12_3$ is the ply stress in the 1-2 direction.

• σzz: the interlaminar stresses. The output is in vector form. The vector has **p - 1** entries. σzz_1 is the interlaminar stress between plies 1 and 2. σzz_2 is the interlaminar stress between plies 2 and 3. σzz_3 is the interlaminar stress between plies 3 and 4, etc.

V. Laminate Strength and Ply Discount

This CLT code is not completely automated to determine laminate first ply failure and laminate rupture using ply discount theory. The user must interact with the program to determine this. To determine first ply failure using maximum stress theory, the user must do the following:

- Enter an initial Nm_1 or Nx value (such as 10) .
- Look at the ply stresses in the material coordinate system, $\sigma 12$.
- Calculate a "factor of safety ratio" for each of the directions (fiber, transverse fiber, 1-2) in each of the plies. This is done using the fiber, transverse fiber, and shear strengths (these should be known by the user). To calculate the "factor of safety", the user must look at the fiber direction stress and determine whether it is tensile or compressive. Then divide

the fiber direction stress bythe appropriate strength in the fiber direction (tensile orcompressive). The same process is used to determine the "factor of safety" ratio for the transverse fiber and 1-2 (shear) directions. This must be done for each ply.

- Once these ratios have been calculated, the user must pick the highest ratio. Then divide the initial Nm_1 or Nx value by the ratio. This will produce another Nx value. Then substitute this new Nx value for the previous value. Continue this process until the highest ratio has a value of 1. At that particular Nx value is when first ply failure occurs.

To determine laminate rupture using ply discount:

- Enter an initial Nm_1 or Nx value (such as 10) .
- Look at the fiber direction stresses in the material coordinate system. Find the highest fiber direction stress. This is the ply that controls rupture.
- Reduce **E2**, **ν12,** and **G12** to 10^{-6} in all plies other than the rupture controlling plies.
- Look at the recalculated stresses in the material coordinate system. Compare the fiber direction stress, $\sigma 12_1$, to the appropriate tensile or compressive fiber strength. Then divide the initial Nx value by this ratio. Continue this process until the ratio becomes 1. At that Nx value is when laminate rupture occurs.

VI. Program Modifications

If the user would like to include more plies then a few minor modifications must be added.

- the column matrices for the following inputs must be be increased such that the number of columns equals the number of plies, **p**:

  θ, E1, E2, ν12, G12, tp

- In the output, to see the stresses and strains for each ply the user must have the remaining plies, in excess of 10, printed out.

VII. Program List

See next page.

Anne Paige Clifton
Classical Laminate Theory

ORIGIN ≡ 1

INPUT DATA

Number of plies:

$p := 8$

$k := 1..p$

Rotation of principle material axes from arbitrary x-y axes:

$r := \frac{\pi}{180}$

$\theta := (0 \quad 45 \quad -45 \quad 90 \quad 90 \quad -45 \quad 45 \quad 0 \quad 0 \quad 0)\cdot r$

$\theta := \theta^T$

Material properties of each lamina:

$E1 := (39 \quad 39 \quad 39 \quad 39 \quad 39 \quad 39 \quad 39 \quad 39 \quad 0 \quad 0)\cdot 10^9$

$E2 := (4.8 \quad 4.8 \quad 4.8 \quad 4.8 \quad 4.8 \quad 4.8 \quad 4.8 \quad 4.8 \quad 0 \quad 0)\cdot 10^9$

$\nu 12 := (0.3 \quad 0.3 \quad 0.3 \quad 0.3 \quad 0.3 \quad 0.3 \quad 0.3 \quad 0.3 \quad 0 \quad 0)$

$G12 := (6.0 \quad 6.0 \quad 6.0 \quad 6.0 \quad 6.0 \quad 6.0 \quad 6.0 \quad 6.0 \quad 0 \quad 0)\cdot 10^9$

$E1 := E1^T \qquad E2 := E2^T \qquad G12 := G12^T \qquad \nu 12 := \nu 12^T$

$$\nu 21_k := \frac{E2_k \cdot \nu 12_k}{E1_k}$$

Ply thickess, tp:

$$tp := (.125 \quad .125 \quad .125 \quad .125 \quad .125 \quad .125 \quad .125 \quad .125 \quad 0 \quad 0) \cdot 10^{-3}$$

$$tp := tp^T$$

Mechanical information:

The resultant force and moment vectors:

$$Nm := (100 \quad 0 \quad 0)$$

$$Mm := (0 \quad 0 \quad 0)$$

Thermal information:

The coefficients of thermal expansion:

$$\alpha 12 := (-1.8 \quad 27 \quad 0) \cdot 10^{-6}$$

$$\alpha 12 := \alpha 12^T$$

Change in temperature (RT-SFT):

$RT := 25$

$SFT := 190$

$\Delta T := RT - SFT$

Moisture information:

Moisture coefficients:

$\beta 12 := (0 \quad 0 \quad 0) \cdot 10^{-6}$

$\beta 12 := \beta 12^{T}$

Change in moisture (M1-M2):

$M1 := 0$

$M2 := 0$

$\Delta M := M1 - M2$

CALCULATIONS:

Determine Q matrix (reduced stiffnesses):

$$Q(k) := \begin{bmatrix} \dfrac{E1_k}{1 - \nu 12_k \cdot \nu 21_k} & \dfrac{\nu 12_k \cdot E2_k}{1 - \nu 12_k \cdot \nu 21_k} & 0 \\ \dfrac{\nu 12_k \cdot E2_k}{1 - \nu 12_k \cdot \nu 21_k} & \dfrac{E2_k}{1 - \nu 12_k \cdot \nu 21_k} & 0 \\ 0 & 0 & G12_k \end{bmatrix}$$

Transformation matrix:

$$T(\theta) := \begin{pmatrix} \cos(\theta)^2 & \sin(\theta)^2 & 2\cdot\sin(\theta)\cdot\cos(\theta) \\ \sin(\theta)^2 & \cos(\theta)^2 & -2\cdot\sin(\theta)\cdot\cos(\theta) \\ -\sin(\theta)\cdot\cos(\theta) & \sin(\theta)\cdot\cos(\theta) & \cos(\theta)^2 - \sin(\theta)^2 \end{pmatrix}$$

Transformed reduced stiffness matrix, Qb:

$$Qb(\theta, k) := T(\theta_k)^{(-1)}\cdot Q(k)\cdot\left[T(\theta_k)^{(-1)}\right]^T$$

Qb matrices :

$$Qb(\theta, 1) = \begin{pmatrix} 3.94368\cdot 10^{10} & 1.45613\cdot 10^{9} & 0 \\ 1.45613\cdot 10^{9} & 4.85376\cdot 10^{9} & 0 \\ 0 & 0 & 6\cdot 10^{9} \end{pmatrix}$$

$$Qb(\theta, 2) = \begin{pmatrix} 1.78007\cdot 10^{10} & 5.80072\cdot 10^{9} & 8.64577\cdot 10^{9} \\ 5.80072\cdot 10^{9} & 1.78007\cdot 10^{10} & 8.64577\cdot 10^{9} \\ 8.64577\cdot 10^{9} & 8.64577\cdot 10^{9} & 1.03446\cdot 10^{10} \end{pmatrix}$$

$$Qb(\theta, 3) = \begin{pmatrix} 1.78007 \cdot 10^{10} & 5.80072 \cdot 10^{9} & -8.64577 \cdot 10^{9} \\ 5.80072 \cdot 10^{9} & 1.78007 \cdot 10^{10} & -8.64577 \cdot 10^{9} \\ -8.64577 \cdot 10^{9} & -8.64577 \cdot 10^{9} & 1.03446 \cdot 10^{10} \end{pmatrix}$$

Laminate thickness, t:

$$t := \sum_k tp_k$$

$$t = 1 \cdot 10^{-3}$$

Calculation of z coordinates:

$$z_1 := -\frac{t}{2}$$

$$z_{k+1} := z_k + tp_k$$

$$z = \begin{bmatrix} -5 \cdot 10^{-4} \\ -3.75 \cdot 10^{-4} \\ -2.5 \cdot 10^{-4} \\ -1.25 \cdot 10^{-4} \\ 0 \\ 1.25 \cdot 10^{-4} \\ 2.5 \cdot 10^{-4} \\ 3.75 \cdot 10^{-4} \\ 5 \cdot 10^{-4} \end{bmatrix}$$

Calculation of A, B, D matrices:

$$A := \sum_k Qb(\theta, k) \cdot (z_{k+1} - z_k)$$

$$B := \sum_k \frac{1}{2} \cdot Qb(\theta, k) \cdot \left[(z_{k+1})^2 - (z_k)^2 \right]$$

$$D := \sum_k \frac{1}{3} \cdot Qb(\theta, k) \cdot \left[(z_{k+1})^3 - (z_k)^3 \right]$$

Calculation of the H matrix:

$X := \text{augment}(A, B)$

$Y := \text{augment}(B, D)$

$X := X^T$

$Y := Y^T$

$Z := \text{augment}(X, Y)$

$H := Z^{-1}$

$$H = \begin{bmatrix} 5.17763 \cdot 10^{-8} & -9.40601 \cdot 10^{-9} & 0 & 0 & 0 & 0 \\ -9.40601 \cdot 10^{-9} & 5.17763 \cdot 10^{-8} & 0 & 0 & 0 & 0 \\ 0 & 0 & 1.22365 \cdot 10^{-7} & 0 & 0 & 0 \\ 0 & 0 & 0 & 0.41432 & -0.11579 & -0.06233 \\ 0 & 0 & 0 & -0.11579 & 1.19567 & -0.22544 \\ 0 & 0 & 0 & -0.06233 & -0.22544 & 1.60548 \end{bmatrix}$$

Calculation of the laminate moduli:

$$Ex := \frac{1}{H_{1,1} \cdot t}$$

$$Ey := \frac{1}{H_{2,2} \cdot t}$$

$$Gxy := \frac{1}{H_{3,3} \cdot t}$$

$$\nu xy := -\frac{H_{2,1}}{H_{1,1}}$$

Transformation of CTE to global coordinates:

$$Id := \begin{pmatrix} 1 & 0 & 0 \\ 0 & 1 & 0 \\ 0 & 0 & 2 \end{pmatrix}$$

$$\alpha xy(k) := Id \cdot T(\theta_k)^{(-1)} \cdot \alpha 12$$

Transformation of moisture coefficients to global coordinates:

$$Id := \begin{pmatrix} 1 & 0 & 0 \\ 0 & 1 & 0 \\ 0 & 0 & 2 \end{pmatrix}$$

$$\alpha xy(k) := Id \cdot T(\theta_k)^{(-1)} \cdot \alpha 12$$

Transformation of moisture coefficients to global coordinates:

$$Id := \begin{pmatrix} 1 & 0 & 0 \\ 0 & 1 & 0 \\ 0 & 0 & 2 \end{pmatrix}$$

$$\beta xy(k) := Id \cdot T(\theta_k)^{(-1)} \cdot \beta 12$$

Calculation of the thermal resultant forces and moments:

$$Nt := \sum_k Qb(\theta, k) \cdot \alpha xy(k) \cdot \Delta T \cdot (z_{k+1} - z_k)$$

$$Mt := \frac{1}{2} \cdot \sum_k Qb(\theta, k) \cdot \alpha xy(k) \cdot \Delta T \cdot \left[(z_{k+1})^2 - (z_k)^2 \right]$$

Calculation of the moisture resultant forces and moments:

$$Nmoist := \sum_k Qb(\theta, k) \cdot \beta xy(k) \cdot \Delta T \cdot (z_{k+1} - z_k)$$

$$Mmoist := \frac{1}{2} \cdot \sum_k Qb(\theta, k) \cdot \beta xy(k) \cdot \Delta T \cdot \left[(z_{k+1})^2 - (z_k)^2 \right]$$

Calculation of total NM vector:

$Nt := Nt^T$

$Mt := Mt^T$

$Nmoist := Nmoist^T$

$Mmoist := Mmoist^T$

$NM := augment(Nm, Mm)^T + augment(Nt, Mt)^T + augment(Nmoist, Mmoist)^T$

Calculation of the midplane strains and curvatures:

$\varepsilon K := H \cdot NM$

$i := 1..3$

$\varepsilon mid_i := \varepsilon K_i$

$K_i := \varepsilon K_{i+3}$

OUTPUT DATA:

A, B, D matrices:

$$A = \begin{pmatrix} 1.9973 \cdot 10^7 & 3.62842 \cdot 10^6 & 0 \\ 3.62842 \cdot 10^6 & 1.9973 \cdot 10^7 & 0 \\ 0 & 0 & 8.17229 \cdot 10^6 \end{pmatrix}$$

$$B = \begin{pmatrix} 0 & 0 & 0 \\ 0 & 0 & 0 \\ 0 & 0 & 0 \end{pmatrix}$$

$$D = \begin{pmatrix} 2.5089 & 0.26843 & 0.13509 \\ 0.26843 & 0.88782 & 0.13509 \\ 0.13509 & 0.13509 & 0.64708 \end{pmatrix}$$

The laminate properties:

$Ex = 1.93138 \cdot 10^{10}$

$Ey = 1.93138 \cdot 10^{10}$

$Gxy = 8.17229 \cdot 10^{9}$

$\nu xy = 0.18167$

Midplane strains and curvatures:

$$\varepsilon mid = \begin{pmatrix} -3.33051 \cdot 10^{-4} \\ -3.39169 \cdot 10^{-4} \\ 0 \end{pmatrix} \qquad K = \begin{pmatrix} 0 \\ 0 \\ 0 \end{pmatrix}$$

Calculation of ply strains in x-y coordinate system:

$$\varepsilon xy(k) := \varepsilon mid + \left(\frac{z_k + z_{k+1}}{2}\right) \cdot K$$

$$\varepsilon xy(1) = \begin{pmatrix} -3.33051 \cdot 10^{-4} \\ -3.39169 \cdot 10^{-4} \\ 0 \end{pmatrix} \quad \varepsilon xy(2) = \begin{pmatrix} -3.33051 \cdot 10^{-4} \\ -3.39169 \cdot 10^{-4} \\ 0 \end{pmatrix} \quad \varepsilon xy(3) = \begin{pmatrix} -3.33051 \cdot 10^{-4} \\ -3.39169 \cdot 10^{-4} \\ 0 \end{pmatrix}$$

$$\varepsilon xy(4) = \begin{pmatrix} -3.33051 \cdot 10^{-4} \\ -3.39169 \cdot 10^{-4} \\ 0 \end{pmatrix} \quad \varepsilon xy(5) = \begin{pmatrix} -3.33051 \cdot 10^{-4} \\ -3.39169 \cdot 10^{-4} \\ 0 \end{pmatrix} \quad \varepsilon xy(6) = \begin{pmatrix} -3.33051 \cdot 10^{-4} \\ -3.39169 \cdot 10^{-4} \\ 0 \end{pmatrix}$$

$$\varepsilon xy(7) = \begin{pmatrix} -3.33051 \cdot 10^{-4} \\ -3.39169 \cdot 10^{-4} \\ 0 \end{pmatrix} \quad \varepsilon xy(8) = \begin{pmatrix} -3.33051 \cdot 10^{-4} \\ -3.39169 \cdot 10^{-4} \\ 0 \end{pmatrix}$$

Calculation of ply strains in material direction (1-2 coordinate system):

$$\varepsilon 12(k) := T(\theta_k) \cdot \varepsilon xy(k)$$

$$\varepsilon 12(1) = \begin{pmatrix} -3.33051 \cdot 10^{-4} \\ -3.39169 \cdot 10^{-4} \\ 0 \end{pmatrix} \quad \varepsilon 12(2) = \begin{pmatrix} -3.3611 \cdot 10^{-4} \\ -3.3611 \cdot 10^{-4} \\ -3.05912 \cdot 10^{-6} \end{pmatrix} \quad \varepsilon 12(3) = \begin{pmatrix} -3.3611 \cdot 10^{-4} \\ -3.3611 \cdot 10^{-4} \\ 3.05912 \cdot 10^{-6} \end{pmatrix}$$

$$\varepsilon 12(4) = \begin{pmatrix} -3.39169 \cdot 10^{-4} \\ -3.33051 \cdot 10^{-4} \\ 0 \end{pmatrix} \quad \varepsilon 12(5) = \begin{pmatrix} -3.39169 \cdot 10^{-4} \\ -3.33051 \cdot 10^{-4} \\ 0 \end{pmatrix} \quad \varepsilon 12(6) = \begin{pmatrix} -3.3611 \cdot 10^{-4} \\ -3.3611 \cdot 10^{-4} \\ 3.05912 \cdot 10^{-6} \end{pmatrix}$$

$$\varepsilon 12(7) = \begin{pmatrix} -3.3611 \cdot 10^{-4} \\ -3.3611 \cdot 10^{-4} \\ -3.05912 \cdot 10^{-6} \end{pmatrix} \quad \varepsilon 12(8) = \begin{pmatrix} -3.33051 \cdot 10^{-4} \\ -3.39169 \cdot 10^{-4} \\ 0 \end{pmatrix}$$

Calculation of the residual ply stresses (x-y coordinate system):

$\sigma xy(k) := Qb(\theta, k)\cdot(\varepsilon xy(k) - \alpha xy(k)\cdot\Delta T)$

$$\sigma xy(1) = \begin{pmatrix} -1.8854\cdot 10^{7} \\ 1.90598\cdot 10^{7} \\ 0 \end{pmatrix} \quad \sigma xy(2) = \begin{pmatrix} 8.67094\cdot 10^{4} \\ 1.32906\cdot 10^{4} \\ -1.90202\cdot 10^{7} \end{pmatrix} \quad \sigma xy(3) = \begin{pmatrix} 8.67094\cdot 10^{4} \\ 1.32906\cdot 10^{4} \\ 1.90202\cdot 10^{7} \end{pmatrix}$$

$$\sigma xy(4) = \begin{pmatrix} 1.90806\cdot 10^{7} \\ -1.90864\cdot 10^{7} \\ -1.82824\cdot 10^{-9} \end{pmatrix} \quad \sigma xy(5) = \begin{pmatrix} 1.90806\cdot 10^{7} \\ -1.90864\cdot 10^{7} \\ -1.82321\cdot 10^{-9} \end{pmatrix} \quad \sigma xy(6) = \begin{pmatrix} 8.67094\cdot 10^{4} \\ 1.32906\cdot 10^{4} \\ 1.90202\cdot 10^{7} \end{pmatrix}$$

$$\sigma xy(7) = \begin{pmatrix} 8.67094\cdot 10^{4} \\ 1.32906\cdot 10^{4} \\ -1.90202\cdot 10^{7} \end{pmatrix} \quad \sigma xy(8) = \begin{pmatrix} -1.8854\cdot 10^{7} \\ 1.90598\cdot 10^{7} \\ 0 \end{pmatrix}$$

Calculation of residual ply stresses in material direction(1-2 coordinate system):

$\sigma 12(k) := T(\theta_k)\cdot\sigma xy(k)$

$$\sigma 12(1) = \begin{pmatrix} -1.8854\cdot 10^{7} \\ 1.90598\cdot 10^{7} \\ 0 \end{pmatrix} \quad \sigma 12(2) = \begin{pmatrix} -1.89702\cdot 10^{7} \\ 1.90702\cdot 10^{7} \\ -3.67094\cdot 10^{4} \end{pmatrix} \quad \sigma 12(3) = \begin{pmatrix} -1.89702\cdot 10^{7} \\ 1.90702\cdot 10^{7} \\ 3.67094\cdot 10^{4} \end{pmatrix}$$

$$\sigma 12(4) = \begin{pmatrix} -1.90864\cdot 10^{7} \\ 1.90806\cdot 10^{7} \\ 0 \end{pmatrix} \quad \sigma 12(5) = \begin{pmatrix} -1.90864\cdot 10^{7} \\ 1.90806\cdot 10^{7} \\ 0 \end{pmatrix} \quad \sigma 12(6) = \begin{pmatrix} -1.89702\cdot 10^{7} \\ 1.90702\cdot 10^{7} \\ 3.67094\cdot 10^{4} \end{pmatrix}$$

$$\sigma 12(7) = \begin{pmatrix} -1.89702\cdot 10^{7} \\ 1.90702\cdot 10^{7} \\ -3.67094\cdot 10^{4} \end{pmatrix} \quad \sigma 12(8) = \begin{pmatrix} -1.8854\cdot 10^{7} \\ 1.90598\cdot 10^{7} \\ 0 \end{pmatrix}$$

Interlaminar stresses:

$n := 1..p-1 \qquad m := 1..p-1$

$$zmid_k := \frac{z_k + z_{k+1}}{2}$$

$zmat_{n,1} := |zmid_n - z_2| \qquad zmat_{n,5} := |zmid_n - z_6|$

$zmat_{n,2} := |zmid_n - z_3| \qquad zmat_{n,6} := |zmid_n - z_7|$

$zmat_{n,3} := |zmid_n - z_4| \qquad zmat_{n,7} := |zmid_n - z_8|$

$zmat_{n,4} := |zmid_n - z_5|$

$zmat_{n,m} := if(n > m, 0, zmat_{n,m})$

$\sigma t_m := \sigma xy(m)_2 \cdot tp_m$

$\sigma t := \sigma t^T$

$Mz := \sigma t \cdot zmat$

$Mz = (\ 0.1489 \quad 0.4468 \quad 0.7449 \quad 0.8941 \quad 0.7449 \quad 0.4468 \quad 0.1489\ )$

$$\sigma zz := \left(\frac{2}{t}\right)^2 \cdot 3.5 \cdot Mz$$

$\sigma zz = (\ 2.08467 \cdot 10^6 \quad 6.25546 \cdot 10^6 \quad 1.04292 \cdot 10^7 \quad 1.25167 \cdot 10^7 \quad 1.04292 \cdot 10^7 \quad 6.25546 \cdot 10^6 \quad 2.08467 \cdot 10^6\ )$

VITA

The author was born September 5, 1969, in Martinsville, Virginia. She attended the University of South Carolina in Columbia, SC, where she earned a Bachelors Degree in Mechanical Engineering. Following graduation in 1992, she went directly to Virginia Polytechnic Institute and State University in Blacksburg, VA, to obtain her Masters Degree in Engineering Mechanics. Three and one-half years later she has finally achieved her goal. The author intends to begin an industrial career following graduation for the first time in her life.